

Combining nonperturbative transverse momentum dependence with TMD evolution

J. O. Gonzalez-Hernandez*

Dipartimento di Fisica, Università degli Studi di Torino, Via P. Giuria 1, 1-10125, Torino, Italy

T. C. Rogers†

*Department of Physics, Old Dominion University, Norfolk, VA 23529, USA and
Jefferson Lab, 12000 Jefferson Avenue, Newport News, VA 23606, USA*

N. Sato‡

Jefferson Lab, 12000 Jefferson Avenue, Newport News, VA 23606, USA

(Dated: May 13, 2022)

Central to understanding the nonperturbative, intrinsic partonic nature of hadron structure are the concepts of transverse momentum dependent (TMD) parton distribution and fragmentation functions. A TMD factorization approach to the phenomenology of semi-inclusive processes that includes evolution, higher orders, and matching to larger transverse momentum, is ultimately necessary for reliably connecting with phenomenologically extracted nonperturbative structures, especially when widely different scales are involved. In this paper, we will address some of the difficulties that arise when phenomenological techniques that were originally designed for very high energy applications are extended to studies of hadron structures, and we will solidify the connection between standard high energy TMD implementations and the more intuitive, parton model based approaches to phenomenology that emphasize nonperturbative hadron structure. In the process, we will elaborate on differences between forward and backward TMD evolution, which in the context of this paper we call “bottom-up” and “top-down” approaches, and we will explain the advantages of a bottom-up strategy. We will also emphasize and clarify the role of the integral relations that connect TMD and collinear correlation functions. We will show explicitly how they constrain the nonperturbative “ g -functions” of standard Collins-Soper-Sterman (CSS) implementations of TMD factorization. This paper is especially targeted toward phenomenologists and model builders who are interested in merging specific nonperturbative models and calculations (including lattice QCD) with TMD factorization at large Q . Our main result is a recipe for incorporating nonperturbative models into TMD factorization, and for constraining their parameters in a way that matches to perturbative QCD and evolution.

I. INTRODUCTION

The techniques of TMD factorization and evolution that are rooted in the CSS [1–3] approach are by now a very widespread, but applications tend to take on superficially different forms depending on their use and the specific phenomenological context. This fact will be very important for understanding the goals of the present paper. To unify different TMD applications, and especially to compare the phenomenologically extracted nonperturbative transverse momentum dependence across many different processes, some translation is still necessary. For our purposes, we will need to consider at least the following two phenomenological settings where TMD factorization has often been applied in the past:

1. Very large Q (Type II): With treatments of the transverse momentum spectra of processes at very large hard scales (say $Q \gtrsim 10$ GeV), it is common to assume (sometimes implicitly) that transverse

momentum dependence is describable mostly as a form of perturbative radiation in collinear factorization. An example is weak boson production in hadron-hadron collisions, where the hard scale is fixed by a heavy boson mass, larger than 80 GeV. When the transverse momentum q_T of the boson is of order the hard scale, calculations can follow a fixed order collinear factorization treatment. The challenge is then to describe the behavior as q_T decreases relative to Q . Term-by-term in fixed order calculations there are logarithms like

$$\sim \alpha_s(Q)^n \ln^m \left(\frac{Q}{q_T} \right), \quad (1)$$

with integer $m, n > 0$, that grow until they spoil truncated perturbation theory. With this as the starting point, the natural strategy is to try to resum as many such logarithms as possible. Most traditional TMD factorization techniques [1–3], along with soft-collinear effective theory (SCET)-based approaches [4–6], as well as approaches that directly resum transverse momentum logarithms [7–11], effectively account for these types of logarithms while also allowing for at least some contribution from nonperturbative transverse momentum in the $q_T \approx \Lambda_{\text{QCD}}$ region.

*Electronic address: joseosvaldo.gonzalezhernandez@unito.it

†Electronic address: tedconantrogers@gmail.com

‡Electronic address: nsato@jlab.org

2. Hadron structure and moderate Q (Type I):

TMD parton distribution functions (pdfs) and fragmentation functions (ffs) also feature prominently in studies whose focus is more directly on the nonperturbative structure of hadrons. In these types of applications, the relevant hard scales tend to be at much lower Q than in Type II situations, such as the $Q \approx \text{few GeV}$ s common in many semi-inclusive deep inelastic scattering (SIDIS) measurements. It is possible to trace the origin of many of the hadron-structure oriented approaches in Type I applications to intuitive pictures of colliding hadrons in a parton model. The hadrons, in this view, are composed entirely of nonperturbative quark and gluon constituents [12–15], and the earliest versions of phenomenological Type I applications usually adopted the approximation that all transverse momentum dependence is nonperturbative in origin. As such, they could mostly ignore the role of perturbative tails at large q_T and of evolution [16–19].

The Type I and Type II classification roughly follows that at Feynman, Field and Fox [20, Fig. 6]. At a formal level, it is now very well understood that approaches to Type I and type II observables can be made equivalent. And, of course, there is no sharp distinction between what constitutes a Type I or a type II scenario. It is possible to merge treatments of hadron structure with the evolution formulas that were traditionally applied at much larger Q [3, 21–24], and indeed much activity over the past decade was devoted to implementing TMD evolution, in the context of hadron structure studies, in ways that include nonperturbative parts [25–37]. (The versions of TMD factorization and evolution that we will focus on in this paper are those rooted in, or very similar to, the CSS formalism as described in Ref. [3] – see also Ref. [38] for translations to other approaches.)

There are, nevertheless, some remaining open issues related to the interpretation of intrinsic nonperturbative transverse momentum dependence that is extracted phenomenologically and its role in cross section calculations, and these can have practical consequences. We will explain what we mean here in much more detail in the main body of this paper. For now, we will prepare the reader by noting how some of the remaining complications originate in a clash between the natural phenomenological strategies that are often implicit in Type I and type II situations.

Starting from a typical Type II perspective, the main issue is that large transverse momentum perturbation theory calculations (with very large Q) receive correction terms like Eq. (1) that diverge as q_T approaches zero. So, the natural strategy is to try to resum as many transverse momentum dependent logarithms as possible as q_T decreases until one is essentially forced to incorporate a nonperturbative transverse momentum dependent component. We call this a “top-down” view because it starts by optimizing a large q_T dependence at large $q_T \approx Q$ in

collinear perturbation theory and then it extends it via evolution and resummation downward to more moderate Q and $q_T \approx 0$.

But, as an alternative strategy, one might instead start from the perspective more common in Type I scenarios. That is, one may begin by considering a moderate input scale Q_0 , low enough so that the accessible range of q_T is either comparable to Q_0 and is perturbative in origin, or is smaller than Q_0 and is mostly nonperturbative.¹ A TMD parton model type of description is the most natural and appropriate approach here. There is no region within the range of $0 < q_T \lesssim Q_0$ where calculations involve large logarithms analogous to Eq. (1). Thus, for $Q \approx Q_0$, the need to resum them does not arise. The only task then is to match a nonperturbative parametrization of transverse momentum dependence to a fixed order $q_T \approx Q_0$ calculation of transverse momentum dependence in collinear factorization.

However, the diverging logarithms will reappear later if we evolve to large Q . In this case, the uncontrolled perturbation theory errors will reappear at large q_T once we consider $Q \gg Q_0$ where the transverse momentum region $q_T \gg Q_0$ becomes accessible. The problematic logarithms are in the correlation functions that were originally defined at the input scale, and they take the form

$$\sim \alpha_s(Q_0)^n \ln^m \left(\frac{q_T}{Q_0} \right). \quad (2)$$

Unlike with the Type II oriented approaches discussed previously, the large logarithms from the bottom-up perspective are due to q_T getting *large* rather than small. We call it a “bottom-up” viewpoint because it starts by optimizing $q_T \sim 0$ treatments at moderate Q_0 , and then uses evolution equations to extend to large q_T and large $Q \gg Q_0$ where terms like Eq. (2) need to be addressed. These aspects of a bottom-up style of approach will be made much clearer in our review of TMD factorization in Sec. II.

In a more general sense, within typical Type II oriented approaches, transverse momentum dependence is seen as primarily perturbative and requiring corrections from non-perturbative behavior, while in typical Type I oriented approaches it is seen as a primarily non-perturbative phenomenon that needs to be improved with perturbative corrections from large transverse momentum. In the former, divergences are seen as a low q_T problem while in the latter they are a large q_T problem.

There is no formal difference between the bottom-up and top-down viewpoints just discussed, and they are generally described by identical sets of factorization and

¹ More specifically, there exists no significant transverse momentum region where m/q_T and q_T/Q_0 are both simultaneously small, though each is small in some region of q_T . Note that it is possible for this to be the situation even if Q_0 is large enough that $\alpha_s(Q_0)$ is small.

evolution equations. The logarithms like Eq. (2) are simply the mirror images of those in Eq. (1). However, they suggest different phenomenological strategies and this can have practical consequences, as we will see. The focus of this paper will be to give a full account of a bottom-up approach, which to our knowledge has never been made entirely explicit. We will also formally link it back to top-down approaches.

As we will see, adopting a bottom-up strategy brings with it some significant practical advantages in situations where extracting nonperturbative transverse momentum dependence is the primary goal. It also raises several important aspects of nonperturbative parametrizations that are often hidden to the foreground. All of this will be made clearer in the main body of the text.

One advantage is that, at the input scale Q_0 , it will be natural from the bottom-up perspective to categorize regions as perturbative or nonperturbative in transverse momentum space rather than in transverse coordinate space. This accords well with standard approaches to interpreting experimental data. For example, Ref. [39] offers some interpretations of recent COMPASS measurements with their Figure 17 and the comment “...the two exponential functions in our parameterisation F_1 can be attributed to two completely different underlying physics mechanisms...”. Much earlier, Feynman, Field, and Fox similarly identified different physical TMD mechanisms in transverse momentum space – see Figures 6 and 7 and the surrounding discussion from Ref. [20]. Associated with observations like these is an implicit choice to categorize physical mechanisms as perturbative or nonperturbative in momentum space.

The most prevalent models of nonperturbative TMDs were also constructed in momentum space, so they also sort regions into perturbative and nonperturbative categories in transverse momentum space. In many models, the large transverse momentum tails are suppressed on the grounds that it is only the small transverse momentum dependence that is nonperturbative or intrinsic to the hadron structure. Examples include at least spectator models [40–43], light-cone wave function descriptions [44–48], bag models [49–53], the Nambu-Jones Lasinio model [54–56], calculations based on the Dyson-Schwinger equations [57], classic quark-hadron model approaches and many others [36, 58, 59]. As will become clear, it is easier to incorporate models like these into full evolution treatments when starting from a bottom-up approach.

It will also turn out to be easier to match these models to perturbative transverse momentum calculations at large q_T in transverse momentum space than in coordinate space. Generally, fixed order perturbation theory calculations in collinear factorization for large transverse momentum ($q_T \approx Q$) observables are performed in momentum space. When we categorize behavior as perturbative or nonperturbative in TMD factorization according to momentum space regions, we will find that we are better able to ensure a consistent transition to the

large- q_T , collinear description where transverse momentum is generated perturbatively. (See also our comments below regarding the “asymptotic” term.) The difficulty of matching regions of q_T with different physics has led to proposals to implement all Type II style resummation entirely in momentum space, such as [60, 61], inspired by earlier pioneering work that resummed leading transverse momentum logarithms [62].

Another issue that will become clearer from a bottom-up perspective is the question of how to describe the transition between perturbative and nonperturbative transverse *coordinate* space dependence. Working in coordinate space has significant advantages for both setting up TMD factorization theoretically and implementing it. For example, most versions of the CSS formalism [1, 2, 63, 64] are in coordinate space. In this paper, we will continue to use coordinate space for implementing evolution. But in most top-down approaches to phenomenology, which are almost always formulated in coordinate (b_T) space, it is only when b_T is very large, usually above some specified transition point b_{\max} , that there is an explicit allowance for a nonperturbative transverse coordinate dependence. The strategy is often to push reliance on perturbation theory, with its well-understood collinear pdfs, normally considered valid only at small b_T , as far into the large b_T region as possible and thereby maximize the predictive power supplied by collinear factorization. However, unless the functions that parametrize the nonperturbative $b_T > b_{\max}$ region are constructed very carefully, there can be undesired side effects, particularly if the nonperturbative b_T -dependent contribution becomes non-negligible. In the original setup of TMD factorization, b_{\max} marks a totally arbitrary line of demarcation between what are labeled “large/nonperturbative” and “small/perturbative” transverse coordinate space regions. Formally, b_{\max} -dependence vanishes exactly from any physical observables. (See, for example, our discussion in section 13.10.4 of [3].) A setup like this ensures that purely perturbative calculations are sequestered from dependence on nonperturbative parameters. However, in practical implementations there is an unsettling tendency for b_{\max} -dependence to propagate into collinear perturbative calculations [65] and affect final results. Thus, purely perturbative calculations can appear to get contaminated by nonperturbative modeling. A significant b_{\max} -dependence in a calculation is a symptom that something is likely non-optimal about the underlying approximations being used. Part of the difficulty is that a valid description over the whole range of b_T needs to interpolate between the perturbative and nonperturbative regions, and varying b_{\max} amounts to simply reshuffling contributions between factors. In many practical applications, however, there is a rather abrupt switch between a purely collinear perturbation-theory calculation and one that involves a nonperturbative ansatz. We will show how switching from a top-down to a bottom-up perspective clarifies the steps that are needed to minimize b_{\max} -dependence in the parametriza-

tions used in phenomenological applications. Indeed, we will find that we are able to avoid the usual b_* -prescription entirely, along with a b_{\max} , and rely instead only on the input hard scale Q_0 to demarcate any transition between large and small transverse momentum.

Part of the work that is necessary in setting up reasonable phenomenological TMD parametrizations involves ensuring that they retain at least an approximate hadron structure interpretation. For example, the probability density interpretation of an unpolarized quark TMD pdf $f_{i/p}(x, k_T)$ gives

$$\int d^2 \mathbf{k}_T f_{i/p}(x, \mathbf{k}_T) \approx f_{i/p}(x) \quad (3)$$

where i is the flavor of a quark in hadron p and $f_{i/p}(x)$ is the corresponding collinear pdf. We use the “ \approx ” symbol here because the actual transverse momentum integral in Eq. (3) is ultraviolet (UV) divergent in QCD and needs to be regulated. After accounting for the UV divergence (by renormalizing the operator definition of the pdf, for example, and introducing regulators), the equality only holds up to order α_s and power-suppressed corrections.

The role that identities like Eq. (3) play in constraining nonperturbative transverse momentum dependence is often unclear in implementations of the CSS and related formalisms. The main reason is that the relation seems to be satisfied automatically in the way that final CSS cross section formulas normally are usually presented. To see how this happens, first consider the TMD pdf expressed in terms of its transverse coordinate space version, $\tilde{f}_{i/p}(x, \mathbf{b}_T)$

$$f_{i/p}(x, \mathbf{k}_T) = \frac{1}{(2\pi)^2} \int d^2 \mathbf{b}_T e^{i \mathbf{k}_T \cdot \mathbf{b}_T} \tilde{f}_{i/p}(x, \mathbf{b}_T). \quad (4)$$

The UV divergence in Eq. (3) manifests itself in Eq. (4) as a divergence in $\tilde{f}_{i/p}(x, \mathbf{b}_T)$ as $b_T \rightarrow 0$, so it may be regulated by freezing the \mathbf{b}_T argument in $\tilde{f}_{i/p}(x, \mathbf{b}_T)$ below some very small \mathbf{b}_{\min} . In that case, the integral of Eq. (3) applied to Eq. (4) is just

$$\int d^2 \mathbf{k}_T f_{i/p}(x, \mathbf{k}_T) = \tilde{f}_{i/p}(x, \mathbf{b}_{\min}). \quad (5)$$

In the next step, one observes that an operator product expansion (OPE) applies to $\tilde{f}_{i/p}(x, \mathbf{b}_{\min})$ in the limit of small \mathbf{b}_{\min} and relates it to the collinear pdf $f_i(x)$,

$$\tilde{f}_{i/p}(x, \mathbf{b}_{\min}) = \sum_j C_{i/j} \otimes f_{j/p} = f_i(x) + O(\alpha_s) + \text{p.s.} \quad (6)$$

The $C_{i/j}$ is a perturbative hard coefficient, $C_{i/j} \otimes f_{j/p}$ is the usual convolution integral of collinear factorization, the sum is over parton flavors, and “p.s.” refers to power suppressed corrections. The perturbation theory expansion on the right hand side is optimized by choosing renormalization scales appropriately in relation to \mathbf{b}_{\min} . So, dropping small corrections from the right side of Eq. (5)/Eq. (6) recovers Eq. (3).

At first sight, the steps leading from Eq. (5) to Eq. (6) can appear to constitute a *derivation* of Eq. (3). The normal presentations (for example, Eq. (22) of [66]) of the evolved CSS cross sections amplify that impression because they almost always include the transition to the OPE in Eq. (6) at small \mathbf{b}_T automatically in the final cross section expressions. From Eq. (6) above, it then appears that any nonperturbative modeling of large \mathbf{b}_T behavior can only impact the right hand side of Eq. (3) through power suppressed terms that are mostly irrelevant.

However, Eq. (6) is itself a restatement of Eq. (3), not a derivation of it. That is, a derivation of Eq. (6) requires that one identify and factorize integrals over the small, nonperturbative region of parton transverse momentum (i.e., the core contribution to the TMD pdf) and identify them with contributions to a collinear pdf, just as in Eq. (3). Therefore, a derivation of Eq. (3) that refers back to Eq. (6) as its starting point is circular. Using Eq. (6) assumes that a version of Eq. (3) already holds nonperturbatively.

There are practical consequences of this for setting up nonperturbative parametrizations of TMD correlations functions. One discards an important and useful constraint from the hadron structure interpretation of the nonperturbative $f_{i/p}(x, \mathbf{k}_T)$ if one assumes that Eq. (3) holds automatically on the basis of the OPE alone. By doing so, one is effectively assuming that, from the outset, all important regions of the integrand on the left side of Eq. (3) are at such large k_T that they are expressible entirely in terms of collinear pdfs, and that the intrinsic transverse momentum is completely irrelevant insofar as the integral is concerned. But there are many practical situations in TMD physics where that is obviously not the case. For example, at moderate scales where $f_{i/p}(x, \mathbf{k}_T)$ can be successfully modeled phenomenologically by a Gaussian distribution, with no collinear perturbative tail present at all, the entire range of the integration is described by a nonperturbative model. Thus, it is a requirement that Eq. (3) be imposed explicitly as a constraint from the outset if the goal is to maintain a connection between the nonperturbative TMD parametrizations of hadron structure interpretations and the corresponding collinear functions.

Many past TMD parton model approaches to Type I phenomenology do of course impose a version of Eq. (3) on TMD pdfs, but they typically do not include the transition to perturbative transverse momentum at large transverse momentum (or small \mathbf{b}_T as in Eq. (6)). Gaussian fits in momentum space are the most prominent examples. The reverse limitation is true of many CSS and similar approaches; these approaches account appropriately for large transverse momentum behavior, but they rarely (if ever) impose conditions analogous to Eq. (3) directly on the models of nonperturbative transverse momentum dependence. We will show in this paper how adopting a bottom-up perspective makes it clearer how to do both simultaneously, and we will give special at-

tention to integral relations like Eq. (3) and expand on the discussions above.

It is worth noting that similar issues also appear in other formalisms that deal with parton transverse momentum, such as the small- x oriented unintegrated pdfs of the Kimber-Martin-Ryskin-Watt [67, 68] treatments [69–71].

The issues that are clarified by a bottom-up perspective are interrelated, and the two just discussed will turn out to be examples of that. On page 2, we mentioned how failing to interpolate explicitly between nonperturbative and perturbative transverse momentum dependence can lead to undesired b_{max} -dependence in perturbative calculations. But, as we will see, setting up that interpolation involves the use of relations like Eq. (3). Conversely, imposing a version of Eq. (3) on small transverse momentum descriptions, in a way that accounts for a cutoff around $k_T \approx Q_0$, naturally requires a careful treatment of the large $k_T \approx Q_0$ region, and thus the interpolation to perturbatively large k_T becomes relevant.

Very broadly speaking, switching to a bottom-up approach helps with the inverse problem that arises from transforming between transverse momentum and coordinate space (see also [72]). Performing exact Fourier transformations to momentum space requires exact knowledge about the full range of the transverse coordinate space correlation functions. But actual measurements only probe specific limited ranges of b_T . Very large Q measurements are only sensitive to small transverse sizes and so they poorly constrain the nonperturbative transverse coordinate dependence at very large b_T . As a consequence, fits evolved from large Q down to moderate Q can be unstable. For instance, [73, 74] pointed out that the nonperturbative evolution extracted from the earlier CSS fits, which were frequently dominated by very large Q data, is too rapid when it is used to evolve down to the Q of only a few GeVs that are relevant for hadron structure studies. Conversely, measurements done at a more moderate $Q \approx Q_0$ might be dominated by nonperturbatively large b_T (or small k_T), but they are usually insensitive to the TMD correlation functions' very small $b_T \ll 1/Q_0$ (or large $k_T \gg Q_0$) behavior. The latter, however, do not generally need to be extracted but are instead calculable in terms of collinear correlation functions. So, a more stable phenomenological strategy is to first emphasize the role of more moderate Q measurements for constraining input nonperturbative transverse momentum and then rely on perturbation theory to evolve to larger Q .

Another aspect of TMD phenomenology that will be easier to control in a bottom-up approach is the matching to a momentum space, large transverse momentum asymptotic term. That step is important for relating the small $q_T \ll Q$ treatment supplied by TMD factorization to the standard momentum space $q_T \approx Q$ treatments in collinear factorization. Agreement between the two types of calculations at large q_T provides an important consistency test. In practice, however, ensur-

ing that the asymptotic term and the TMD factorization calculations match can be difficult at moderate Q . That is especially the case near the lowest scales, around $Q_0 \approx 1 - 2$ GeV, that are conventionally accepted as reasonable input scales. The difficulties can be largely traced back to those that we have discussed so far in this introduction. Errors that grow as Q evolves downward propagate, at least to some degree, to all values of transverse momentum, including the large transverse momentum. The range of accessible q_T shrinks, so there is a less well-defined separation between different transverse momentum regions.

We have so far emphasized a dichotomy between bottom-up/top-down approaches to phenomenology to highlight steps that continue to be a challenge when merging nonperturbative TMD parton model descriptions with TMD factorization and evolution in phenomenology, and to provide readers a basic foundation from which to read the rest of this paper. We reassure readers who find the discussion to be rather vague so far that it likely will become much clearer in the main body of this paper; some of the points noted above require explicit examples in order to be made entirely clear. We will provide some such examples within the main text.

Another way to understand the goals of this paper is to recall that nonperturbative transverse momentum dependence enters the standard CSS implementations in the form of extra coordinate space factors, often expressed as exponential factors $e^{-g_{j/A}(x, b_T)}$ for a flavor j in hadron A or $e^{-g_K(b_T) \ln \frac{Q}{Q_0}}$ for the nonperturbative TMD evolution. (For example, consider again Eq. (22) of Ref. [66].) Our purpose is to explain, in much more detail than is usual, how to optimally parametrize these functions in phenomenological applications, such that they match to existing models or calculations of intrinsic nonperturbative transverse momentum dependence. Nothing about the standard TMD factorization formalism itself will change. The final outcome will be a recipe for merging arbitrary nonperturbative models of $g_{j/A}(x, b_T)$ and $g_K(b_T)$ with TMD evolution in the CSS style. To our knowledge, this is the first instance of such a discussion. We will connect the bottom-up strategy with more standard presentations that involve $g_{j/A}(x, b_T)$ and $g_K(b_T)$ in Sec. IX. Some of our goals overlap with those recently addressed in [72], which introduced techniques for disentangling large and small b_T contributions to cross sections, and these techniques will likely be helpful in future efforts to identify and separate perturbative and nonperturbative contributions.

To further prepare the reader, we end this introduction by listing the main aspects of what we will advocate that differ from what is sometimes done:

- When we discuss phenomenology at an input scale Q_0 , we will work mainly in transverse momentum space rather than in coordinate space.
- We will nevertheless account for the perturbative behavior at $q_T \gg Q_0$ in TMD correlation func-

tions. We will do this even for $Q \approx Q_0$ where such contributions are often phenomenologically irrelevant.

- For the region where $Q \approx Q_0$, $q_T \approx Q_0$, all renormalization scales will be fixed at order Q_0 and not $1/b_T$ since there is no need for resummation of logarithms of the type $\ln(q_T/Q_0)$ or $\ln(b_T Q_0)$.
- We will nevertheless perform evolution to $Q \gg Q_0$ in coordinate space, and switch to a $\sim 1/b_T$ scale, but only at a later step.
- Also for $Q \approx Q_0$, we will explicitly impose approximate matching to the fixed order asymptotic behavior at $q_T \approx Q_0$.
- In nonperturbative parametrizations of TMD correlation functions at $Q = Q_0$, we will explicitly impose a version of Eq. (3). We will do this in momentum space with a large transverse momentum cutoff to regulate UV divergences and to match with what is typically done in phenomenological models.
- Our approach will include an explicit interpolation between purely nonperturbative and purely perturbative descriptions of transverse momentum dependence in the TMD correlation functions.

Along the way, we will highlight the advantages of these choices by using explicit examples. At the end, we will translate the expressions into forms that are more familiar from standard TMD factorization implementations in the CSS formalism.

We will start by reminding the reader of the basic setup of TMD factorization and evolution in Sec. II. Section III discusses the role of integral constraints for nonperturbative parametrizations of TMD correlation functions in more detail. Sections IV and V will focus on the details of modeling nonperturbative parts of TMD functions at an input scale Q_0 and in momentum space. The steps for using input parametrizations to evolve to higher scales are summarized in a practical phenomenological recipe in Sec. VI. In Sec. VII we use concrete toy examples to illustrate the steps, including plots. In Sec. VIII we return the integral relation and discuss it in light of the bottom-up approach. In Sec. IX we explain how to connect the bottom-approach to standard CSS expressions. We offer our concluding remarks in Sec. X.

Explaining some intermediate steps will require a more pedantic system of notation than what is normally necessary. To help the reader keep track of symbols and conventions, we have therefore included a notation glossary in Appendix A.

II. TMD FACTORIZATION AND EVOLUTION

We begin by reviewing some of the basic setup of TMD factorization to establish context and introduce notation

for later sections. While all of what we discuss is meant to apply to any of the basic processes for which there are TMD factorization theorems, it will be instructive to work within a specific example. For this we will use semi-inclusive annihilation (SIA) of a lepton-antilepton pair (usually electron-positron) into a pair of nearly back-to-back hadrons with a sum over all other final state particles X ,

$$e^-(l) + e^+(\bar{l}) \rightarrow H_A(p_A) + H_B(p_B) + X. \quad (7)$$

A quark-antiquark pair is produced in the hard vertex, and hadrons H_A and H_B are measured in the final state. This is among the simplest processes to work with theoretically, and it is ideal for illustrating the basics of TMD factorization. (See, for example, the discussion in chapter 13 of Ref. [3].)

The process is illustrated graphically in Figure 1: An electron (l) and a positron (\bar{l}) annihilate to create a virtual photon of momenta q , which creates a quark-antiquark pair. The two hadrons measured in the final state with momenta p_A and p_B are then produced when partons A and B fragment. The momentum of the virtual photon sets the hard scale of the process Q , with $q^2 \equiv Q^2$. See also Refs.[75–77] for more details about the general kinematical setup.

In a reference frame where the hadrons are back-to-back, the transverse momentum of the photon q_T is the relevant observed final state transverse momentum. When it is small relative to the hard scale, $q_T \ll Q$, it is sensitive to intrinsic transverse momenta of the hadronizing quark and antiquark respectively. The usual Lorentz

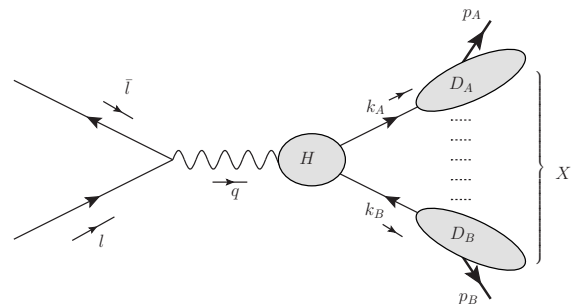


FIG. 1: Schematic of the semi-inclusive e^+e^- -annihilation process.

invariant kinematic variables related to collinear momentum fractions are

$$z_A = \frac{p_A \cdot p_B}{q \cdot p_B} \approx \frac{p_{A,h}^+}{q_h^+}, \quad z_B = \frac{p_A \cdot p_B}{q \cdot p_A} \approx \frac{p_{B,h}^-}{q_h^-} \quad (8)$$

where the “ \approx ” means we drop terms that are power suppressed in the current fragmentation region (by which we mean z_A and z_B are fixed and not too small relative to 1). The “ h ” subscripts on lightcone momentum components indicate that they are with respect to the hadron frame.

In TMD factorization, the unpolarized cross section differential in z_A , z_B and q_T^2 is written [3]

$$\begin{aligned}
& Q^2 \frac{d\sigma^{A,B}}{dz_A dz_B dq_T^2} \\
&= H_{j\bar{j}}(\mu_Q; C_2) \int d^2\mathbf{k}_{AT} d^2\mathbf{k}_{BT} D_{j/A}(z_A, z_A \mathbf{k}_{AT}; \mu_Q, Q^2) D_{\bar{j}/B}(z_B, z_B \mathbf{k}_{BT}; \mu_Q, Q^2) \delta^{(2)}(\mathbf{q}_T - \mathbf{k}_{AT} - \mathbf{k}_{BT}) + \\
& Y^{A,B}(q_T, Q; \mu_Q) + O(m/Q) .
\end{aligned} \tag{9}$$

The second line has the familiar form from the TMD parton model, but with extra auxiliary arguments for evolution. The capital $D_{j/A}$ and $D_{\bar{j}/B}$ are the TMD ffs for a quark of flavor j (\bar{j}) to fragment into hadron A (B). A sum over flavors is implied.

In addition to the longitudinal and transverse parton momentum arguments $z_{A,B}$ and $\mathbf{k}_{A,BT}$, the TMD ffs also depend on a renormalization group scale μ and a rapidity evolution scale ζ , which in Eq. (9) we have already fixed equal to $\mu = \mu_Q \equiv C_2 Q$ and $\zeta = Q^2$ to optimize perturbation theory. Here, C_2 is an arbitrary numerical constant of order unity. (Throughout this paper, we will assume $C_2 = 1$.) $H(\mu_Q; C_2)$ is a hard factor of the form $H = 1 + O(\alpha_s(\mu_Q))$, up to an uninteresting overall constant. The $Y(q_T, Q)$ -term on the last line is an abbreviation for the correction needed for the $q_T \approx Q$ behavior, and it is calculable entirely in fixed order collinear factorization. The second line in Eq. (14) is exactly the TMD parton model familiar from typical Type I appli-

cations if we drop the auxiliary μ and ζ arguments and set $H(\mu_Q; C_2) = 1$.

We will focus on a very specific combination of physical observables in order to simplify later illustrative examples. Say that hadron A is h^+ and hadron B is its antiparticle h^- . Then we can consider the combination

$$\begin{aligned}
& \frac{d\sigma^{\text{NS}}}{dz_A dz_B dq_T^2} = \\
& \frac{d\sigma^{h^+, h^-}}{dz_A dz_B dq_T^2} + \frac{d\sigma^{h^-, h^+}}{dz_A dz_B dq_T^2} \\
& - \frac{d\sigma^{h^+, h^+}}{dz_A dz_B dq_T^2} - \frac{d\sigma^{h^-, h^-}}{dz_A dz_B dq_T^2} .
\end{aligned} \tag{10}$$

We will also consider only the $j = \text{“up quark”}$ contribution to Eq. (9). Then, summing the corresponding terms on the right hand side of Eq. (9) gives

$$\begin{aligned}
& H_{u\bar{u}}(\mu_Q; C_2) \int d^2\mathbf{k}_{AT} d^2\mathbf{k}_{BT} [D_{u/h^+}(z_A, z_A \mathbf{k}_{AT}; \mu_Q, Q^2) - D_{u/h^-}(z_A, z_A \mathbf{k}_{AT}; \mu_Q, Q^2)] \\
& \times [D_{\bar{u}/h^-}(z_B, z_B \mathbf{k}_{BT}; \mu_Q, Q^2) - D_{\bar{u}/h^+}(z_B, z_B \mathbf{k}_{BT}; \mu_Q, Q^2)] \delta^{(2)}(\mathbf{q}_T - \mathbf{k}_{AT} - \mathbf{k}_{BT}) \\
& + Y^{\text{NS}}(q_T, Q; \mu_Q) + O(m/Q) .
\end{aligned} \tag{11}$$

Then we can define non-singlet TMD fragmentation functions,

$$D_A(z_A, z_A \mathbf{k}_{AT}; \mu_Q, Q^2) \equiv D_{j/h^+}(z_A, z_A \mathbf{k}_{AT}; \mu_Q, Q^2) - D_{j/h^-}(z_A, z_A \mathbf{k}_{AT}; \mu_Q, Q^2) \tag{12}$$

$$D_B(z_B, z_B \mathbf{k}_{BT}; \mu_Q, Q^2) \equiv D_{\bar{j}/h^-}(z_B, z_B \mathbf{k}_{BT}; \mu_Q, Q^2) - D_{\bar{j}/h^+}(z_B, z_B \mathbf{k}_{BT}; \mu_Q, Q^2) . \tag{13}$$

And, we can drop the j index for the rest of this paper and rewrite Eq. (9) in a more abbreviated way as

$$\begin{aligned}
& Q^2 \frac{d\sigma^{\text{NS}}}{dz_A dz_B dq_T^2} \\
&= H(\mu_Q; C_2) \int d^2\mathbf{k}_{AT} d^2\mathbf{k}_{BT} D_A(z_A, z_A \mathbf{k}_{AT}; \mu_Q, Q^2) D_B(z_B, z_B \mathbf{k}_{BT}; \mu_Q, Q^2) \delta^{(2)}(\mathbf{q}_T - \mathbf{k}_{AT} - \mathbf{k}_{BT}) \\
&+ Y^{\text{NS}}(q_T, Q; \mu_Q) + O(m/Q) .
\end{aligned} \tag{14}$$

Our results are general and independent of the specific hadrons in the final state, but organizing the discussion

around this channel will simplify illustrative example calculations later on by allowing us to drop explicit flavor indices and consider only non-singlet ffs in parts of calculations that involve collinear DGLAP evolution. Specifically, in our examples we will use the JAM20 collinear fragmentation functions for π^+ and its corresponding grid for α_s values [78]. Note that because of charge conjugation, to construct the TMDs in Eq. (12) and Eq. (13), only the non-singlet combination $u - \bar{u}$ are involved. We use the set= 0, from LHAPDF[79], since we will not be making any comparison to data. All that is needed for our present purposes is that the collinear ffs employed in

our numerical examples obey non-singlet DGLAP evolution equations.

Since our focus for this paper is on the $q_T \ll Q$ region at leading power, where TMD correlation functions are relevant, we will also drop any mention of the $Y(q_T, Q)$ -term from here forward.

The second line in Eq. (14) is exactly the TMD parton model familiar from typical Type I applications if we drop the auxiliary μ and ζ arguments and set $H(\mu_Q; C_2) = 1$. This term is sometimes called the W -term.

It can be convenient to write the W -term in terms of coordinate space TMD ffs,

$$W(q_T, Q) = H(\mu_Q; C_2) \int \frac{d^2 \mathbf{b}_T}{(2\pi)^2} e^{-i \mathbf{q}_T \cdot \mathbf{b}_T} \tilde{D}_A(z_A, \mathbf{b}_T; \mu_Q, Q^2) \tilde{D}_B(z_B, \mathbf{b}_T; \mu_Q, Q^2), \quad (15)$$

where the transverse coordinate and momentum space TMD ffs are related to one another via

$$D(z, z \mathbf{k}_T; \mu, \zeta) = \int \frac{d^2 \mathbf{b}_T}{(2\pi)^2} e^{-i \mathbf{k}_T \cdot \mathbf{b}_T} \tilde{D}(z, \mathbf{b}_T; \mu, \zeta). \quad (16)$$

The TMD ffs D_A and D_B are hadron-vacuum correlation functions defined in a very particular way in terms of quark field operators. An explanation of these definitions and their origins in factorization theorems would involve topics like Wilson lines, rapidity divergences, soft factors, and other related issues that are beyond the scope of this article. In recent years, they have been reviewed in many places, so to avoid repetition we refer the reader to [80] which includes an overview and a list references associated with TMD definitions derived in the style relevant for this article, and also to [81] which includes additional relevant references.

With regard to the TMD definitions, what is important for our purposes is only that they satisfy an exact set of evolution equations for the auxiliary variables μ and ζ . For a TMD ff in coordinate space, the evolution equations are

$$\frac{\partial \ln \tilde{D}(z, \mathbf{b}_T; \mu, \zeta)}{\partial \ln \sqrt{\zeta}} = \tilde{K}(b_T; \mu), \quad (17)$$

$$\frac{d \tilde{K}(b_T; \mu)}{d \ln \mu} = -\gamma_K(\alpha_s(\mu)), \quad (18)$$

$$\begin{aligned} \frac{d \ln \tilde{D}(z, \mathbf{b}_T; \mu, \zeta)}{d \ln \mu} &= \gamma(\alpha_s(\mu); \zeta/\mu^2) \\ &= \gamma(\alpha_s(\mu); 1) - \gamma_K(\alpha_s(\mu)) \ln \left(\frac{\sqrt{\zeta}}{\mu} \right). \end{aligned} \quad (19)$$

The evolution kernels, γ , γ_K and \tilde{K} are known by many different names in the literature. In keeping with our earlier work, we will refer to $\tilde{K}(b_T; \mu)$ as the Collins-Soper (CS) kernel.

For large enough μ , the anomalous dimensions γ_K and γ are both calculable in perturbation theory and they are independent of b_T . $\tilde{K}(b_T; \mu)$ is also perturbatively calculable at small $b_T \sim 1/\mu$, but it becomes nonperturbative over large distances, $b_T \rightarrow \infty$. However, since it is independent of the identity of external hadrons, it has very strong universality properties related to the QCD vacuum.

The evolution equations are first order linear differential equations that relate the TMD ffs in Eq. (15) at an input scale Q_0 to a different scale Q , so they can be easily solved exactly and analytically. The general solutions to the evolution equations for D_A and D_B , substituted into Eq. (15), allow us to write $W(q_T, Q)$ as

$$W(q_T, Q) = H(\alpha_s(\mu_Q); C_2) \int \frac{d^2 \mathbf{b}_T}{(2\pi)^2} e^{-i\mathbf{q}_T \cdot \mathbf{b}_T} \tilde{D}_A(z_A, \mathbf{b}_T; \mu_{Q_0}, Q_0^2) \tilde{D}_B(z_B, \mathbf{b}_T; \mu_{Q_0}, Q_0^2) \\ \times \exp \left\{ \tilde{K}(b_T; \mu_{Q_0}) \ln \left(\frac{Q^2}{Q_0^2} \right) + \int_{\mu_{Q_0}}^{\mu_Q} \frac{d\mu'}{\mu'} \left[2\gamma(\alpha_s(\mu'); 1) - \ln \frac{Q^2}{\mu'^2} \gamma_K(\alpha_s(\mu')) \right] \right\}. \quad (20)$$

We could express the same evolved W with TMD ffs in transverse momentum space, and in some cases that might help with intuition since it more closely matches the TMD parton model. But then the Fourier transforms of simple factors become transverse momentum convolu-

tion integrals of several functions. For the purposes of implementing evolution, we will continue to work with Eq. (20) in coordinate space, as is normally done.

When $Q = Q_0$, Eq. (20) exactly reproduces the TMD parton model form of the factorization,

$$W(q_T, Q_0) = H(\mu_{Q_0}; C_2) \int \frac{d^2 \mathbf{b}_T}{(2\pi)^2} e^{-i\mathbf{q}_T \cdot \mathbf{b}_T} \tilde{D}_A(z_A, \mathbf{b}_T; \mu_{Q_0}, Q_0^2) \tilde{D}_B(z_B, \mathbf{b}_T; \mu_{Q_0}, Q_0^2) \\ = H(\mu_{Q_0}; C_2) \int d^2 \mathbf{k}_{AT} d^2 \mathbf{k}_{BT} D_A(z_A, z_A \mathbf{k}_{AT}; \mu_{Q_0}, Q_0^2) D_B(z_B, z_B \mathbf{k}_{BT}; \mu_{Q_0}, Q_0^2) \delta^{(2)}(\mathbf{q}_T - \mathbf{k}_{AT} - \mathbf{k}_{BT}). \quad (21)$$

So far, Eq. (20) and Eq. (21) still involve no approximations at all on the W -term. However, approximations are ultimately necessary, of course, for getting practical results.

Rather different kinds of approximations to Eq. (20) can enter in a number of different ways, so the language can become confusing. We will be as precise as possible with our wording here. There are at least four different types of approximation that generally take place simultaneously, including

1. The choices of models, assumptions, or approximations used to describe nonperturbative contributions,
2. The neglect of power suppressed corrections to factorization, like the last term in Eq. (14),
3. Truncation of high powers of α_s in perturbative parts of the calculation and,
4. In phenomenological applications involving fits, whatever assumptions and approximations are used at the level of fit extractions.

When we discuss an “ n^{th} -order” perturbative treatment, we will mean by this that all parts that are calculable in fixed order perturbative QCD have been included through order n , and they are optimized using the renormalization group and Collins-Soper evolution (Eq. (17)). These “perturbative parts” include the right sides of Eqs. (17)–(19), which in Eq. (20) appear as $\gamma_K(\alpha_s(\mu'))$, $\gamma(\alpha_s(\mu'); 1)$ and $\tilde{K}(b_T; \mu_{Q_0})$ when b_T (or k_T) is small

(large) enough that its b_T -dependence is perturbative. In Eq. (20) it also includes $H(\mu_Q; C_2)$ and the \tilde{D}_A , \tilde{D}_B functions in regions of small b_T (or large k_T). An “(n)” superscript on a function means that it has been replaced by its truncated, fixed order perturbation theory calculation through order n . When we discuss nonperturbative parts in later sections, it should be understood to be in the context of phenomenological extractions. We will *assume* for the sake of our discussion here that all nonperturbative parametrizations have been made flexible enough that the significant errors come only from the limitations of factorization and truncated perturbation theory, and not from a poor choice of nonperturbative parametrizations or artifacts of the fitting procedure. Thus, a function like $\tilde{D}_A^{(n)}$ should be read as “a \tilde{D}_A parametrization including nonperturbative parts extracted from measurements and using an n^{th} -order perturbation theory treatment for its perturbative ingredients.”

Also, when we use the phrase “nonperturbative part,” (e.g., the g -functions of the CSS formalism) it should generally be understood that we are not necessarily referring to parts of a calculation that cannot ever be improved with small coupling techniques. It only refers to contributions that we choose to exclude from those factors that we explicitly identify as perturbative.

Now consider how one might use Eq. (20) to do phenomenology in a Type I scenario and from a bottom-up perspective. Near the input scale, $Q \approx Q_0$, the evolution factor on the second line is nearly unity and we can, to a good approximation, just work with Eq. (21). If Q_0 is only of order $\sim 1 - 2$ GeV, then a phenomenolog-

ical measurement of $W(q_T, Q_0)$ is only sensitive to the region of nonperturbatively large b_T parts of \tilde{D}_A and \tilde{D}_B whereas the $b_T \ll 1/Q_0$ contributions is strongly suppressed in cross sections. Therefore, measurements of the $Q \approx Q_0$ region place rigid constraints on the nonperturbative transverse momentum dependence while remaining mostly insensitive to perturbative tails from

large $k_{A,BT}$ (or small b_T). Indeed, past phenomenology with Eq. (21) has confirmed that the basic TMD parton model is quite successful at describing moderate Q data with entirely nonperturbative k_T parametrizations like Gaussians [18, 82–84]. Work that is done in this style effectively replaces the exact Eq. (21) with the approximation

$$W^{(n)}(q_T, Q_0) = H^{(n)}(\mu_{Q_0}; C_2) \int \frac{d^2 \mathbf{b}_T}{(2\pi)^2} e^{-i\mathbf{q}_T \cdot \mathbf{b}_T} \tilde{D}_{A,\text{np}}(z_A, \mathbf{b}_T; \mu_{Q_0}, Q_0^2) \tilde{D}_{B,\text{np}}(z_B, \mathbf{b}_T; \mu_{Q_0}, Q_0^2), \quad (22)$$

where the “np” subscripts on the TMD ffs refer to Fourier-Bessel transforms of entirely nonperturbative model parametrizations for $D_A(z_A, z_A \mathbf{k}_{AT}; \mu_{Q_0}, Q_0^2)$ and $D_B(z_B, z_B \mathbf{k}_{BT}; \mu_{Q_0}, Q_0^2)$ (e.g., Gaussians, etc), with no matching to perturbative large- k_T tails. If most of the $0 \lesssim q_T \lesssim Q_0$ region of transverse momentum dependence is nonperturbative at $Q \approx Q_0$, then there is nothing more to do at this scale, and replacing $H(\mu_{Q_0}; C_2)$ by $H^{(n)}(\mu_{Q_0}; C_2)$ in Eq. (22) is the maximum amount of perturbative input that is possible.

Notice that, if we have perfectly constrained the input TMD ffs for all k_T at the input scale Q_0 , then evolving them to larger $Q \gg Q_0$ with Eq. (20) is almost trivial. All that is necessary are $\gamma_K(\alpha_s(\mu'))$, $\gamma(\alpha_s(\mu'); 1)$ and $\tilde{K}(b_T; \mu_{Q_0})$ calculated to n^{th} order in perturbation theory and a way to perform the inverse Fourier-Bessel transform. Thus, traditional Type I extractions of TMD ffs near an input scale might appear at first sight to be all the input that is necessary, aside from a treatment of the evolution kernels, for evolution to any other scale.

However, this will fail to work if applied directly to traditional Type I oriented styles of phenomenological extractions that neglect large k_T tails. The reason is that $D_A(z_A, z_A \mathbf{k}_{AT}; \mu_{Q_0}, Q_0^2)$ and $D_B(z_B, z_B \mathbf{k}_{BT}; \mu_{Q_0}, Q_0^2)$ need to be well-described over their *entire* k_T ranges, not just over the $0 \lesssim k_T \lesssim Q_0$ regions that moderate Q_0 measurements effectively probe, in order for the evolution to larger Q to be accurate. Fortunately, the large- k_T behavior of TMD ffs is calculable in collinear factorization, so nothing prevents us from simply interpolating between phenomenological fits of the small k_T region and a large- k_T perturbative description of the input TMD correlation functions at $k_T > Q_0$. We will discuss how to make this adjustment to standard Type II oriented approaches in later sections.

If Q_0 is, as we intend, a lower bound on what is considered a reasonable hard scale, near the boundary between large and small coupling, then there is a very rapid scale dependence when a choice of $\mu \propto Q_0$ is varied downward. Therefore, it is preferable to keep renormalization and rapidity scales fixed around μ_{Q_0} and Q_0 in the moderate $k_T \approx Q_0$ or $b_T \approx 1/Q_0$ regions. (We elaborate on this

slightly subtle point in Appendix B to avoid breaking the flow of our main discussion here.)

But in the $k_T \gg Q_0$ region, large logarithms of the form $\ln(k_T/Q_0)$ start to degrade the accuracy of such a treatment. Extending calculations to the very large $k_T \gg Q_0$ region requires another iteration of the evolution equations to switch scales. (Actually, when we do this in later sections, it will be in coordinate space as is more common, and we will switch to the usual $\sim 1/b_T$ scale.) We will explain the details of both the interpolation and the scale transformation in Sec. V. The discussion of Eq. (2) in the introduction was in reference to these types of logarithmic errors.

For readers accustomed to more standard presentations of the CSS formalism, the above discussion might seem like a slightly odd starting point because normally one does not stop with Eq. (20). Rather, one immediately performs the step of evolving $\tilde{D}_A(z_A, \mathbf{b}_T; \mu_{Q_0}, Q_0^2)$ and $\tilde{D}_B(z_B, \mathbf{b}_T; \mu_{Q_0}, Q_0^2)$ to scales of order $1/b_T$ to optimize collinear factorization calculations with the OPE in the region of $b_T \sim 1/Q$. The resulting expressions (see for example Eq.(22) of [66]) highlight the role of the $b_T \sim 1/Q$ calculation. Ultimately, we will perform an equivalent step, but we choose to delay it for now for reasons that we hope will become clear later. The connection between Eq. (20) and the usual CSS presentation will be made in Sec. IX.

III. INTEGRAL RELATIONS

As we will see in later sections, consistently interpolating between nonperturbatively small k_T and perturbatively large k_T will require integral relations like Eq. (3). In this section we will define and discuss a collinear ff that obeys an analogous equation with a cutoff on large transverse momentum. This section also introduces additional notation that will be necessary in later sections. We remind the reader of our notation glossary, Appendix A.

We will use a superscript “ (n, d_r) ” on a TMD ff to indicate that it is calculated in a large ($k_T \approx Q$) transverse

momentum approximation. Thus,

$$D(z, z\mathbf{k}_T \approx Q; \mu_Q, Q^2) \equiv D^{(n, d_r)}(z, z\mathbf{k}_T; \mu_Q, Q^2) + O\left(\frac{m}{k_T}, \alpha_s(k_T)^{n+1}\right). \quad (23)$$

As usual, “ n ” is the order of collinear perturbation theory. Thus, $D^{(n, d_r)}(z, z\mathbf{k}_T; \mu_Q, Q^2)$ is calculated *through* order α_s^n , with powers of α_s^{n+1} and $\sim m/k_T$ errors neglected. However, now we have also included a “ d_r ” in the superscript. This is to indicate that the collinear factorization calculation uses a renormalized collinear ff $d_r(z; \mu_Q)$. The subscript “ r ” on “ d_r ” in turn labels the UV renormalization or regularization scheme (such as, for example, $r = \overline{\text{MS}}$ renormalization). We also define

$$D^{(n, d_r)}(z, z\mathbf{k}_T; \mu_Q, Q^2) \equiv 0 \quad \forall \quad n < 1. \quad (24)$$

The m/k_T in the error term of Eq. (23) symbolizes contributions that are power suppressed when $k_T \approx Q$. Throughout this paper, an “ m ” will always represent any generic mass scale that is of order a small hadronic size like Λ_{QCD} or an intrinsic transverse momentum. Also, to simplify notation, any power-suppressed contributions of the form $(m/Q)^\beta$ or $(m/k_T)^\beta$, with $\beta > 0$ will always simply be written as $O(m/Q)$ or $O(m/k_T)$, regardless of the power β .

To summarize, the symbol $D^{(n, d_r)}(z, z\mathbf{k}_T; \mu_Q, Q^2)$ is the approximation to an individual TMD ff wherein it is calculated in fixed order collinear perturbation theory, optimized to the region $k_T \approx Q$ and $Q \rightarrow \infty$, and using d_r collinear fragmentation functions. The fixed order perturbative expression for $D^{(n, d_r)}(z, z\mathbf{k}_T; \mu_Q, Q^2)$ in collinear factorization has the form

$$D^{(n, d_r)}(z, z\mathbf{k}_T; \mu_Q, Q^2) = \left[\mathcal{C}_D^{(n)}(z\mathbf{k}_T) \otimes d_r \right](z; \mu_Q). \quad (25)$$

The “ \otimes ” here symbolizes the usual collinear convolution integral,

$$(f \otimes g)(z; \mu) \equiv \int_z^1 \frac{d\xi}{\xi} f(z/\xi) g(\xi; \mu). \quad (26)$$

In Eq. (25), $\mathcal{C}_D^{(n)}(z\mathbf{k}_T)$ is a hard coefficient. We have written its $z\mathbf{k}_T$ argument explicitly as a reminder that this particular hard factor has k_T -dependence. Approximations to $D(z, z\mathbf{k}_T; \mu_Q, Q^2)$ appropriate to regions other than $k_T \approx Q$ will be left unaddressed for now. They will be discussed in Sec. V.

The TMD ff is related to a collinear ff by an integral over transverse momentum,

$$2\pi z^2 \int_0^{\mu_Q} dk_T k_T D(z, z\mathbf{k}_T; \mu_Q, Q^2) = d_r(z; \mu_Q) + \Delta^{(n, d_r)}(\alpha_s(\mu_Q)) + O\left(\frac{m}{Q}, \alpha_s(\mu_Q)^{n+1}\right), \quad (27)$$

with the details of the notation to be explained below. In a literal probability density interpretation, μ_Q would

be set equal to infinity and the second two terms on the right-hand side would be zero. In a renormalizable theory like QCD, the integral needs to be regulated, and corrections are necessary to relate the cutoff integral to collinear ffs defined in standard schemes. The $\Delta^{(n, d_r)}(\alpha_s(\mu_Q))$ term on the right-hand side of Eq. (27) is our notation for the perturbative correction through n^{th} -order that relates the cutoff integral to the collinear ff $d_r(z; \mu_Q)$ in scheme r . There are also, in general, power-suppressed corrections, as indicated by the error term in Eq. (27). The correction term $\Delta^{(n, d_r)}(\alpha_s(\mu_Q))$ is related to collinear ffs via another factorization theorem,

$$\Delta^{(n, d_r)}(\alpha_s(\mu_Q)) = \left[\mathcal{C}_\Delta^{(n)} \otimes d_r \right](z; \mu_Q). \quad (28)$$

and $\mathcal{C}_\Delta^{(n)}$ is an order- $\alpha_s(\mu_Q)^n$ hard coefficient, with a Δ subscript included here to distinguish it from the k_T -dependent hard coefficient in Eq. (25). The “ (n, d_r) ” superscript in $\Delta^{(n, d_r)}(\alpha_s(\mu_Q))$ is to symbolize that Eq. (28) is to be calculated through order $\alpha_s(\mu_Q)^n$, and that the collinear ff is defined in the r renormalization and/or regularization scheme. Note that $\Delta^{(n, d_r)}(\alpha_s(\mu_Q))$ is also a function of z and Q , but we have dropped explicit dependence on those variables to maintain as compact a notation as possible. We also define

$$\Delta^{(n, d_r)}(\alpha_s(\mu_Q)) \equiv 0 \quad \forall \quad n < 1. \quad (29)$$

To make the above more explicit, let us *define* a new collinear ff that is the transverse momentum integral of a TMD ff regulated with a cutoff on all $k_T > \mu_Q$:

$$d_c(z; \mu_Q) \equiv 2\pi z^2 \int_0^{\mu_Q} dk_T k_T D(z, z\mathbf{k}_T; \mu_Q, Q^2). \quad (30)$$

The $r = c$ subscript on the left indicates that this is an ff defined in the “cutoff” scheme.² Equation (30) is just the left side of Eq. (27). Dropping the power-suppressed and order- $\alpha_s^{n+1}(\mu_Q)$ terms on the right side of Eq. (27) gives an equation that is satisfied only approximately. To give this a notation, we also define

$$d_c^{(n, d_r)}(z; \mu_Q) \equiv d_r(z; \mu_Q) + \Delta^{(n, d_r)}(\alpha_s(\mu_Q)). \quad (31)$$

Then, Eq. (27) is

$$d_c^{(n, d_r)}(z; \mu_Q) - d_c(z; \mu_Q) = O\left(\frac{m}{Q}, \alpha_s(\mu_Q)^{n+1}\right), \quad (32)$$

If the scheme for dealing with UV transverse momentum divergences is the cutoff scheme itself, $r = c$, then

$$\Delta^{(n, d_c)}(\alpha_s(\mu_Q)) = 0 \quad (33)$$

² For the renormalization of the TMD ff in the integrand of Eq. (30), it is to be understood that the scheme is a standard one like $\overline{\text{MS}}$.

exactly by definition. If the scheme is modified minimal subtraction, $r = \overline{\text{MS}}$, then

$$\Delta^{(n, d_{\overline{\text{MS}}})}(\alpha_s(\mu_Q)) = \frac{\alpha_s(\mu_Q)}{2\pi} \times \int_z^1 \frac{dz'}{z'} d_{\overline{\text{MS}}}(z/z'; \mu_Q) [2P_{qq}(z') \ln z' + C_F(1 - z')] + O(\alpha_s(\mu_Q)^2), \quad (34)$$

where we have used the standard splitting function notation

$$P_{qq}(z) = P_{q\bar{q}}(z) = C_F \left[\frac{1+z^2}{(1-z)_+} + \frac{3}{2} \delta(1-z) \right]. \quad (35)$$

The quantities in Eqs. (23)–(32) are so far intended to be exact. That is, $D(z, z\mathbf{k}_T; \mu_Q, Q^2)$, $d_r(z; \mu_Q)$, etc are the operator definitions.

Equation (30) is a version of Eq. (3) wherein the collinear ff $d_c(z; \mu_Q)$ is defined such that the integral relation is satisfied exactly when the UV divergent integral is regulated with a cutoff. A collinear pdf or ff defined in this way does have some practical advantages. It is a natural definition when regions are categorized as perturbative or nonperturbative in transverse momentum space, and it is the preferred definition in some work associated with hadron structure (see, for example, the work of Brodsky and collaborators [85]). It is also a natural definition for matching to fixed order large- q_T calculations, which of course are almost always performed in momentum space. However, it also comes with significant disadvantages as well; see, for example, reference [86] for a discussion of the different ways of handling UV divergences in definitions of collinear pdfs and the pitfalls of each. An important point is that the correction terms relating cut-off scheme and renormalized pdfs are not just perturbative, but include also the power-suppressed errors in Eq. (27).

IV. THE COLLINS-SOPER KERNEL NEAR THE INPUT SCALE Q_0

Up to now, our discussion has mainly focused on establishing context and defining notation. In the bulleted list of Sec. I, we explained that we will explicitly interpolate between nonperturbatively small k_T and perturbatively large k_T in our parametrizations of TMD functions at an input scale. With the language and notation of Sec. II and Sec. III, we are ready to step through the interpolation details.

Inspection of Eq. (20) shows that there are actually two separate types of functions in which we will need to interpolate between nonperturbative parametrizations and perturbative regions of transverse momentum when we do calculations for phenomenology. First, there

are the TMD ffs themselves, $\tilde{D}_A(z_A, \mathbf{b}_T; \mu_{Q_0}, Q_0^2)$ and $\tilde{D}_B(z_B, \mathbf{b}_T; \mu_{Q_0}, Q_0^2)$, at the input scale Q_0 . Second, there is the CS kernel $\tilde{K}(\mathbf{b}_T; \mu_{Q_0})$, also at the input scale Q_0 , which will be necessary for evolving away from $Q = Q_0$.

Between these two, it is actually the CS kernel that is the simpler to handle, so we will begin by focusing on it. In fact, the steps for interpolating a full parametrization of an input TMD ff $D(z, z\mathbf{k}_T; \mu_{Q_0}, Q_0^2)$ between large and small k_T will turn out to be very analogous to what we do for the CS kernel.

It is straightforward to calculate $K(k_T; \mu_{Q_0})$ in fixed order perturbative theory if $k_T \approx Q_0$. Using notation analogous to that of Sec. III, we express this as

$$K(k_T; \mu_{Q_0}) = K^{(n)}(k_T; \mu_{Q_0}) + O\left(\alpha_s(\mu_{Q_0})^{n+1}, \frac{m}{k_T}\right). \quad (36)$$

$K^{(n)}(k_T; \mu_{Q_0})$ is our notation for the fixed order perturbative calculation through order n and with all nonperturbative effects ignored. It takes the form

$$K^{(n)}(k_T; \mu_{Q_0}) = \frac{1}{k_T^2} \kappa\left(\alpha_s(\mu_{Q_0}), \frac{k_T}{\mu_{Q_0}}\right), \quad (37)$$

where κ is a function of $\alpha_s(\mu_{Q_0})$ and logarithms involving k_T/μ_{Q_0} . For example, in $\overline{\text{MS}}$ renormalization it is

$$K^{(1)}(k_T; \mu_{Q_0}) = \frac{\alpha_s(\mu_{Q_0}) C_F}{\pi^2} \frac{1}{k_T^2}. \quad (38)$$

Away from $k_T \approx \mu_{Q_0}$, the accuracy of $K^{(n)}(k_T; \mu_{Q_0})$ as an approximation to $K(k_T; \mu_{Q_0})$ degrades. The reason for $k_T < \mu_{Q_0}$ is simply that the k_T -dependence of the zero momentum soft radiation is nonperturbative. Conversely, the reason for the approximation failing at $k_T \gg Q_0$ is that the error terms in Eq. (36) include logarithms of k_T/μ_{Q_0} that diverge in the large k_T/μ_{Q_0} limit.

The $k_T \gg Q_0$ contribution is numerically unimportant in Eq. (21) or Eq. (22) because the region of transverse momenta far above Q_0 is suppressed at the input scale (for reasonable fixed values of z_A and z_B). With regard to $Q \approx Q_0$ cross sections, therefore, a suitable parametrization of $K(k_T; \mu_{Q_0})$ only requires that we deal with the region $0 < k_T \lesssim Q_0$. That is to say, near the input scale we only need to extend the perturbative $k_T \approx Q_0$ treatment in $K^{(n)}(k_T; \mu_{Q_0})$ downward into the nonperturbative $k_T < \mu_{Q_0}$ region in order to have a parametrization of $K(k_T; \mu_{Q_0})$ that is useful for all k_T accessible at the input scale. Let us therefore start by defining an “input” parametrization for $K^{(n)}(k_T; \mu_{Q_0})$ that equals the fixed order calculation, Eq. (38), when $k_T \approx \mu_{Q_0}$ or larger, but interpolates to a nonperturbative parametrization for $k_T < \mu_{Q_0}$.

$$K_{\text{input}}^{(n)}(\mathbf{k}_T; \mu_{Q_0}) \equiv \begin{cases} K^{(n)}(\mathbf{k}_T; \mu_{Q_0}) & \text{if } k_T \gtrsim \mu_{Q_0}, \\ \text{nonperturbative parametrization} & \text{otherwise} \end{cases}. \quad (39)$$

Now the “(n)” superscript on the left side of this equation refers to the perturbative order of the large k_T tail in this input nonperturbative parametrization. When we work with Eq. (20), we will need its coordinate space version of the CS kernel,

$$\tilde{K}_{\text{input}}^{(n)}(b_T; \mu_{Q_0}) \equiv \int d^2 \mathbf{k}_T e^{i \mathbf{k}_T \mathbf{b}_T} K_{\text{input}}^{(n)}(k_T; \mu_{Q_0}). \quad (40)$$

The scale-dependence of the exact \tilde{K} is exactly b_T -independent by the RG equation Eq. (18), so we will enforce the condition that an n^{th} -order parametrization satisfies Eq. (18) to order $\alpha_s(\mu)^n$, with only $O(\alpha_s(\mu)^{n+1})$ errors,

$$\frac{d\tilde{K}_{\text{input}}^{(n)}(b_T; \mu)}{d \ln \mu} = -\gamma_K^{(n)}(\alpha_s(\mu)) + O(\alpha_s(\mu)^{n+1}). \quad (41)$$

In Sec. VII A we will provide an example of a specific trial functional form for Eq. (39). In general, however, any phenomenologically successful parametrization that satisfies Eq. (39) and Eq. (41) is allowed. The parametrizations in Eq. (39) and Eq. (40) are appropriate specifically when $Q \approx Q_0$ such that only the region of $0 < k_T \lesssim Q_0$ is important.

However, it is a poor approximation to the true $\tilde{K}(b_T; \mu_{Q_0})$ in the $k_T \gg Q_0$ region, and this matters if we evolve to large enough Q for contributions from $k_T \gg Q_0$ to become significant. In Eq. (40), the large errors manifest themselves as higher order terms logarithmic in $b_T \mu_{Q_0}$, which diverge in the $b_T \rightarrow 0$ limit. There needs to be a change in renormalization scale. Thus, in coordinate space the more common choice for the RG scale is $\mu = C_1/b_T$, with C_1 being an order unity proportionality constant. The truncated RG improved perturbation theory then increases in accuracy as $b_T \rightarrow 0$.

To obtain a $K(\mathbf{k}_T; \mu_{Q_0})$ parametrization that works well for all Q , we need steps that combine the stability of fixed scale calculations in the $Q \approx Q_0$, $k_T \approx Q_0$ region with the RG-improved calculations that optimize for the $b_T \rightarrow 0$ limit. Specifically, we need to perform a scale transformation on the above parametrization using the RG equation at a b_T somewhat below $1/Q_0$. If we implement this scale transformation at small enough b_T , it will have a negligible effect on phenomenology that uses the above parametrization near $Q \approx Q_0$ where the $b_T \ll 1/Q_0$ is strongly suppressed. Therefore, fits that use Eq. (39) will be largely unaffected. And, if the transformation takes place in a range of b_T at least comparable to $\lesssim 1/Q_0$, then its overall effect will only appear at order $n+1$ or higher, so the effect of the transformation

will always be one order higher in perturbation theory than the working order. So, the transformation will ensure an accurate treatment of evolution to large Q in any subsequent steps. We will show how this works in detail below.

The first step in implementing the scale transformation is to define a b_T -dependent mass scale, which we will call $\bar{Q}_0(b_T)$, that smoothly transitions between Q_0 and a $1/b_T$ -dependence in the region just below $b_T \approx 1/Q_0$. Specifically,

$$\bar{Q}_0(b_T) = \begin{cases} C_1/b_T & b_T \ll C_1/Q_0, \\ Q_0 & \text{otherwise,} \end{cases} \quad (42)$$

where C_1 is an order unity numerical constant, typically taken to be $C_1 = 2e^{-\gamma_E}$. When b_T is comparable to C_1/Q_0 , the scales Q_0 and C_1/b_T are numerically similar, so any sensitivity to the difference between the two scale is a higher order effect that can be reduced by including higher orders in perturbation theory. Therefore, the exact form of $\bar{Q}_0(b_T)$ is arbitrary so long as it provides a reasonably smooth interpolation between the Q_0 and C_1/b_T behavior at large and small b_T . Some example suggestions for $\bar{Q}_0(b_T)$, which we will call the transformation function, are shown in Appendix C.

Next, we need to combine this with the RG equation Eq. (18), whose exact solution is

$$\tilde{K}(b_T; \mu) = \tilde{K}(b_T; \mu_i) - \int_{\mu_i}^{\mu} \frac{d\mu'}{\mu'} \gamma_K(\alpha_s(\mu')). \quad (43)$$

Here, μ_i is an arbitrary initial scale. To make it useful in applications of Eq. (20), let us evolve from an initial scale $\mu_i = \mu_{\bar{Q}_0}$ (where $\mu_{\bar{Q}_0} = C_2 \bar{Q}_0$) so that the right side contains $\tilde{K}(b_T; \mu_{\bar{Q}_0})$:

$$\tilde{K}(b_T; \mu) = \tilde{K}(b_T; \mu_{\bar{Q}_0}) - \int_{\mu_{\bar{Q}_0}}^{\mu} \frac{d\mu'}{\mu'} \gamma_K(\alpha_s(\mu')). \quad (44)$$

For any $\mu \approx Q_0$, the second term in Eq. (44) is calculable in perturbation theory with the n^{th} -order anomalous dimension, $\gamma_K(\alpha_s(\mu')) \rightarrow \gamma_K^{(n)}(\alpha_s(\mu'))$, and it vanishes for $b_T \approx C_1/Q_0$ or larger.

The original parametrization in Eq. (40) was designed to provide an accurate perturbative description of $\tilde{K}(b_T; \mu_{Q_0})$ in the region of $b_T \approx 1/Q_0$ and larger. Now if we replace the first term on the right side of Eq. (44) with $\tilde{K}_{\text{input}}^{(n)}(b_T; \mu_{\bar{Q}_0})$, it continues to describe the $b_T \gtrsim 1/Q_0$ region, by our construction of $\bar{Q}_0(b_T)$. However, now the RG-improved perturbative contribution to

$\tilde{K}(b_T; \mu_{\overline{Q}_0})$ also remains accurate into the $b_T \ll 1/Q_0$ region.

Therefore, we obtain an optimal parametrization by replacing the exact $\tilde{K}(b_T; \mu_{\overline{Q}_0})$ on the right side of Eq. (44) by the approximate $\tilde{K}_{\text{input}}^{(n)}(b_T; \mu_{\overline{Q}_0})$ and the exact $\gamma_K(\alpha_s(\mu'))$ by $\gamma_K^{(n)}(\alpha_s(\mu'))$. We define this as

$$\begin{aligned} \underline{\tilde{K}}^{(n)}(b_T; \mu) \\ \equiv \tilde{K}_{\text{input}}^{(n)}(b_T; \mu_{\overline{Q}_0}) - \int_{\mu_{\overline{Q}_0}}^{\mu} \frac{d\mu'}{\mu'} \gamma_K^{(n)}(\alpha_s(\mu')). \end{aligned} \quad (45)$$

The underline on $\underline{\tilde{K}}^{(n)}(b_T; \mu)$ is our notation for the final parametrization to be used with evolution. The above applies to the cases where $\mu \approx Q_0$, so as a final step we set $\mu = \mu_{Q_0}$ and write the underlined parametrization as

$$\begin{aligned} \underline{\tilde{K}}^{(n)}(b_T; \mu_{Q_0}) \\ \equiv \tilde{K}_{\text{input}}^{(n)}(b_T; \mu_{\overline{Q}_0}) - \int_{\mu_{\overline{Q}_0}}^{\mu_{Q_0}} \frac{d\mu'}{\mu'} \gamma_K^{(n)}(\alpha_s(\mu')). \end{aligned} \quad (46)$$

This is the form of the parametrization for the CS kernel that we will ultimately use in Eq. (20). The errors in $\underline{\tilde{K}}^{(n)}(b_T; \mu_{Q_0})$, as an approximation to $\tilde{K}(b_T; \mu_{Q_0})$, are suppressed by at least $\alpha_s(\mu_{Q_0})^{n+1}$ point-by-point for all b_T .

A final constraint on parametrizations of $K_{\text{input}}^{(n)}(\mathbf{k}_T; \mu_{Q_0})$ is obtained by recalling that soft gluon effects cancel in collinear factorization when we integrate over all transverse momentum. Thus, after an integration of $K_{\text{input}}^{(n)}(\mathbf{k}_T; \mu_{Q_0})$ over \mathbf{k}_T up to a cutoff k_{max} of order μ_{Q_0} , sensitivity to any nonperturbative mass parameters must vanish as $m/\mu_{Q_0} \rightarrow 0$. We may express this by demanding that

$$\begin{aligned} \pi \int_0^{k_{\text{max}}^2} dk_T^2 K_{\text{input}}^{(n)}(\mathbf{k}_T; \mu_{Q_0}) \\ = \chi^{(n)}(k_{\text{max}}/\mu_{Q_0}, \alpha_s(\mu_{Q_0})) + O\left(\frac{m}{\mu_{Q_0}}, \frac{m}{k_{\text{max}}}\right), \end{aligned} \quad (47)$$

where $\chi^{(n)}(k_{\text{max}}/\mu, \alpha_s(\mu))$ is either zero or a perturbatively calculable function, independent of any nonperturbative mass parameters in $K_{\text{input}}^{(n)}(\mathbf{k}_T; \mu_{Q_0})$.

Before continuing, let us summarize the basic properties of the parametrization, $\underline{\tilde{K}}^{(n)}(b_T; \mu_{Q_0})$:

- For $b_T \approx 1/Q_0$ or larger, it differs negligibly from $\tilde{K}_{\text{input}}^{(n)}(b_T; \mu_{Q_0})$, by construction. Therefore, both $\underline{\tilde{K}}^{(n)}(b_T; \mu_{Q_0})$ and $\tilde{K}_{\text{input}}^{(n)}(b_T; \mu_{Q_0})$ are equally appropriate for describing the $Q \approx Q_0$ region phenomenologically.
- For small b_T , the RG scale transitions to the usual $\mu \sim 1/b_T$ RG-improved form, but only when b_T is very small relative to the input scale, $b_T \ll 1/Q_0$.

- The parametrization in Eq. (45) obeys an exact RG equation,

$$\frac{d\underline{\tilde{K}}^{(n)}(b_T; \mu)}{d \ln \mu} = -\gamma_K^{(n)}(\alpha_s(\mu)), \quad (48)$$

with no error terms present.

- By contrast, the “input” parametrization defined in Eqs. (39)–(41) obeys the approximate RG equation in Eq. (41) with possible perturbative error terms, as shown in the equation.
- Both Eq. (41) and Eq. (48) are satisfied for all b_T .

The resulting $\underline{\tilde{K}}^{(n)}(b_T; \mu_{Q_0})$ is an accurate representation of the exact $\tilde{K}(b_T; \mu_{Q_0})$ up to at most (non-logarithmic) order $\alpha_s(\mu_{Q_0})^{n+1}$ errors.

There is an ambiguity in the exact choice of functional form for $\overline{Q}_0(b_T)$ in Eq. (42) in the region of $b_T \approx 1/Q_0$, but this is just the usual scale uncertainty that appears in any truncated perturbation theory, akin to the dependence on the exact numerical choices for C_1 and C_2 . Since Q_0 and C_1/b_T are of similar size when $b_T \approx 1/Q_0$ the effect of the transformation is under perturbative control and the ambiguity diminishes as one incorporates higher orders.

To state this more explicitly, consider a family of different choices for $\overline{Q}_0(b_T)$ smoothly connected by an extra parameter a :

$$\overline{Q}_0(b_T) \rightarrow \overline{Q}_0(b_T, a). \quad (49)$$

The only requirement is that Eq. (49) satisfies Eq. (42) for all the a one might consider. Then,

$$\begin{aligned} \frac{d}{da} \underline{\tilde{K}}^{(n)}(b_T; \mu) &= \frac{1}{\mu_{\overline{Q}_0}} \frac{d\mu_{\overline{Q}_0}}{da} \frac{d}{d \ln \mu_{\overline{Q}_0}} \underline{\tilde{K}}^{(n)}(b_T; \mu) \\ &= \frac{1}{\mu_{\overline{Q}_0}} \frac{d\mu_{\overline{Q}_0}}{da} \left[\frac{d}{d \ln \mu_{\overline{Q}_0}} \tilde{K}_{\text{input}}^{(n)}(b_T; \mu_{\overline{Q}_0}) + \gamma_K(\alpha_s(\mu_{\overline{Q}_0})) \right] \\ &\sim \frac{1}{\mu_{\overline{Q}_0}} \frac{d\mu_{\overline{Q}_0}}{da} \alpha_s(\mu_{\overline{Q}_0})^{n+1} \ln^{(n+1)}(b_T \mu_{\overline{Q}_0}). \end{aligned} \quad (50)$$

In the second line, we have substituted Eq. (45) and in the last line we have used Eq. (41) while noting that at small b_T the suppressed errors are enhanced by terms logarithmic in $b_T \mu_{\overline{Q}_0}$. However, by construction $\frac{1}{\mu_{\overline{Q}_0}} \frac{d\mu_{\overline{Q}_0}}{da}$ is only allowed to be nonzero in a region of b_T where $1/b_T$, Q_0 , and \overline{Q}_0 are all of comparable size. So Eq. (50) is just

$$\frac{d}{da} \underline{\tilde{K}}^{(n)}(b_T; \mu) = O(\alpha_s(\mu_{Q_0})^{n+1}), \quad (51)$$

So effects from varying the precise choice of transition function $\overline{Q}_0(b_T)$ are always one order higher in $\alpha_s(Q_0)$ than the working order n .

We will illustrate the steps above more concretely with specific examples in Sec. VII A.

V. PARAMETRIZATION OF THE TMD FFs AT $Q = Q_0$

Now we turn to the parametrizations of the input TMD ffs themselves. Following the strategy outlined in the introduction, we will categorize regions as perturbative or nonperturbative for the input scale TMD ff in transverse momentum space. The steps will be very analogous to those just described in the previous section for $\tilde{K}(b_T; \mu)$.

$$D_{\text{input}}^{(n,d_r)}(z, z\mathbf{k}_T; \mu_{Q_0}, Q_0^2) \equiv \begin{cases} D^{(n,d_r)}(z, z\mathbf{k}_T; \mu_{Q_0}, Q_0^2) & \text{if } k_T \gtrsim Q_0 \\ \text{nonperturbative parametrization otherwise} \end{cases}. \quad (52)$$

The only condition on the intermediate region between $k_T \ll Q_0$ and $k_T \approx Q_0$ is that it should be reasonably smooth. The input parametrization in Eq. (52) has the coordinate space representation,

$$\begin{aligned} \tilde{D}_{\text{input}}^{(n,d_r)}(z, \mathbf{b}_T; \mu_{Q_0}, Q_0^2) \\ \equiv \int d^2\mathbf{k}_T e^{i\mathbf{k}_T \cdot \mathbf{b}_T} D_{\text{input}}^{(n,d_r)}(z, z\mathbf{k}_T; \mu_{Q_0}, Q_0^2). \end{aligned} \quad (53)$$

We will require that the input coordinate space parametrizations satisfy the evolution equations through n^{th} -order in the evolution kernels, at least for the $b_T \approx 1/Q_0$ region:

$$\begin{aligned} \frac{\partial \ln \tilde{D}_{\text{input}}^{(n,d_r)}(z, \mathbf{b}_T; \mu, Q^2)}{\partial \ln Q} \\ = \tilde{K}_{\text{input}}^{(n)}(b_T; \mu) + O(\alpha_s(\mu)^{n+1}) + O(b_T m), \quad (54) \\ \frac{d \ln \tilde{D}_{\text{input}}^{(n,d_r)}(z, \mathbf{b}_T; \mu, Q^2)}{d \ln \mu} \\ = \gamma^{(n)}(\alpha_s(\mu); Q^2/\mu^2) + O(\alpha_s(\mu)^{n+1}) + O(b_T m). \end{aligned} \quad (55)$$

Usually, these will be satisfied automatically if the parametrization follows Eq. (52). Note the analogy between Eqs. (52)–(55) above and Eqs. (39)–(41) for the CS kernel.

Finally, for the integrated TMD ff to be consistent with the definition in Eq. (30) we must impose it directly on the parametrization,

$$\begin{aligned} 2\pi z^2 \int_0^{\mu_{Q_0}} dk_T k_T D_{\text{input}}^{(n,d_r)}(z, z\mathbf{k}_T; \mu_{Q_0}, Q_0^2) \\ \equiv \underline{d}_c^{(n,d_r)}(z; \mu_{Q_0}). \end{aligned} \quad (56)$$

Here we have introduced new notation and another definition. The underline on $\underline{d}_c^{(n,d_r)}(z; \mu_{Q_0})$ is meant to indicate that this is a specific *parametrization* (one determined by the $D_{\text{input}}^{(n,d_r)}(z, z\mathbf{k}_T; \mu_{Q_0}, Q_0^2)$ parametrization)

As in that case, we will use an “input” subscript to label the TMD ff parametrization that applies phenomenologically at the input scale $Q = Q_0$, and which is to be used in Eq. (22). For $k_T < Q_0$, the input parametrization will be defined to have a mainly nonperturbative transverse momentum dependence while for $k_T \approx Q_0$ or larger it will transition into its n^{th} -order perturbative description, the first term in Eq. (23). Specifically, we define

of the $d_c(z; \mu_{Q_0})$ defined in Eq. (30). In accordance with Eq. (32), it is to have, by its definition, the property that

$$\underline{d}_c^{(n,d_r)}(z; \mu_{Q_0}) = d_c^{(n,d_r)}(z; \mu_{Q_0}) + O\left(\frac{m}{\mu_{Q_0}}\right). \quad (57)$$

The parametrization $\underline{d}_c^{(n,d_r)}(z; \mu_{Q_0})$ is a description of the definition $d_c(z; \mu_{Q_0})$, with an n^{th} -order collinear treatment of the high transverse momentum region. It is simply the $d_c^{(n,d_r)}(z; \mu_{Q_0})$ from Eq. (31), but with account taken of the power-suppressed behavior in Eq. (27) that vanishes as $m/\mu_{Q_0} \rightarrow 0$.

It is worth pausing to review the different types of cut-off collinear ffs that we have introduced so far, given that there are now at least three. First, the version in Eq. (30) with no underlines or superscripts is the exact $d_c(z; \mu_{Q_0})$ that follows from the abstract operator definitions. Second, the $\underline{d}_c^{(n,d_r)}(z; \mu_{Q_0})$ above is a specific parametrization of that definition, with the only requirement being that in the limit of large μ_{Q_0} it reduces to n^{th} -order collinear perturbation theory in terms of renormalized ffs with scheme r . Finally, there is the $d_c^{(n,d_r)}(z; \mu_{Q_0})$ defined in Eq. (31), which is just the limit of $\underline{d}_c^{(n,d_r)}(z; \mu_{Q_0})$ where power-suppressed terms are dropped. An equally valid definition is

$$\underline{d}_c^{(n,d_r)}(z; \mu_{Q_0}) \equiv \lim_{\mu_{Q_0} \rightarrow 0} d_c^{(n,d_r)}(z; \mu_{Q_0}). \quad (58)$$

Because Eq. (56) is just a definition, it contains no constraint by itself. The constraint is in Eq. (57).

So far, the steps for constructing the TMD ff parametrizations are very analogous to those of Sec. IV for $K(k_T; \mu_{Q_0})$, but there are some differences. The most significant is that the “perturbative” large k_T part of Eq. (52) is not *entirely* perturbative because it involves non-perturbative collinear ffs as input in Eq. (25). The perturbative contribution to large transverse momentum dependence only enters in the coefficient func-

tion $C_D^{(n)}(zk_T)$. By contrast, the only input to the perturbative calculation in Eq. (37) is the strong coupling α_s .

The conditions in Eqs. (52)–(56) are all that we need for constructing phenomenologically useful parametrizations in the $Q \approx Q_0$ region. Any model or parametrization that satisfies them is acceptable, but we will give some explicit examples in later sections.

However, the perturbative part of the parametrization in Eq. (52) does not provide an accurate description in the region of $k_T \gg Q_0$, where ratios of k_T and Q_0 diverge. In coordinate space, the same issue arises at $b_T \ll 1/Q_0$ in the form of large logarithms of μb_T . That does not create a problem for phenomenological applications near $Q \approx Q_0$ where the $k_T \gg Q_0$ contributions are suppressed in the integral of Eq. (21). However, it becomes impor-

tant as one evolves to $Q \gg Q_0$ and the $k_T \gg Q_0$ region starts to contribute more significantly.

Therefore, there needs to be a scale transformation from $\mu = \mu_{Q_0}$ to $\mu = C_1/b_T$ in the coordinate space TMD ff in the region of b_T just below $b_T \approx 1/Q_0$. This of course is exactly the same issue that we faced in the case of $\tilde{K}_{\text{input}}^{(n)}(b_T; \mu_{Q_0})$ in the previous section. For the TMD ff, it also implies that we have to evolve the CS scale $\sqrt{\zeta}$ from Q_0 to C_1/b_T . For the scale change we can reuse the same scale transformation function from Eq. (42).

The exact solution to the TMD evolution equations for an individual TMD ff evolving from scales μ_i, Q_i to μ_{Q_0}, Q_0 is

$$\tilde{D}(z, \mathbf{b}_T; \mu_{Q_0}, Q_0^2) = \tilde{D}(z, \mathbf{b}_T; \mu_i, Q_i^2) \exp \left\{ \int_{\mu_i}^{\mu_{Q_0}} \frac{d\mu'}{\mu'} \left[\gamma(\alpha_s(\mu'); 1) - \ln \frac{Q_0}{\mu'} \gamma_K(\alpha_s(\mu')) \right] + \ln \frac{Q_0}{Q_i} \tilde{K}(b_T; \mu_i) \right\}. \quad (59)$$

Or, if we use $\mu_i = \mu_{\bar{Q}_0}$, $Q_i = \bar{Q}_0$ for the input scale,

$$\tilde{D}(z, \mathbf{b}_T; \mu_{Q_0}, Q_0^2) = \tilde{D}(z, \mathbf{b}_T; \mu_{\bar{Q}_0}, \bar{Q}_0^2) \exp \left\{ \int_{\mu_{\bar{Q}_0}}^{\mu_{Q_0}} \frac{d\mu'}{\mu'} \left[\gamma(\alpha_s(\mu'); 1) - \ln \frac{Q_0}{\mu'} \gamma_K(\alpha_s(\mu')) \right] + \ln \frac{Q_0}{\bar{Q}_0} \tilde{K}(b_T; \mu_{\bar{Q}_0}) \right\}. \quad (60)$$

As of yet, there are still no approximations on $\tilde{D}(z, \mathbf{b}_T; \mu_{Q_0}, Q_0^2)$. The left side has no dependence on \bar{Q}_0 ; any \bar{Q}_0 -dependence in $\tilde{D}(z, \mathbf{b}_T; \mu_{\bar{Q}_0}, \bar{Q}_0^2)$ is exactly canceled by an opposite \bar{Q}_0 -dependence in the exponential factor.

Now we can substitute approximations into the right side of Eq. (60) in a way that is again very analogous to the way we handled $\tilde{K}(b_T; \mu)$ in the previous section by making substitutions on the right side of Eq. (44). We approximate $\tilde{D}(z, \mathbf{b}_T; \mu_{\bar{Q}_0}, \bar{Q}_0^2)$ on the right side of Eq. (60) by replacing it with the $D_{\text{input}}^{(n, d_r)}(z, z\mathbf{k}_T; \mu_{\bar{Q}_0}, \mu_{\bar{Q}_0}^2)$ from

Eq. (52). Because of the scale transformation, the result is a parametrization of $\tilde{D}(z, \mathbf{b}_T; \mu_{\bar{Q}_0}, \bar{Q}_0^2)$ that is an accurate description not only for $b_T \approx 1/Q_0$ and larger but also for all $b_T \ll 1/Q_0$. For the $\tilde{K}(b_T; \mu_{\bar{Q}_0})$ in the exponent on the right side of Eq. (60), we already have the analogous result from Eq. (46) in Sec. IV, and we can reuse it here. All that remains then is to substitute $\gamma(\alpha_s(\mu'); 1)$ and $\gamma_K(\alpha_s(\mu'))$ by their truncated n^{th} -order perturbation theory approximations. Thus, our final parametrization of the input TMD ff is

$$\begin{aligned} & \underline{\tilde{D}}^{(n, d_r)}(z, \mathbf{b}_T; \mu_{Q_0}, Q_0^2) \\ &= \underline{\tilde{D}}_{\text{input}}^{(n, d_r)}(z, \mathbf{b}_T; \mu_{\bar{Q}_0}, \bar{Q}_0^2) \exp \left\{ \int_{\mu_{\bar{Q}_0}}^{\mu_{Q_0}} \frac{d\mu'}{\mu'} \left[\gamma^{(n)}(\alpha_s(\mu'); 1) - \ln \frac{Q_0}{\mu'} \gamma_K^{(n)}(\alpha_s(\mu')) \right] + \ln \frac{Q_0}{\bar{Q}_0} \tilde{K}_{\text{input}}^{(n)}(b_T; \mu_{\bar{Q}_0}) \right\}. \end{aligned} \quad (61)$$

The underline on $\underline{\tilde{D}}^{(n, d_r)}(z, \mathbf{b}_T; \mu_{Q_0}, Q_0^2)$ is our notation for the final parametrization of the TMD ff at the input scale $\mu = \mu_{Q_0}$, $\zeta = Q_0^2$.

To summarize, $\underline{\tilde{D}}(z, \mathbf{b}_T; \mu_{Q_0}, Q_0^2)$ has the following

properties:

- Each factor in Eq. (61) is an accurate approximation to the corresponding factor in the exact Eq. (60) point-by-point in b_T .

- For $b_T \approx 1/Q_0$ or larger, the exponential evolution factor deviates from unity by a negligible amount. This is by our construction of $\bar{Q}_0(b_T)$. $\tilde{D}^{(n,d_r)}(z, \mathbf{b}_T; \mu_{Q_0}, Q_0^2)$ therefore deviates negligibly from $\tilde{D}_{\text{input}}^{(n,d_r)}(z, \mathbf{b}_T; \mu_{Q_0}, Q_0^2)$ when $Q \approx Q_0$. Both $\tilde{D}^{(n,d_r)}(z, \mathbf{b}_T; \mu_{Q_0}, Q_0^2)$ and $\tilde{D}_{\text{input}}^{(n,d_r)}(z, \mathbf{b}_T; \mu_{Q_0}, Q_0^2)$ with Eq. (22) are equally appropriate for applications to phenomenology when $Q \approx Q_0$. Also, recall that the $\tilde{D}_{\text{input}}^{(n,d_r)}(z, \mathbf{b}_T; \mu_{Q_0}, Q_0^2)$ was originally formulated in transverse momentum space.
- There is a smooth scale transformation to $\mu \sim \sqrt{\zeta} \sim 1/b_T$ at small b_T , but only when $b_T \ll 1/Q_0$. Therefore, $\tilde{D}^{(n,d_r)}(z, \mathbf{b}_T; \mu_{Q_0}, Q_0^2)$ continues to provide an accurate approximation to the exact TMD ff after $Q \gg Q_0$ where the $b_T \ll 1/Q_0$ region starts to be relevant.
- Thus, at small b_T we may express the TMD ff in terms of collinear ffs d_r using the usual OPE methods.
- $\tilde{D}^{(n,d_r)}(z, \mathbf{b}_T; \mu_{Q_0}, Q_0^2)$ satisfies the exact evolution equations

$$\frac{\partial \ln \tilde{D}^{(n,d_r)}(z, \mathbf{b}_T; \mu_{Q_0}, Q_0^2)}{\partial \ln Q_0} = \tilde{K}^{(n)}(b_T; \mu_{Q_0}), \quad (62)$$

$$\begin{aligned} \frac{d \ln \tilde{D}^{(n,d_r)}(z, \mathbf{b}_T; \mu_{Q_0}, Q_0^2)}{d \ln \mu_{Q_0}} &= \gamma^{(n)}(\alpha_s(\mu_{Q_0}); 1) \\ &\quad - \gamma_K^{(n)}(\alpha_s(\mu_{Q_0})) \ln \left(\frac{Q_0}{\mu_{Q_0}} \right). \end{aligned} \quad (63)$$

There are no error terms in either of these equations, and both Eq. (62) and Eq. (63) are valid for all b_T .

- By contrast, the evolution equations for the “input” subscript TMD ffs in Eqs. (54)–(55) do come with explicit error terms.

As was the case for $\tilde{K}^{(n)}(b_T; \mu_{Q_0})$, sensitivity to the choice of functional form for $\bar{Q}_0(b_T)$ is the standard scale uncertainty in truncated perturbation theory, and it vanishes in the limit that Q_0 is large and/or high enough orders in $\alpha_s(Q_0)$ are included. To see this, we may repeat

steps analogous to those after Eq. (49):

$$\begin{aligned} &\frac{d}{da} \ln \tilde{D}^{(n,d_r)}(z, \mathbf{b}_T; \mu_{Q_0}, Q_0^2) \\ &= \frac{1}{\mu_{\bar{Q}_0}} \frac{d\mu_{\bar{Q}_0}}{da} \frac{d}{d \ln \mu_{\bar{Q}_0}} \ln \tilde{D}^{(n,d_r)}(z, \mathbf{b}_T; \mu_{Q_0}, Q_0^2) \\ &\quad + \frac{1}{\bar{Q}_0} \frac{d\bar{Q}_0}{da} \frac{\partial}{\partial \ln \bar{Q}_0} \ln \tilde{D}^{(n,d_r)}(z, \mathbf{b}_T; \mu_{Q_0}, Q_0^2) \\ &= \frac{1}{\mu_{\bar{Q}_0}} \frac{d\mu_{\bar{Q}_0}}{da} \left[\tilde{K}_{\text{input}}^{(n)}(b_T; \mu_{\bar{Q}_0}) + \gamma^{(n)}(\alpha_s(\mu_{\bar{Q}_0}); 1) \right. \\ &\quad \left. - \tilde{K}_{\text{input}}^{(n)}(b_T; \mu_{\bar{Q}_0}) - \gamma^{(n)}(\alpha_s(\mu_{\bar{Q}_0}); 1) \right. \\ &\quad \left. + O(\alpha_s(\mu_{\bar{Q}_0})^{n+1}) + O(b_T m) \right] \\ &= O(\alpha_s(\mu_{Q_0})^{n+1}) + O\left(\frac{m}{Q_0}\right). \end{aligned} \quad (64)$$

After the second equality, we have substituted the expression for $\tilde{D}^{(n,d_r)}(z, \mathbf{b}_T; \mu_{Q_0}, Q_0^2)$ from Eq. (61) and applied Eqs. (54)–(55) to $\tilde{D}_{\text{input}}^{(n,d_r)}(z, \mathbf{b}_T; \mu_{\bar{Q}_0}, \bar{Q}_0^2)$. We have also used that $\mu_{\bar{Q}_0} = \bar{Q}_0$ when $C_2 = 1$ to simplify expressions. On the last line, we have used the fact that $\frac{1}{\mu_{Q_0}} \frac{d\mu_{Q_0}}{da}$ vanishes by construction everywhere except where $b_T \sim 1/Q_0$.

Thus, sensitivity to the choice of $\bar{Q}_0(b_T)$, at any order n , vanishes as $m/Q_0 \rightarrow 0$.

Since our notation has now grown rather extensive, we remind the reader that it is summarized in Appendix A.

VI. SUMMARY OF STEPS

So far, we have focused on describing $\tilde{D}(z, \mathbf{b}_T; \mu_{Q_0}, Q_0^2)$ only at a fixed input scale Q_0 . Now all that is necessary to calculate $W(q_T, Q)$ at any other scale using $\tilde{D}^{(n,d_r)}(z, \mathbf{b}_T; \mu_{Q_0}, Q_0^2)$ and $\tilde{K}^{(n)}(b_T; \mu_{Q_0})$ is to substitute them into the right side of Eq. (20), along with the n^{th} -order perturbative expressions for $H(\alpha_s(\mu_Q); C_2)$, $\gamma(\alpha_s(\mu'); 1)$, and $\gamma_K(\alpha_s(\mu'))$. The result is an approximation for $W(q_T, Q)$ that includes evolution and is accurate for $Q \geq Q_0$,

$$W^{(n)}(q_T, Q) \equiv H^{(n)}(\alpha_s(\mu_Q); C_2) \int \frac{d^2 \mathbf{b}_T}{(2\pi)^2} e^{-i \mathbf{q}_T \cdot \mathbf{b}_T} \underline{\tilde{D}}_A^{(n, d_r)}(z_A, \mathbf{b}_T; \mu_{Q_0}, Q_0^2) \underline{\tilde{D}}_B^{(n, d_r)}(z_B, \mathbf{b}_T; \mu_{Q_0}, Q_0^2) \\ \times \exp \left\{ \tilde{K}^{(n)}(b_T; \mu_{Q_0}) \ln \left(\frac{Q^2}{Q_0^2} \right) + \int_{\mu_{Q_0}}^{\mu_Q} \frac{d\mu'}{\mu'} \left[2\gamma^{(n)}(\alpha_s(\mu'); 1) - \ln \frac{Q^2}{\mu'^2} \gamma_K^{(n)}(\alpha_s(\mu')) \right] \right\}. \quad (65)$$

The approximation, notated by the “(n)” superscript on $W^{(n)}(q_T, Q)$, is such that the scale dependence given by the evolution equations in Eqs. (17)–(19) is accurate point-by-point for $Q \geq Q_0$ with errors at most of order $O(\alpha_s(Q_0)^{n+1})$ – see Eqs. (62)–(63). When $Q = Q_0$ the $W^{(n)}(Q_0, q_T)$ defined in Eq. (65) reduces to the TMD parton model up to the overall factor of $H^{(n)}(\alpha_s(\mu_Q); C_2)$ and

$$W(q_T, Q_0) - W^{(n)}(q_T, Q_0) \\ = O(\alpha_s(\mu_{Q_0})^{n+1}) + O\left(\frac{m}{Q_0}\right). \quad (66)$$

While it might appear that we have only succeeded at introducing an excessive amount of notation, the end result is a fairly simple recipe for combining any arbitrary model of nonperturbative transverse momentum dependence with full TMD factorization and evolution. After some basic initial decisions like choosing a value for Q_0 and fixing renormalization schemes, the steps are as follows:

A) Model Building

A1: Choose a nonperturbative model, or a nonperturbative technique more generally, to phenomenologically parametrize the small transverse momentum dependence in the TMD $D(z_A, z_A \mathbf{k}_{AT}; \mu_{Q_0}, Q_0^2)$ and in $K(k_T; \mu_{Q_0})$ at the input scale. (See, for example, the list of models in the introduction. These can likely be used here.)

A2: For step A1, make any modifications to the models that are necessary to ensure that they satisfy Eq. (39), Eq. (41), Eq. (47), Eq. (52), and Eqs. (54)–(57). This step mostly amounts to extrapolating existing models to low order perturbative descriptions of $k_T \approx Q_0$ behavior. The result is a set of parametrizations for $\tilde{D}_{\text{input}, A}^{(n, d_r)}(z_A, \mathbf{b}_T; \mu_{Q_0}, Q_0^2)$, $\tilde{D}_{\text{input}, B}^{(n, d_r)}(z_B, \mathbf{b}_T; \mu_{Q_0}, Q_0^2)$, and $\tilde{K}_{\text{input}}^{(n)}(b_T; \mu_{Q_0})$.

A3: Choose a functional form for the $\bar{Q}_0(b_T)$ in Eq. (42) to implement the transition between scales. Use the “input” functions from step A2 to construct $\tilde{K}^{(n)}(b_T; \mu_{Q_0})$ and $\underline{\tilde{D}}^{(n, d_r)}(z, \mathbf{b}_T; \mu_{Q_0}, Q_0^2)$ via Eq. (45) and Eq. (61).

B) Phenomenology at $Q \approx Q_0$

B1: Apply factorization phenomenologically to $Q = Q_0$, Type I processes by taking

$$\underline{\tilde{D}}^{(n, d_r)}(z, \mathbf{b}_T; \mu_{Q_0}, Q_0^2) \rightarrow \tilde{D}_{\text{input}}^{(n, d_r)}(z, \mathbf{b}_T; \mu_{Q_0}, Q_0^2)$$

in Eq. (65). This corresponds to the TMD parton model formula in Eq. (22) with the input function of step A2. Fix any parameters in the nonperturbative model. This step is essentially no different from traditional TMD parton model motivated approaches to describing Type I processes. Thus, prior existing phenomenological results can likely be reused here.

B2: Consider the phenomenological behavior of cross sections in a region of Q around $Q \approx Q_0$. Take

$$\tilde{\underline{D}}^{(n, d_r)}(z, \mathbf{b}_T; \mu_{Q_0}, Q_0^2) \rightarrow \tilde{D}_{\text{input}}^{(n, d_r)}(z, \mathbf{b}_T; \mu_{Q_0}, Q_0^2) \\ \tilde{\underline{K}}^{(n)}(b_T; \mu_{Q_0}) \rightarrow \tilde{K}_{\text{input}}^{(n)}(b_T; \mu_{Q_0})$$

in Eq. (65), and use the resulting formula in phenomenological fits to fix any nonperturbative parameters in $\tilde{K}_{\text{input}}^{(n)}(b_T; \mu_{Q_0})$ in the $Q \approx Q_0$ region.

B3: Verify that the effect of replacing $\tilde{\underline{K}}^{(n)}(b_T; \mu_{Q_0})$ and $\underline{\tilde{D}}^{(n, d_r)}(z, \mathbf{b}_T; \mu_{Q_0}, Q_0^2)$ by $\tilde{K}_{\text{input}}^{(n)}(b_T; \mu_{Q_0})$ and $\tilde{D}_{\text{input}}^{(n, d_r)}(z, \mathbf{b}_T; \mu_{Q_0}, Q_0^2)$ respectively is negligible for numerical calculations around $Q \approx Q_0$.

C) Phenomenology at large Q

C1: Use Eq. (65) to evolve to significantly larger Q and make predictions for Type II observables. Then re-fit and/or tune the nonperturbative parameters and improve the agreement with the higher Q observables. The adjustment of parameters should be expected to be minimal since the larger Q measurements are less sensitive to large b_T .

C2: Continue to repeat step C1 with even higher Q . One should expect the accuracy of predictions to increase, both because of the growing constraints on nonperturbative parameters from previous steps and because larger Q is less sensitive to large b_T and more sensitive to small $\alpha_s(Q)$ perturbative contributions.

It is possible to transform Eq. (65) into a form more familiar from traditional implementations of the CSS formalism. While that is not necessary, and indeed we would

advocate for using Eq. (65) directly, at least for hadron structure applications, there may still be situations where it is desirable. The steps for transforming Eq. (65) into the more familiar form will be explained later in Sec. IX.

We have used the example of SIA and TMD ffs to have a concrete factorization formula for illustration purposes,

$$W^{(n)}(q_T, Q) = H^{(n)}(\alpha_s(\mu_Q); C_2) \int \frac{d^2 \mathbf{b}_T}{(2\pi)^2} e^{-i \mathbf{q}_T \cdot \mathbf{b}_T} \tilde{D}_A^{(n, dr)}(z_A, \mathbf{b}_T; \mu_{\overline{Q}_0}, \overline{Q}_0^2) \tilde{D}_B^{(n, dr)}(z_B, \mathbf{b}_T; \mu_{\overline{Q}_0}, \overline{Q}_0^2) \\ \times \exp \left\{ \tilde{K}^{(n)}(b_T; \mu_{\overline{Q}_0}) \ln \left(\frac{Q^2}{\overline{Q}_0^2} \right) + \int_{\mu_{\overline{Q}_0}}^{\mu_Q} \frac{d\mu'}{\mu'} \left[2\gamma^{(n)}(\alpha_s(\mu'); 1) - \ln \frac{Q^2}{\mu'^2} \gamma_K^{(n)}(\alpha_s(\mu')) \right] \right\} \quad (67)$$

by directly substituting Eq. (46) and Eq. (61) into Eq. (65). Which form to use is a matter of convenience, but each highlights different aspects of evolution at moderate and/or large Q . Equation (65) is written in a way that makes it obvious that TMD factorization exactly follows a TMD parton model description at $Q = Q_0$. That form of $W^{(n)}(q_T, Q)$ also makes it clear that if the TMD ffs and $\tilde{K}(b_T; \mu_{Q_0})$ are known exactly for all b_T at a fixed input scale, the evolution to larger Q becomes technically trivial. Conversely, in Eq. (67) we have been able to eliminate Q_0 entirely from the expression, and the RG improved treatment of the $Q \gg Q_0$ limit is automatic in the $\sim 1/b_T$ scale dependence at small b_T . Indeed, this form is very similar to the standard presentation of the $W^{(n)}(q_T, Q)$, as we will see in Sec. IX.

VII. LOW ORDER EXAMPLES

We mean for the steps in Sec. VI to apply to any model or nonperturbative method of parametrizing the intrinsic transverse momentum, so we have left the nonperturbative parts in Eq. (39) and Eq. (52) completely general. But specific examples make the steps much clearer, so we will illustrate them in this section with very minimalistic models of the nonperturbative intrinsic transverse momentum dependence.

We caution that the nonperturbative parametrizations that we will use below should be regarded only as toy examples at this stage, only to be used for illustration purposes. In future work, we hope to implement the steps in Sec. VI with input from at least some of the more sophisticated models or nonperturbative techniques referenced in the introduction.

Since this section makes much use of the notation we have introduced in earlier sections, we remind the reader once more of our notation glossary Appendix A. We will assume that $\overline{\text{MS}}$ renormalization is used everywhere, and we will always use $Q_0 = 2 \text{ GeV}$ for making example plots.

but everything up to now carries over in obvious ways to TMD pdfs and processes like Drell-Yan scattering. The steps bridge standard approaches to Type I and Type II phenomenology.

Before continuing on to examples, notice that we may rewrite Eq. (65) as

A. CS kernel example

To motivate a simple model for the nonperturbative part of the CS kernel, let us recall the physical effect that a nonzero $\tilde{K}(b_T; \mu_{Q_0})$ has on momentum-space cross sections at small transverse momentum. Consider the CS evolution equation for $W(Q, q_T)$ in transverse momentum space. Fourier-Bessel transforms become transverse momentum convolutions so

$$\frac{\partial}{\partial \ln Q^2} W(Q, \mathbf{q}_T) = \int d^2 \mathbf{k}_T K(\mathbf{k}_T; \mu) W(Q, \mathbf{q}_T - \mathbf{k}_T) + \text{Const.} \times W(Q, \mathbf{q}_T). \quad (68)$$

(See, for example, Eq. (25) of [66].) The partial derivative here indicates that z_A and z_B should be fixed. The “Const.” is independent of transverse momentum and is related to the anomalous dimension γ . It only contributes to a Q -dependent normalization. Our task is to find a reasonable input $K(\mathbf{k}_T; \mu_{Q_0})$ parametrization that satisfies Eq. (39) and also gives a good phenomenological description of cross sections in the region of $Q \approx Q_0$ close to the input scale. One way that $K(\mathbf{k}_T; \mu)$ can contribute to the evolution of $W(Q \approx Q_0, \mathbf{q}_T)$ is simply through a normalization. To capture that behavior in Eq. (68), the model parametrization should include a term proportional to a δ -function,

$$K_{\text{input}}(k_T; \mu_{Q_0}) \propto \delta^{(2)}(\mathbf{k}_T). \quad (69)$$

This is an example of step A1 applied to $K(k_T; \mu_{Q_0})$. But as step A2 prescribes, $K_{\text{input}}(k_T; \mu_{Q_0})$ also needs to match the large k_T perturbative description,

$$K_{\text{input}}(k_T; \mu_{Q_0}) \stackrel{k_T \approx Q_0}{\approx} K^{(1)}(k_T; \mu_{Q_0}), \quad (70)$$

where for now we work at order $n = 1$. We also know that

$$K^{(1)}(k_T; \mu_{Q_0}) = \frac{\alpha_s(\mu_{Q_0}) C_F}{\pi^2} \frac{1}{k_T^2}. \quad (71)$$

(For a textbook derivation of Eq. (71), see section 13.10.2 of [3]. Also see Ref. [87] for earlier calculations. For higher order \tilde{K} expressions, see also [88–91], and see Ref. [38] for translating between different notations. See also [92] for more discussion of the operator definition.)

As k_T decreases below Q_0 , Eq. (70) needs to transition into a nonperturbative eparametrization in a way that is still phenomenologically successful at describing $Q \approx Q_0$ behavior. Existing evidence, both theoretical and phenomenological [73, 74, 93] and from lattice calculations [94], points toward a shape for TMD pdfs and ffs that varies only very weakly with scale in the $Q \approx Q_0$ region. Our trial parametrization will reproduce this behavior if it is fairly sharply peaked around $k_T \ll Q_0$ and then falls off rapidly for larger k_T . Equation (68) with $K^{(1)}(k_T; \mu_{Q_0})$ captures that general behavior if we make the replacement $k_T^2 \rightarrow k_T^2 + m_K^2$ and keep the non-perturbative parameter m_K small relative to Q_0 . Thus, we obtain a reasonable candidate for a $K_{\text{input}}^{(1)}(k_T; \mu_{Q_0})$ parametrization that satisfies Eq. (39) if we combine the $k_T^2 \rightarrow k_T^2 + m_K^2$ modification of Eq. (71) with Eq. (69):

$$K_{\text{input}}^{(1)}(k_T; \mu_{Q_0}) = \frac{\alpha_s(\mu_{Q_0})C_F}{\pi^2} \frac{1}{k_T^2 + m_K^2} + C_K \delta^{(2)}(\mathbf{k}_T). \quad (72)$$

The transformation into coordinate space is

$$\tilde{K}_{\text{input}}^{(1)}(b_T; \mu_{Q_0}) = \frac{2\alpha_s(\mu_{Q_0})C_F}{\pi} K_0(b_T m_K) + C_K. \quad (73)$$

Satisfying both Eq. (41) and Eq. (47) with the $\overline{\text{MS}}$ expression for $\gamma_K^{(1)}$ requires

$$C_K = \frac{2\alpha_s(\mu_{Q_0})C_F}{\pi} \ln\left(\frac{m_K}{\mu_{Q_0}}\right) \quad (74)$$

So the input CS kernel is just the single parameter function

$$\tilde{K}_{\text{input}}^{(1)}(b_T; \mu_{Q_0}) = \frac{2\alpha_s(\mu_{Q_0})C_F}{\pi} \left[K_0(b_T m_K) + \ln\left(\frac{m_K}{\mu_{Q_0}}\right) \right]. \quad (75)$$

Note that the same mass m_K appears in Eq. (74) and the first term of Eq. (75) reproduces the known lowest order coordinate space $\tilde{K}^{(1)}(b_T; \mu_{Q_0})$ in $\overline{\text{MS}}$ at small b_T :

$$\begin{aligned} \lim_{b_T \rightarrow 0} \tilde{K}_{\text{input}}^{(1)}(b_T; \mu_{Q_0}) &= \\ &= -\frac{2\alpha_s(\mu_{Q_0})C_F}{\pi} \left[\ln\left(\frac{b_T \mu_{Q_0} e^{\gamma_E}}{2}\right) + \ln\left(\frac{m_K}{\mu_{Q_0}}\right) \right] + C_K \\ &= -\frac{2\alpha_s(\mu_{Q_0})C_F}{\pi} \ln\left(\frac{b_T \mu_{Q_0} e^{\gamma_E}}{2}\right). \end{aligned} \quad (76)$$

At large b_T , we get the expected (see [66, Sec. VII-A]) constant negative behavior,

$$\lim_{b_T \rightarrow \infty} \tilde{K}_{\text{input}}^{(1)}(b_T; \mu_{Q_0}) = \frac{2\alpha_s(\mu_{Q_0})C_F}{\pi} \ln\left(\frac{m_K}{\mu_{Q_0}}\right). \quad (77)$$

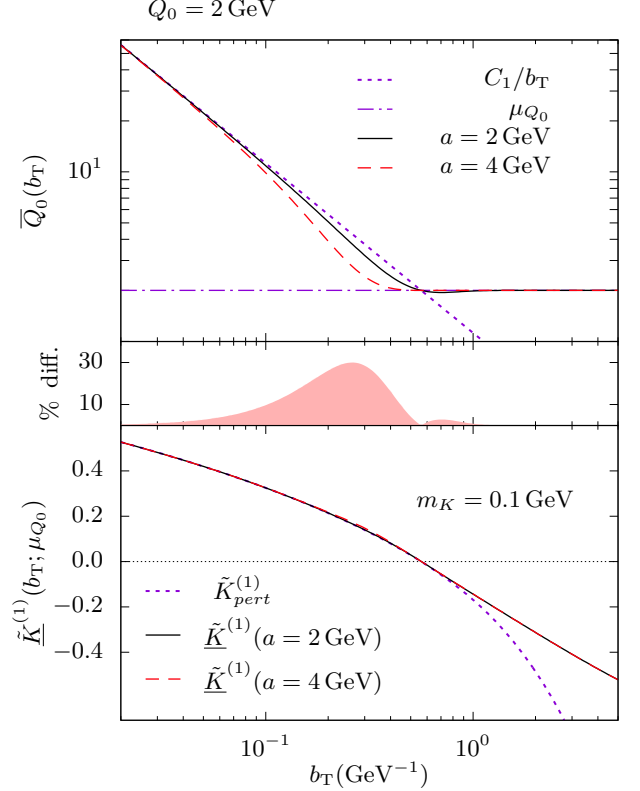


FIG. 2: The example parametrization for $\tilde{K}^{(1)}(b_T; \mu_{Q_0})$ from Eq. (78), obtained after performing the steps A1, A2 and A3 of Sec. VI. The top panel shows two scale transformation functions $\tilde{Q}_0(b_T)$ that satisfy Eq. (42). The choice of functional form is Eq. (C2) from Appendix C, shown for two choices of a (solid black and dashed red curves). For comparison, lines for the scales $\mu_{Q_0} = 2$ GeV (dash-dotted violet) and C_1/b_T (dashed violet) are also shown. The central panel is the percent difference between the $\tilde{Q}_0(b_T)$ obtained from the two values $a = 2$ GeV and $a = 4$ GeV, calculated as the difference divided by the average. The bottom panel is a plot of the actual $\tilde{K}^{(1)}(b_T; \mu_{Q_0})$ parametrization in Eq. (78). The results are shown for both $a = 2$ GeV and $a = 4$ GeV (black solid and red dashed curves), but the difference between the curves is not visible on the graph. The violet dashed curve in the lower plot is a $b_T \rightarrow 0$ purely perturbative calculation, Eq. (80), shown for comparison. See text for details.

This completes steps A1 and A2 insofar as they pertain to the CS kernel.

To get a $\tilde{K}^{(1)}(b_T; \mu_{Q_0})$ that can be extended to calculations of $\tilde{K}(b_T; \mu_{Q_0})$ at $b_T \ll 1/Q_0$, we need to proceed with step A3 and choose a form for the scale transition function $\tilde{Q}_0(b_T)$. For now we will use the form in Eq. (C1) from Appendix C for any numerical calculations and plots. Later, we will demonstrate that the details of this choice do not significantly affect calculations.

Finally, we get $\tilde{K}^{(1)}(b_T; \mu_{Q_0})$ by substituting the trial

$\tilde{K}_{\text{input}}^{(1)}(b_T; \mu_{Q_0})$ from Eq. (75) into Eq. (46),

$$\begin{aligned} \tilde{K}^{(1)}(b_T; \mu_{Q_0}) &= \tilde{K}_{\text{input}}^{(1)}(b_T; \mu_{\bar{Q}_0}) - \int_{\mu_{\bar{Q}_0}}^{\mu_{Q_0}} \frac{d\mu'}{\mu'} \gamma_K^{(1)}(\alpha_s(\mu')) \\ &= \frac{2\alpha_s(\mu_{\bar{Q}_0})C_F}{\pi} \left[K_0(b_T m_K) + \ln \left(\frac{m_K}{\mu_{\bar{Q}_0}} \right) \right] \\ &\quad - \int_{\mu_{\bar{Q}_0}}^{\mu_{Q_0}} \frac{d\mu'}{\mu'} \gamma_K^{(1)}(\alpha_s(\mu')), \end{aligned} \quad (78)$$

Repeating Eq. (50) confirms that variations in the form of $\bar{Q}_0(b_T)$ only enter at order $\alpha_s(\mu_{Q_0})^2$,

$$\begin{aligned} \frac{d}{da} \tilde{K}^{(1)}(b_T; \mu_{Q_0}) &= \frac{1}{\mu_{\bar{Q}_0}} \frac{d\mu_{\bar{Q}_0}}{da} \frac{2\beta(\mu_{\bar{Q}_0})C_F}{\pi} \left[K_0(b_T m_K) + \ln \left(\frac{m_K}{\mu_{\bar{Q}_0}} \right) \right] \\ &= O(\alpha_s(\mu_{Q_0})^2) \end{aligned} \quad (79)$$

for all b_T .

This completes step A3 from Sec. VI, and it completes the model building for the CS kernel with $n = 1$. To determine the phenomenological parameter m_K , one would need to then proceed to the next steps in Sec. VI, in particular B2. But for that, one needs to first construct a model for the TMD ff itself, which we will do in the next subsection.

Before proceeding to that step, it is instructive to examine the trial $\tilde{K}^{(1)}(b_T; \mu_{Q_0})$ graphically, and to verify that the properties described above hold. For example, we expect only a numerically mild, perturbatively suppressed, dependence in $\tilde{K}^{(1)}(b_T; \mu_{Q_0})$ on the scale transformation parameter a in the region between small and large b_T , consistent with Eq. (79). The lower panel of Fig. 2 shows plots of our trial $\tilde{K}^{(1)}(b_T; \mu_{Q_0})$ with $Q_0 = 2$ GeV and $m_K = 0.1$ GeV, while the top panel shows two slightly different functional forms for $\bar{Q}_0(b_T)$ from Eq. (42), as given in Appendix C and Eq. (C2). The two transition functions are generated by using two different values of a , $a = 2$ GeV and $a = 4$ GeV. The narrow central panel shows the % variation between the two $\bar{Q}_0(b_T)$, and it can be seen from the graph that they differ by a maximum of about $\approx 30\%$ for $b_T \approx 0.3$ GeV $^{-1}$, but for b_T much larger or smaller than this the variation vanishes as per our requirements.

The $\tilde{K}^{(1)}(b_T; \mu_{Q_0})$ calculation in the lower panel of Fig. 2 was performed using both of the two $\bar{Q}_0(b_T)$ functions in the top panel. We have plotted them as solid black and dashed-red curves, but the two are visually indistinguishable, confirming the good approximate scale insensitivity in Eq. (79). Despite the clearly visible difference between the two $\bar{Q}_0(b_T)$ functions in the upper panel in the region just below $b_T \approx C_1/Q_0 \approx 0.5$ GeV $^{-1}$, the effect of switching between them essentially vanishes in the $\tilde{K}^{(1)}(b_T; \mu_{Q_0})$ calculations of the lower panel.

The normal way to calculate $\tilde{K}(b_T; \mu_{Q_0})$ in the small- b_T limit is to transform to an RG scale, $\mu_{Q_0} \rightarrow C_1/b_T$, and use low order perturbative calculations. We should thus expect to recover this in the small- b_T limit of the $\tilde{K}^{(1)}(b_T; \mu_{Q_0})$ from Fig. 2. To check this, let us define a “purely perturbative” calculation of the small- b_T $\tilde{K}(b_T; \mu_{Q_0})$ called $\tilde{K}_{\text{pert}}^{(1)}(b_T; \mu_{Q_0})$:

$$\begin{aligned} \tilde{K}_{\text{pert}}^{(1)}(b_T; \mu_{Q_0}) &\equiv \\ \tilde{K}^{(1)}(b_T; C_1/b_T) &- \int_{C_1/b_T}^{\mu_{Q_0}} \frac{d\mu'}{\mu'} \gamma_K^{(1)}(\alpha_s(\mu')). \end{aligned} \quad (80)$$

We have shown $\tilde{K}_{\text{pert}}^{(1)}(b_T; \mu_{Q_0})$ as the violet dashed curve in the lower panel of Fig. 2. As expected, the purely perturbative curve diverges at large b_T , while it merges with the $\tilde{K}^{(1)}(b_T; \mu_{Q_0})$ curves for $b_T \ll 1/\Lambda_{\text{QCD}}$.

Care is needed when interpreting the numerically small $\bar{Q}_0(b_T)$ dependence observed in plots like Fig. 2. In cross section calculations like Eq. (20), $\tilde{K}^{(1)}(b_T; \mu_{Q_0})$ multiplies a $\ln(Q^2/Q_0^2)$, so small errors will be amplified as $Q \gg Q_0$. The effect of $\tilde{K}^{(1)}(b_T; \mu_{Q_0})$ on the b_T -space cross section is entirely through the overall factor of $\exp \left\{ \tilde{K}^{(1)}(b_T; \mu_{Q_0}) \ln(Q^2/Q_0^2) \right\}$, as seen in Eq. (20). So, we get a better sense of the size of errors after evolution by plotting this exponent for a wide range of $Q > Q_0$. For example, we may calculate $\tilde{K}^{(1)}(b_T; \mu_{Q_0})$ using different $\bar{Q}_0(b_T)$ and compare the resulting $\exp \left\{ \tilde{K}^{(1)}(b_T; \mu_{Q_0}) \ln(Q^2/Q_0^2) \right\}$ for several $Q > Q_0$. We have shown an example of this in Fig. 3 for the two different choices of $\bar{Q}_0(b_T)$ in the top panel of Fig. 2. In the top panel of Fig. 3, we have replotted the two $\tilde{K}^{(1)}(b_T; \mu_{Q_0})$ curves from the lower pane in Fig. 2, but now with axis ranges shifted until the variation between the two calculations starts to become visible on the plot. It is evident from the curves that we should expect any effect from varying a to be significant only in a band around $b_T \approx 0.3$ GeV $^{-1}$. In the lower panel we have plotted the ratio of $\exp \left\{ \tilde{K}^{(1)}(b_T; \mu_{Q_0}) \ln(Q^2/Q_0^2) \right\}$ for the two different values of a from the top panel. That is, we plot

$$r(a_1, a_2) \equiv \frac{\exp \left\{ \tilde{K}^{(1)}(b_T; \mu_{Q_0}) \ln(Q^2/Q_0^2) \right\} \Big|_{a=a_2}}{\exp \left\{ \tilde{K}^{(1)}(b_T; \mu_{Q_0}) \ln(Q^2/Q_0^2) \right\} \Big|_{a=a_1}} \quad (81)$$

for $Q = 4$ GeV and $Q = 100$ GeV. After evolving from $Q = 2$ GeV to $Q = 100$ GeV, the maximum effect is just under 6%. We will see in more detail how the scale sensitivity propagates to the cross section in Sec. VII C.

So far, our example plots have only used $m_K = 0.1$ GeV, but nonperturbative parameters like these will in general need to be adjusted in fits. In our setup, adjustments to parameters like m_K will have a negligible

effect on the $b_T \lesssim 1/Q_0$ region of $\tilde{K}^{(1)}(b_T; \mu_{Q_0})$ so long as m_K is kept small relative to Q_0 . To illustrate this, we have plotted $\tilde{K}^{(1)}(b_T; \mu_{Q_0})$ once again in Fig. 4 for several values of m_K , now on a linear horizontal axis to magnify the effect on the large b_T region. The plot confirms that the region of $b_T \lesssim 0.5 \text{ GeV}^{-1}$ is essentially unaffected by the values of the m_K parameter between $\approx 0.1 \text{ GeV}$ and $\approx 0.5 \text{ GeV}$, so long as those values are kept reasonably small relative to Q_0 . A vertical line indicates the $b_T = 0.3 \text{ GeV}^{-1}$ position where we previously found the greatest scale sensitivity in the perturbative part of the calculation – the peak of the bump in Fig. 3. In contrast to the small scale sensitivity in the bottom panel of Fig. 2, sensitivity to changes in the value of m_K is large and clearly visible, but only in the region of large b_T . The step of fitting the purely nonperturbative parameter has been sequestered from the treatment of the transition into the perturbative regime.

In phenomenological applications, one converges on an unambiguous \tilde{K} as one repeats the steps above but with higher orders for the large k_T region. That amounts to constructing parametrizations for $\tilde{K}^{(2)}(b_T; \mu_{Q_0})$, $\tilde{K}^{(3)}(b_T; \mu_{Q_0})$, etc. Going to larger n reduces sensitivity to arbitrary choices like the functional form for $\tilde{Q}_0(b_T)$. Quantities like a and m_K are also increasingly constrained as more data from larger Q are included in fitting.

Extending the above construction of $\tilde{K}^{(1)}(b_T; \mu_{Q_0})$ to the case of $\tilde{K}^{(2)}(b_T; \mu_{Q_0})$ is straightforward and instructive, but we leave it to future work.

B. TMD ff example

Next we need to repeat steps A1-A3 from Sec. VI for the TMD ffs themselves. To keep the discussion here simple, we will assume that the TMD ffs are the same for hadrons A and B, and we will continue to focus only on the $n = 1$ case. Fortunately, the steps are very analogous to the CS kernel, so much of the below will be repetition.

A typical parametrization, common in TMD parton-model descriptions of Type I processes, is a Gaussian,

$$D_{\text{input}}^{(0, d_r)}(z, z\mathbf{k}_T; \mu_{Q_0}, Q_0^2) = \frac{C}{\pi M^2} e^{-z^2 k_T^2 / M^2}. \quad (82)$$

This fails to satisfy Eq. (52) when we try to extend it directly to $n = 1$ because it does not have the right functional form to match to $D^{(n, d_r)}(z, z\mathbf{k}_T; \mu_{Q_0}, Q_0^2)$ when $k_T \approx Q_0$. In order to construct a TMD ff for $n = 1$, we need to describe the transition from a nonperturbative peak like Eq. (82) to a perturbative large k_T power-law tail. The simplest way to do this is to just append $D^{(n, d_r)}(z, z\mathbf{k}_T; \mu_{Q_0}, Q_0^2)$ to Eq. (82) as an additive term. Inside $D^{(n, d_r)}(z, z\mathbf{k}_T; \mu_{Q_0}, Q_0^2)$, we can then make the replacement $k_T^2 \rightarrow k_T^2 + m_D^2$, where m_D is a nonperturbative parameter, to smooth the $k_T \rightarrow 0$ behavior into

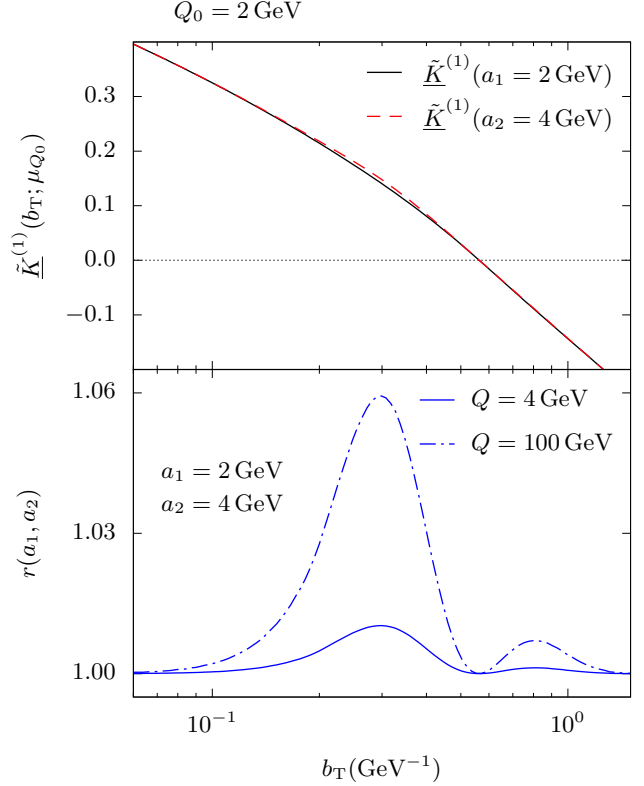


FIG. 3: Top panel: A blown-up version of the curves in the lower panel of Fig. 2. The axes have been adjusted so that the deviation between the two $\tilde{K}^{(1)}(b_T; \mu_{Q_0})$ calculations for different $\tilde{Q}_0(b_T)$ are visible, and we can see that the most significant variation is in a narrow band around $b_T \approx 0.3 \text{ GeV}^{-1}$. Bottom panel: The effect of the choice of the transformation function on the ratio in Eq. (81). All curves are obtained from our trial $n = 1$ parametrization for $Q = 4 \text{ GeV}$ and $Q = 100 \text{ GeV}$. At $Q = 100 \text{ GeV}$, the ratio $r(a_1, a_2)$ deviates from unity by a maximum of about 6% in a transition region around $b_T \approx 0.3 \text{ GeV}^{-1}$.

a nonperturbative peak, analogous to what we did in Eq. (72). Thus, our trial input parametrization is

$$\begin{aligned} D_{\text{input}}^{(1, d_r)}(z, z\mathbf{k}_T; \mu_{Q_0}, Q_0^2) &= \frac{1}{2\pi z^2} \frac{1}{k_T^2 + m_D^2} \left[A^{(d_r)}(z; \mu_{Q_0}) \right. \\ &\quad \left. + B^{(d_r)}(z; \mu_{Q_0}) \ln \frac{Q_0^2}{k_T^2 + m_D^2} \right] + \frac{C^{(d_r)}}{\pi M^2} e^{-z^2 k_T^2 / M^2}, \end{aligned} \quad (83)$$

where we have utilized the following abbreviations,

$$A^{(d_r)}(z; \mu) \equiv \frac{\alpha_s(\mu)}{\pi} \left\{ [(P_{qq} \otimes d_r)(z; \mu)] - \frac{3C_F}{2} d_r(z; \mu) \right\}, \quad (84)$$

$$B^{(d_r)}(z; \mu) \equiv \frac{\alpha_s(\mu) C_F}{\pi} d_r(z; \mu). \quad (85)$$

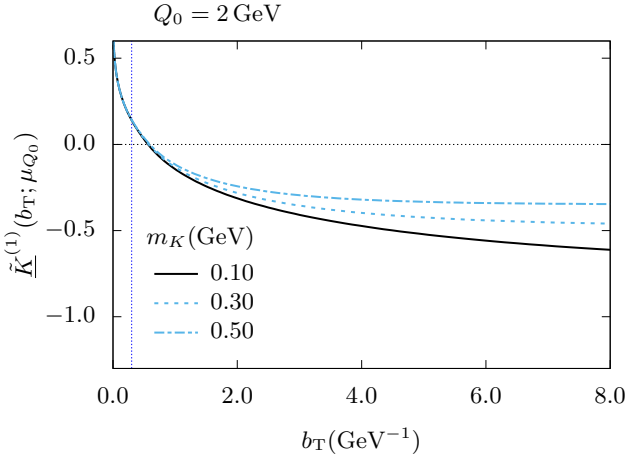


FIG. 4: The trial $\tilde{K}^{(1)}(b_T; \mu_{Q_0})$ from Eq. (78) calculated for three different values of the nonperturbative parameter m_K . The transformation function that was used is Eq. (C2) for $a = 2$ GeV as before. The black solid curve is identical to the black solid curve in the lower panel of Fig. 2, but now we show two additional values of m_K , and with a linear horizontal axis. The sensitivity to m_K is only visible for $b_T \gtrsim C_1/Q_0 \approx 0.5 \text{ GeV}^{-1}$, as expected. The vertical line at $b_T = 0.3 \text{ GeV}^{-1}$ marks the point where we previously found significant scale sensitivity, as seen in Fig. 3.

For a textbook derivation of the large k_T perturbative behavior see, for example, Eq.(13.101) and Eq.(13.66) of Ref. [3]. At the order- α_s we are working in, the expressions are independent of the exact renormalization scheme r used for the collinear ffs, so we have left it general in Eq. (83) for now. We will specialize to $r = \overline{\text{MS}}$ later.

The TMD ff should at least approximately match its collinear perturbative expansion for $k_T \approx Q_0$, so m_D and M should be kept small relative to Q_0 in any fits.

One of our requirements from step A2 is that parametrizations of the TMD ffs must satisfy the integral relation in Eq. (56) with Eq. (57) satisfied. We will use this constraint to fix $C^{(d_r)}$, which so far is just another nonperturbative parameter. Evaluating the transverse momentum integral of Eq. (83), expanding in small m/μ_{Q_0} , and solving for $C^{(d_r)}$ in terms of $\underline{d}_c^{(1,d_r)}(z; \mu_{Q_0})$ gives

$$\begin{aligned} C^{(d_r)} &= \underline{d}_c^{(1,d_r)}(z; \mu_{Q_0}) - A^{(d_r)}(z; \mu_{Q_0}) \ln \left(\frac{\mu_{Q_0}}{m_D} \right) \\ &\quad - B^{(d_r)}(z; \mu_{Q_0}) \ln \left(\frac{\mu_{Q_0}}{m_D} \right) \ln \left(\frac{Q_0^2}{\mu_{Q_0} m_D} \right) \\ &\quad + O \left(\frac{m}{\mu_{Q_0}} \right). \end{aligned} \quad (86)$$

We still need to choose a form for $\underline{d}_c^{(1,d_r)}(z; \mu_{Q_0})$, but our requirement is that it must satisfy Eq. (57), where we allow the m/μ_{Q_0} -suppressed contributions to be chosen to give an optimal parametrization. Thus, let us define the power-suppressed terms in Eq. (57) (again, for $n = 1$)

to exactly equal those in Eq. (86). Then,

$$\begin{aligned} C^{(d_r)} &= \underline{d}_c^{(1,d_r)}(z; \mu_{Q_0}) - A^{(d_r)}(z; \mu_{Q_0}) \ln \left(\frac{\mu_{Q_0}}{m_D} \right) \\ &\quad - B^{(d_r)}(z; \mu_{Q_0}) \ln \left(\frac{\mu_{Q_0}}{m_D} \right) \ln \left(\frac{Q_0^2}{\mu_{Q_0} m_D} \right) \\ &= \underline{d}_r(z; \mu_{Q_0}) - A^{(d_r)}(z; \mu_{Q_0}) \ln \left(\frac{\mu_{Q_0}}{m_D} \right) \\ &\quad - B^{(d_r)}(z; \mu_{Q_0}) \ln \left(\frac{\mu_{Q_0}}{m_D} \right) \ln \left(\frac{Q_0^2}{\mu_{Q_0} m_D} \right) \\ &\quad + \Delta^{(n,d_r)}(\alpha_s(\mu_Q)), \end{aligned} \quad (87)$$

where in the last line we have used Eq. (31). These last few steps are necessary if we wish to relate $C^{(d_r)}$ to known collinear ffs in standard schemes.

Equation (83), with Eq. (87) now for $C^{(d_r)}$, is the parametrization of the TMD ff that is to be substituted into Eq. (22) and, in accordance with step B1, used phenomenologically for describing Type I processes with standard TMD parton model techniques near the input scale $Q \approx Q_0$.

To get a general sense of what the Eq. (83) parametrization of the TMD ff looks like at $Q = Q_0$, we have plotted it in Fig. 5 using $\overline{\text{MS}}$ collinear ffs and reasonable values of the mass parameters m_D , and M . (The nonperturbative mass parameters are kept small relative to $Q_0 = 2.0 \text{ GeV}$.) For this case, $\Delta^{(n,d_{\overline{\text{MS}}})}(\alpha_s(\mu_Q))$ is given by Eq. (34). The plot is for a sample value of $z = 0.3$, but other values of z produce qualitatively similar curves, as can be easily checked. Since there is a general expectation from existing Type I TMD phenomenology that the small transverse momentum region in moderate Q processes is well-described by Gaussian TMDs, we have overlaid a Gaussian curve on top of Eq. (83), confirming that the $k_T \ll Q_0$ region retains a generally Gaussian shape.

As per step B1, the small k_T region is to be described by fitting the m_D and M parameters to measurements. So long as these mass parameters are reasonably small compared to Q_0 , the parametrization at least approximately recovers the lowest order perturbative description in collinear factorization around $k_T \approx Q_0$. In principle M and m_D can both have z -dependence:

$$M \rightarrow M(z), \quad m_D \rightarrow m_D(z), \quad (88)$$

but we will not include this in any of our example plots.

While we intend for the above parametrization to be only a toy example to illustrate broader procedural points, it is worth noting that at least some phenomenological support for an additive two-component model (like Eq. (83)) exists in the observation from [39] that a sum of two peaked nonperturbative functions provides a good fit to data in the moderate Q region. In that case, the two peaked functions were both Gaussians, but the trend is nevertheless suggestive of a two component form more generally. Reference [95] has also confirmed that

a combination of a Gaussian peak at small transverse momentum and a power-law tail at large transverse momentum provides a reasonable description of moderate Q data.

The two model parameters in our construction have natural interpretations: The lower-case m_D describes exactly how the TMD ff transitions from the Gaussian-like behavior typically ascribed to nonperturbative dependence to the power-law behavior more typical of a perturbative tail, while the capital M parameters controls the precise shape of the Gaussian peak at small k_T .

The inverse Fourier-Bessel transform into transverse coordinate space is

$$\begin{aligned} z^2 \tilde{D}_{\text{input}}^{(1,d_r)}(z, \mathbf{b}_T; \mu_{Q_0}, Q_0^2) &= A^{(d_r)}(z; \mu_{Q_0}) K_0(b_T m_D) \\ &+ B^{(d_r)}(z; \mu_{Q_0}) K_0(b_T m_D) \ln \left(\frac{b_T}{2m_D} Q_0^2 e^{\gamma_E} \right) \\ &+ C^{(d_r)} \exp \left(-\frac{b_T^2 M^2}{4z^2} \right), \end{aligned} \quad (89)$$

$$\begin{aligned} z^2 \tilde{D}_{\text{input}}^{(1,d_r)}(z, \mathbf{b}_T; \mu_{Q_0}, Q_0^2) &= \\ &- A^{(d_r)}(z; \mu_{Q_0}) \ln \left(\frac{b_T \mu_{Q_0} e^{\gamma_E}}{2} \right) - B^{(d_r)}(z; \mu_{Q_0}) \left[\ln^2 \left(\frac{b_T \mu_{Q_0} e^{\gamma_E}}{2} \right) + \ln \left(\frac{b_T \mu_{Q_0} e^{\gamma_E}}{2} \right) \ln \left(\frac{Q_0^2}{\mu_{Q_0}^2} \right) \right] \\ &+ d_r(z; \mu_{Q_0}) + \Delta^{(1,d_r)}(\alpha_s(\mu_Q)) + O(mb_T), \end{aligned} \quad (90)$$

Or, specializing to $r = \overline{\text{MS}}$,

$$\begin{aligned} z^2 \tilde{D}_{\text{input}}^{(1,d_{\overline{\text{MS}}})}(z, \mathbf{b}_T; \mu_{Q_0}, Q_0^2) &= \\ &- A^{(d_{\overline{\text{MS}}})}(z; \mu_{Q_0}) \ln \left(\frac{b_T \mu_{Q_0} e^{\gamma_E}}{2} \right) - B^{(d_{\overline{\text{MS}}})}(z; \mu_{Q_0}) \left[\ln^2 \left(\frac{b_T \mu_{Q_0} e^{\gamma_E}}{2} \right) + \ln \left(\frac{b_T \mu_{Q_0} e^{\gamma_E}}{2} \right) \ln \left(\frac{Q_0^2}{\mu_{Q_0}^2} \right) \right] \\ &+ \frac{\alpha_s(\mu_Q)}{2\pi} \int_z^1 \frac{dz'}{z'} d_{\overline{\text{MS}}}(z/z', \mu_Q) [2P_{qq}(z') \ln z' + C_F(1 - z')] + d_{\overline{\text{MS}}}(z; \mu_{Q_0}) + O(mb_T), \end{aligned} \quad (91)$$

Equation (91) is the usual small- b_T OPE applied to $\tilde{D}(z, \mathbf{b}_T; \mu_{Q_0}, Q_0^2)$ in the $\overline{\text{MS}}$ scheme through order $\alpha_s(\mu_{Q_0})$. Using Eq. (90), it is straightforward to verify Eqs. (54)–(55) by directly applying to Eq. (90) a partial derivative with respect to Q_0 and a total derivative with respect to μ_{Q_0} .

This completes our steps A1 and A2 from Sec. VI. Now we have a $\tilde{D}_{\text{input}}^{(1,d_c)}(z, \mathbf{b}_T; \mu_{Q_0}, Q_0^2)$ parametrization that is suitable for Type I phenomenological applications.

Finally, for step A3 we need to construct a parametrization $\tilde{D}^{(n,d_r)}(z, \mathbf{b}_T; \mu_{Q_0}, Q_0^2)$ that applies not

where $C^{(d_c)}$ is now defined as in Eq. (87). For checking various properties of the input TMD ff, it will also be useful to have the $mb_T \rightarrow 0$ limit,

only near the input scale $Q \approx Q_0$ but also to $Q \gg Q_0$. To switch to the final underlined parametrization, we can continue to use the same $\tilde{Q}_0(b_T)$ from Sec. IV and Appendix C that we used for the CS kernel. Implementing step A3 amounts to simply substituting our $\tilde{D}_{\text{input}}^{(1,d_c)}(z, \mathbf{b}_T; \mu_{Q_0}, Q_0^2)$ from Eq. (89) into the right-hand side of Eq. (61) along with the $\tilde{K}_{\text{input}}^{(1)}(b_T; \mu_{\tilde{Q}_0})$ that we already constructed in Sec. VII A, Eq. (75). The final expression is,

$$\begin{aligned} & \tilde{D}^{(1,d_{\overline{\text{MS}}})}(z, \mathbf{b}_T; \mu_{Q_0}, Q_0^2) \\ &= \tilde{D}_{\text{input}}^{(1,d_{\overline{\text{MS}}})}(z, \mathbf{b}_T; \mu_{\overline{Q}_0}, \overline{Q}_0^2) \exp \left\{ \int_{\mu_{\overline{Q}_0}}^{\mu_{Q_0}} \frac{d\mu'}{\mu'} \left[\gamma^{(1)}(\alpha_s(\mu'); 1) - \ln \frac{Q_0}{\mu'} \gamma_K^{(1)}(\alpha_s(\mu')) \right] + \ln \frac{Q_0}{\overline{Q}_0} \tilde{K}_{\text{input}}^{(1)}(b_T; \mu_{\overline{Q}_0}) \right\}. \end{aligned} \quad (92)$$

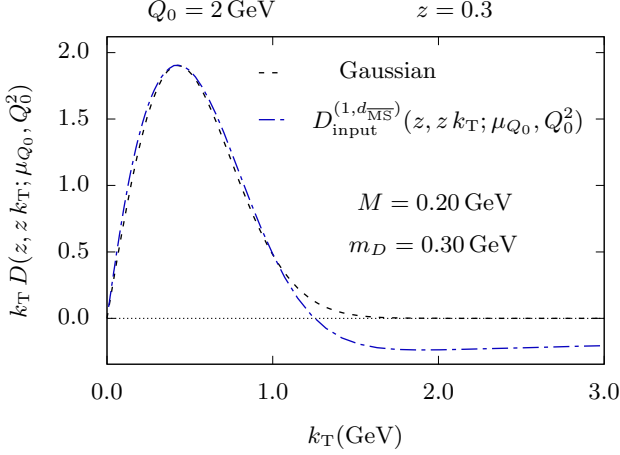


FIG. 5: The $n = 1$ input TMD ff from Eq. (83). The function is shown for $M = 0.2 \text{ GeV}$ and $m_D = 0.3 \text{ GeV}$ at a fixed value of $z = 0.3$ (blue dot-dashed). For comparison, we have also overlaid a Gaussian (black dashed) curve. Up to $k_T \approx 1.0 \text{ GeV}$, both lines exhibit similar profiles. The change in sign at larger k_T is due to matching to the perturbative collinear factorization expression using $\overline{\text{MS}}$ collinear ffs.

This is simply Eq. (61) again but now we mean it to be implied that it is being used with the specific models from Eq. (72) and Eq. (83). From Eq. (89),

$$\begin{aligned} & z^2 \tilde{D}_{\text{input}}^{(1,d_{\overline{\text{MS}}})}(z, \mathbf{b}_T; \mu_{\overline{Q}_0}, \overline{Q}_0^2) = \\ & A^{(d_{\overline{\text{MS}}})}(z; \mu_{\overline{Q}_0}) K_0(b_T m_D) \\ & + B^{(d_{\overline{\text{MS}}})}(z; \mu_{\overline{Q}_0}) K_0(b_T m_D) \ln \left(\frac{b_T}{2m_D} \overline{Q}_0^2 e^{\gamma_E} \right) \\ & + C^{(d_{\overline{\text{MS}}})} \exp \left(-\frac{b_T^2 M^2}{4z^2} \right), \end{aligned} \quad (93)$$

and $\tilde{K}^{(1)}(b_T; \mu_{\overline{Q}_0})$ is the same $n = 1$ result already written in Eq. (78). $C^{(d_{\overline{\text{MS}}})}$ is given by Eq. (87).

For illustration, Fig. 6 is a plot of our trial $\tilde{D}^{(1,d_{\overline{\text{MS}}})}(z, \mathbf{b}_T; \mu_{Q_0}, Q_0^2)$ from Eq. (92), plotted in coordinate space, where as before we have used an input scale $Q_0 = 2 \text{ GeV}$ and $z = 0.3$. We have chosen typical sizes for the nonperturbative mass parameters: $M = 0.2 \text{ GeV}$, $m_D = 0.3 \text{ GeV}$ and $m_K = 0.1 \text{ GeV}$. As in the case of $\tilde{K}^{(1)}(b_T; \mu_{Q_0})$, we are able to test scale sensitivity in the intermediate b_T region by varying the transition function $\tilde{Q}_0(b_T)$. In Fig. 6, we do this by again switching between the two $\tilde{Q}_0(b_T)$ functions from the upper panel of Fig. 2;

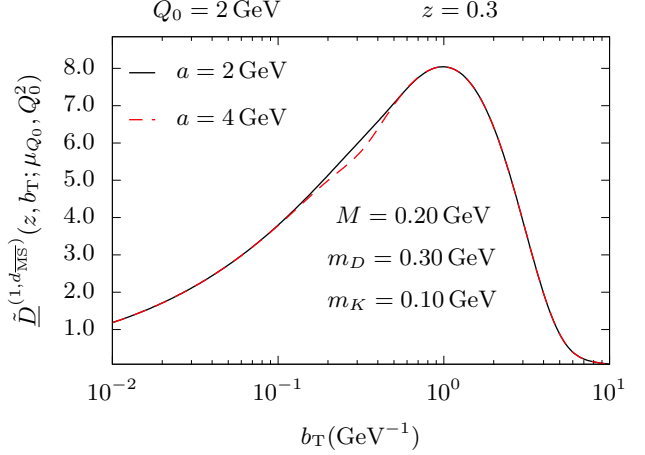


FIG. 6: A plot of the example $\tilde{D}^{(1,d_{\overline{\text{MS}}})}(z, \mathbf{b}_T; \mu_{Q_0}, Q_0^2)$ from Eq. (92), with typical nonperturbative mass parameters chosen for illustration purposes; m_D and M have the same values as in Fig. 5 while m_K has the same value as in the lower panel of Fig. 2. As in all previous plots, we have also fixed $Q_0 = 2 \text{ GeV}$. The difference between the two curves corresponds to switching between the two transition functions $\tilde{Q}_0(b_T)$ in the upper panel of Fig. 2, as indicated by the two values of a . This figure is the culmination of steps A1, A2 and A3 from Sec. VI.

the solid black and dashed red curves are for $a = 2 \text{ GeV}$ and $a = 4 \text{ GeV}$ respectively. The weakness of the observed variation confirms that the setup is behaving as intended (recall Eq. (64)). As with $\tilde{K}^{(1)}(b_T; \mu_{Q_0})$, sensitivity to parameters like a can in principle be reduced still further by including higher orders and fitting at larger Q . This requires matching to a higher order treatment of the large q_T tail – see, for example, Refs. [90, 96, 97].

C. Cross section examples

With Eq. (92) now completely set up, all that is needed to get the cross section is to substitute it, along with Eq. (78), into Eq. (65) to obtain a calculation of $W^{(1)}(q_T, Q)$ for any $Q \geq Q_0$. To illustrate how the features of the $\tilde{D}^{(1,d_{\overline{\text{MS}}})}(z, \mathbf{b}_T; \mu_{Q_0}, Q_0^2)$ and $\tilde{K}^{(1)}(b_T; \mu_{Q_0})$ parametrizations from the previous subsections influence $W^{(1)}(q_T, Q)$, and to finish reviewing the steps of Sec. VI, we will end this section below by examining several example plots of $W^{(1)}(q_T, Q)$.

First, Fig. 7 shows $q_T W^{(1)}(q_T, Q)$ (divided by an un-

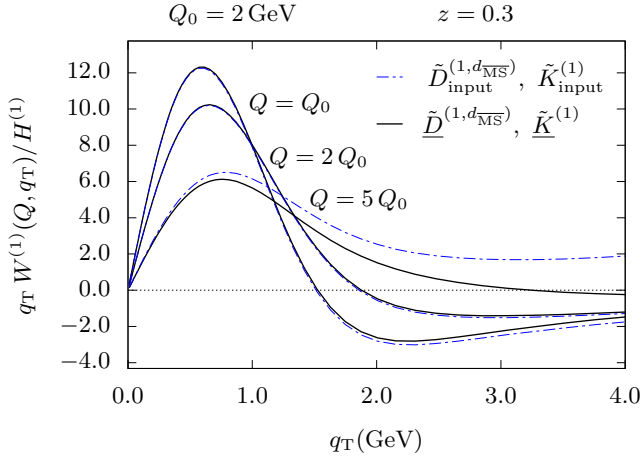


FIG. 7: $W^{(1)}(q_T, Q)$ from Eq. (65) calculated using $\tilde{D}^{(1, d_{\overline{\text{MS}}})}(z, \mathbf{b}_T; \mu_{Q_0}, Q_0^2)$ and $\tilde{K}^{(1)}(b_T; \mu_{Q_0})$ from Eq. (78) and Eq. (92) (solid black curves) for $Q = Q_0, 2Q_0$ and $5Q_0$. Here, as in all remaining plots that we will show, we use an input scale of $Q_0 = 2 \text{ GeV}$ and $z = 0.3$. The scale transformation function $\bar{Q}_0(b_T)$ used to produce these curves is the solid black function in the upper panel of Fig. 2 corresponding to $a = 2 \text{ GeV}$. The model parameters are the same $M = 0.2 \text{ GeV}$, $m_D = 0.3 \text{ GeV}$ and $m_K = 0.1 \text{ GeV}$ that we used in the plots of the previous subsection. For comparison, $W^{(1)}(q_T, Q)$ calculations are also shown wherein $\tilde{K}_{\text{input}}^{(1)}(b_T; \mu_{\bar{Q}_0})$ and $\tilde{D}_{\text{input}}^{(1, d_{\overline{\text{MS}}})}(z, \mathbf{b}_T; \mu_{Q_0}, Q_0^2)$ from Eq. (75) and Eq. (91) are used in Eq. (65) (blue dot-dashed curves), in place of the underlined parametrizations. Note the negligible difference for $Q \approx Q_0$ and small q_T . See text for further discussion.

interesting normalization $H^{(1)}$), plotted versus q_T and with a selection of Q values just above the input scale $Q_0 = 2 \text{ GeV}$. The nonperturbative parameters are the same $M = 0.2 \text{ GeV}$, $m_D = 0.3 \text{ GeV}$ and $m_K = 0.1 \text{ GeV}$ values that we used in our illustrations from the previous subsection, and the $\bar{Q}_0(b_T)$ is the same transition function from the upper panel of Fig. 2 with $a = 2 \text{ GeV}$. The solid black curves are what are obtained if we substitute the underlined functions of Eq. (78) and Eq. (92) into Eq. (65). For comparison, the blue dot-dashed curves are what are obtained when we simply substitute the input parametrizations, Eq. (75) and Eq. (91) into Eq. (65), instead of the final underlined parametrizations optimized for the small b_T limit. Showing both curves confirms that switching between “input” and underlined parametrizations results in a negligible difference in the cross section calculation at $q_T \ll Q$ when Q is only slightly larger than Q_0 . In Fig. 7, the difference between the solid black and dot-dashed blue curves is nearly invisible for Q between Q_0 and $2Q_0$, and only becomes significant for $Q \approx 5Q_0$ and larger q_T . Making these observations corresponds to step B3 from Sec. VI. They confirm that the input or the underlined parametrizations are both valid and interchangeable for phenomenological Type I applications near $Q \approx Q_0$.

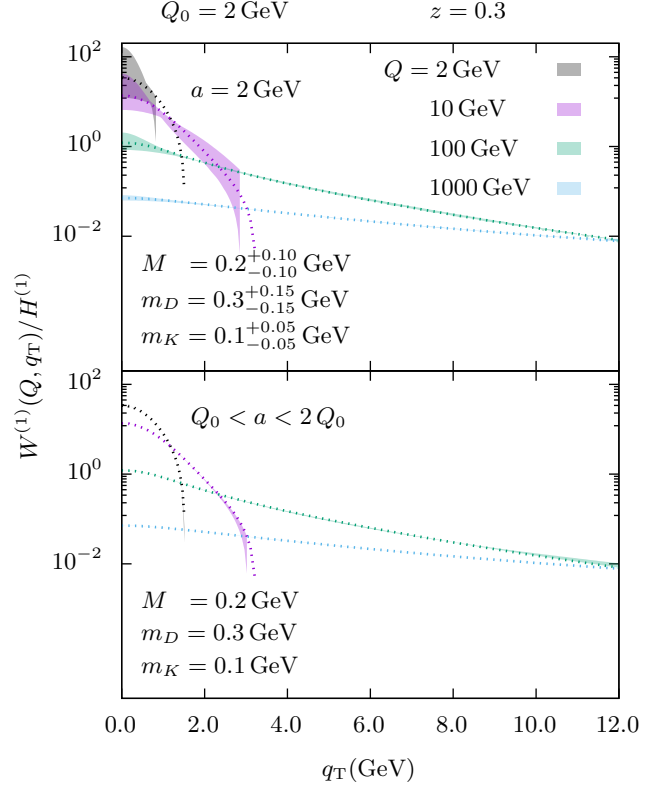


FIG. 8: $W^{(1)}(q_T, Q)$, calculated using the trial underlined parametrizations from this section and evolved to scales much larger than Q_0 . The dotted lines are calculated using fixed intrinsic scales $M = 0.2 \text{ GeV}$, $m_D = 0.3 \text{ GeV}$ and $m_K = 0.1 \text{ GeV}$ and the usual scale transformation function with $a = 2 \text{ GeV}$. The colored bands in the top panel show the effect of varying nonperturbative mass parameters by $\pm 50\%$ with respect to the values used for dotted lines. The bands in the bottom panel show the perturbative scale sensitivity from varying a between 2 GeV and 4 GeV , with masses fixed to those of the dotted lines. For reference, we also show the $Q = Q_0$ case as the black dotted line.

Next, Fig. 8 shows the $W^{(1)}(q_T, Q)$ calculation (from now on, we will always use the underlined parametrizations), plotted against q_T on a logarithmic scale for a selection of Q covering a large range between $Q_0 = 2 \text{ GeV}$ and $Q = 1000 \text{ GeV}$. The top panel is calculated with a fixed scale transformation function $\bar{Q}_0(b_T)$, specifically the $a = 2 \text{ GeV}$ curve in Fig. 2. The bands in the top panel were generated by varying the parameters M , m_D , and m_K associated with intrinsic transverse momentum by 50% around the values we used in the previous subsections, $M = 0.2 \text{ GeV}$, $m_D = 0.3 \text{ GeV}$ and $m_K = 0.1 \text{ GeV}$. The lower panel in Fig. 8 shows the same $W^{(1)}(q_T, Q)$ calculations, but now with the intrinsic nonperturbative scales fixed to their previous values. Instead, the bands are generated by varying the scale transformation function $\bar{Q}_0(b_T)$ between the two curves in the upper panel of Fig. 2 corresponding to $a = 2 \text{ GeV}$ and $a = 4 \text{ GeV}$. Com-

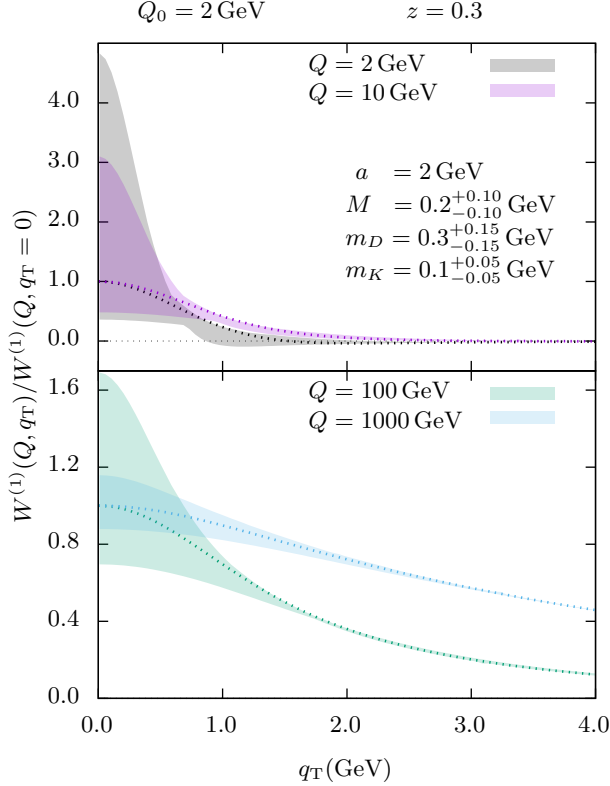


FIG. 9: Same as the top panel of Fig. 8, but with the horizontal axes now restricted to $q_T < 4$ GeV, linear vertical axes, and with each $W^{(1)}(q_T, Q)$ curve normalized to its value at $q_T = 0$. The upper panel shows the lower Q values, $Q = Q_0 = 2$ GeV and $Q = 10$ GeV while the lower panel shows the large Q values $Q = 100, 1000$ GeV.

paring the upper and lower panels in Fig. 8 shows that, within the range of parameters considered here, scale sensitivity is far weaker than the sensitivity to intrinsic transverse momentum parameters. On the logarithmic scale, the scale sensitivity is only visible, even at large Q , around the node where $W^{(1)}(q_T, Q)$ crosses zero.

Nevertheless, sensitivity to intrinsic transverse momentum parameters does clearly diminish with increasing Q , especially for $q_T \gtrsim Q_0$. To get a sense of how rapidly it decreases with our parametrizations, we have plotted the top curves from Fig. 8 again in Fig. 9, but now with linear axes and only for the region of $q_T < 4.0$ GeV in order to magnify sensitivity to variations in M , m_D , and m_K . We have also normalized the curves by their values at $q_T = 0$. The upper panel in Fig. 9 shows the bands for smaller $Q = 2$ GeV and $Q = 10$ GeV scales, and it shows that the small transverse momentum region $q_T \ll Q$ is very sensitive to nonperturbative intrinsic mass scales. At $q_T = 0$, the width of the band is about an order of magnitude for $Q \approx Q_0$. The lower panel of Fig. 9 shows the bands for the larger $Q = 100$ GeV and $Q = 1000$ GeV scales. There, the sensitivity to intrinsic mass param-

eters at $q_T = 0$ is much weaker than for the smaller Q , and it becomes essentially invisible above about $q_T \gtrsim 0.02Q$. This weak sensitivity to intrinsic nonperturbative transverse momentum parameters at $q_T \gg m$ will be especially important if we need to consistently match to fixed order asymptotic calculations [98].

In phenomenological applications such as fitting, non-perturbative parameters like M , m_D , and m_K , along with scale setting choices like the value of a , become better constrained each time data from somewhat higher Q are included in the fitting. As higher Q are incorporated into fits, and input parameters become better constrained, it eventually becomes unambiguous how to evolve to still higher Q . The steps that we have described in this subsection, along with the plots used to illustrate them, correspond to steps C1 and C2 in Sec. VI.

The illustrative examples in this subsection are to confirm that the setup in Sec. VI reproduces general expectations. We emphasize once again, before closing the discussion of examples, that our purpose here is not to advocate for a particular choice of a model parametrization for small k_T dependence, but rather to illustrate the general steps from Sec. VI in concrete situations. Ultimately, it is up to phenomenological tests to assess the success of any particular model or calculation of nonperturbative transverse momentum dependence.

VIII. INTEGRAL RELATIONS II

It is worthwhile to return again to the integral relations discussed in Sec. III in light of parametrizations like the one we constructed above. Now recall how integral relations often appear in phenomenological extractions of TMD functions near the input scale. For $Q \approx 1 - 2$ GeV and $k_T \ll Q_0$, it is well-known that the shapes of transverse momentum distributions are generally well approximated by Gaussians, so one might reasonably adopt a parametrization of the form

$$D(z, z\mathbf{k}_T; \mu_{Q_0}, Q_0^2) \stackrel{??}{=} \frac{d(z; \mu_{Q_0})}{\pi M^2} e^{-z^2 k_T^2 / M^2}, \quad (94)$$

where we have dropped renormalization subscripts etc to simplify expressions. The TMD and collinear ffs parametrized in this way automatically satisfy the parton model integral relation

$$2\pi z^2 \int d\mathbf{k}_T k_T D(z, z\mathbf{k}_T; \mu_{Q_0}, Q_0^2) = d(z; \mu_{Q_0}). \quad (95)$$

A parametrization like Eq. (94) imposes a strong suppression on large k_T , cutting off the large k_T tail. Because large k_T -dependence is generally regarded as perturbatively calculable, it is tempting to assume that it is possible to fix Eq. (94) in later steps simply by appending a purely perturbative tail for the region of $k_T \gtrsim Q_0$ while leaving the initial Gaussian of Eq. (94) completely unchanged. Taking that view literally would mean that, as

regards the integral relation, one does not need to modify either Eq. (94) or Eq. (95) other than to explicitly indicate an upper cutoff on the integral on the right-hand side of Eq. (95) and to specify that higher orders in α_s and/or $1/Q_0$ are neglected:

$$2\pi z^2 \int_0^{\mu_{Q_0}} dk_T k_T D(z, z\mathbf{k}_T; \mu_{Q_0}, Q_0^2) \stackrel{??}{=} d(z; \mu_{Q_0}) + \text{small corrections}. \quad (96)$$

A problem with this approach can be seen, however, in our examples from the previous section, where Eq. (96) would amount to applying the transverse momentum integral in Eq. (96) to Eq. (83) with $C^{(d_r)} = d_r(z; \mu_{Q_0})$ instead of Eq. (87) so that

$$\begin{aligned} z^2 \tilde{D}_{\text{input}}^{(1, d_r)}(z, \mathbf{b}_T; \mu_{Q_0}, Q_0^2) &= A^{(d_r)}(z; \mu_{Q_0}) K_0(b_T m_D) \\ &+ B^{(d_r)}(z; \mu_{Q_0}) K_0(b_T m_D) \ln \left(\frac{b_T}{2m_D} Q_0^2 e^{\gamma_E} \right) \\ &+ d_r(z; \mu_{Q_0}) \exp \left(-\frac{b_T^2 M^2}{4z^2} \right). \end{aligned} \quad (97)$$

But then the integral on the left side of Eq. (96) becomes

$$\begin{aligned} 2\pi z^2 \int_0^{\mu_{Q_0}} dk_T k_T D_{\text{input}}(z, z\mathbf{k}_T; \mu_{Q_0}, Q_0^2) &= \\ d_r(z; \mu_{Q_0}) + A^{(d_r)}(z; \mu_{Q_0}) \ln \left(\frac{\mu_{Q_0}}{m_D} \right) \\ &+ B^{(d_r)}(z; \mu_{Q_0}) \ln^2 \left(\frac{\mu_{Q_0}^2}{m_D^2} \right). \end{aligned} \quad (98)$$

The last two terms involving $A^{(d_r)}$ and $B^{(d_r)}$ would thus need to be identified with the “small corrections” of Eq. (96). However, the factorization theorem applies to the limit that $m/\mu_{Q_0} \rightarrow 0$, so the last two terms are not the purely perturbative corrections implied by an expression like Eq. (96). While $A^{(d_r)}(z; \mu_{Q_0})$ and $B^{(d_r)}(z; \mu_{Q_0})$ involve a coupling $\alpha_s(\mu_{Q_0})$ that vanishes asymptotically like

$$\alpha_s(\mu_{Q_0}) \sim \frac{1}{\ln(\mu_{Q_0}/\Lambda_{\text{QCD}})},$$

at large μ_{Q_0} , the logarithms in Eq. (98) more than compensate for this in the limit of large μ_{Q_0} . Indeed, the term in Eq. (98) involving $B^{(d_r)}(z; \mu_{Q_0})$ blows up as $\mu_{Q_0}/m \rightarrow \infty$. To keep a consistent integral relation that matches a parton model interpretation while also accounting for tails, evolution, etc, the coefficient of the Gaussian in Eq. (94) needs to be an expression like Eq. (87) rather than a simple collinear ff.

To write a version of Eq. (96), that is consistent with the presence of a large k_T tail region, as with our example in Sec. VII B with Eq. (89), it was necessary to interpolate between the nonperturbative and tail regions first.

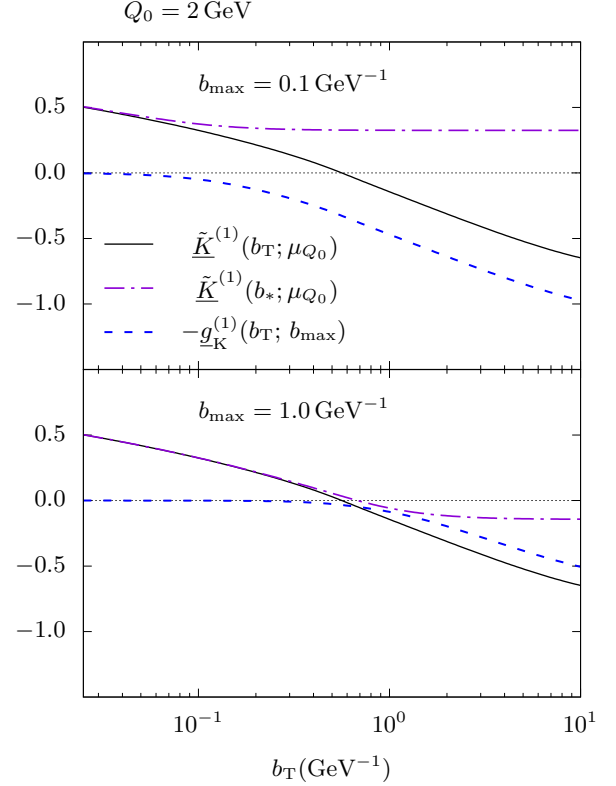


FIG. 10: The example $\tilde{K}^{(1)}(b_T; \mu_{Q_0})$ from Eq. (78) and the corresponding $\underline{g}_K^{(1)}(b_T)$ (Eq. (115)) and $\tilde{K}^{(1)}(b_*; \mu_{Q_0})$ calculated in the b_* -prescription with Eq. (101). Results are obtained using the same $m_K = 0.1 \text{ GeV}$ and $a = 2 \text{ GeV}$ as in Fig. 2. The top panel is the case of $b_{\text{max}} = 0.1 \text{ GeV}^{-1}$ and the bottom panel is the case of $b_{\text{max}} = 1.0 \text{ GeV}^{-1}$. The b_{max} -dependence in $\tilde{K}^{(1)}(b_*; \mu_{Q_0})$ (violet dot-dashed) cancels that of $-\underline{g}_K^{(1)}(b_T)$ (blue-dashed). The solid black curve showing $\tilde{K}^{(1)}(b_T; \mu_{Q_0})$ is identical in the top and bottom.

IX. COMPARISON WITH THE STANDARD PRESENTATION

After step C2 of Sec. VI, we noted that it is possible to recast final results into a form more familiar from past applications of TMD evolution in Type II contexts. We will show how to perform that translation in this section. We emphasize that the steps below are not necessary for implementing the approach above, so this section may be skipped without missing the main points of this article. Most of the steps below amount to reshuffling factors in the cross section expression. Ultimately, however, the translation is important for comparing approaches.

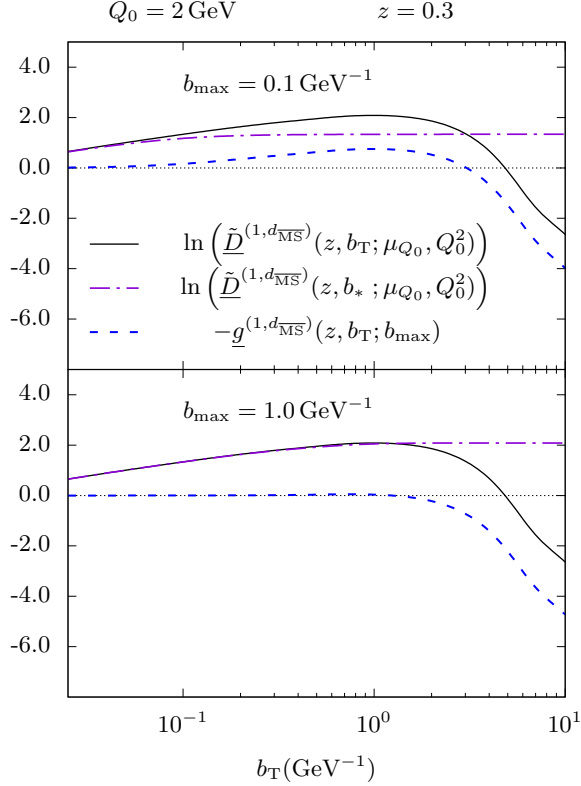


FIG. 11: The example $\tilde{D}^{(1,d_{\overline{\text{MS}}})}(z, b_T; \mu_{Q_0}, Q_0^2)$ from Eq. (92), and the corresponding $\underline{g}^{(1,d_{\overline{\text{MS}}})}(z, b_T)$ (Eq. (116)) and $\tilde{D}^{(1,d_{\overline{\text{MS}}})}(z, b_*; \mu_{Q_0}, Q_0^2)$ from the b_* -prescription (Eq. (101)). The curves are generated using the same $M = 0.2 \text{ GeV}$, $m_D = 0.3 \text{ GeV}$, and $a = 2 \text{ GeV}$ as in Fig. 7. The top panel is the case of $b_{\text{max}} = 0.1 \text{ GeV}^{-1}$ and the bottom panel is the case of $b_{\text{max}} = 1.0 \text{ GeV}^{-1}$. The b_{max} -dependence in $\ln(\tilde{D}^{(1,d_{\overline{\text{MS}}})}(z, b_*; \mu_{Q_0}, Q_0^2))$ (violet dot-dashed) cancels that of $-\underline{g}^{(1,d_{\overline{\text{MS}}})}(z, b_T)$ (blue-dashed). The solid black curves for $\tilde{D}^{(1,d_{\overline{\text{MS}}})}(z, b_T; \mu_{Q_0}, Q_0^2)$ are identical in the top and bottom panels.

A. The b_* method

Readers who are familiar with standard implementations of the CSS formalism might find the surface appearance of our expressions for the evolved $W^{(n)}(q_T, Q)$ in sections Sec. IV-Sec. VII somewhat odd. Normally, the cross section is written with nonperturbative TMD effects contained in separate exponential factors usually notated

$$e^{-g_A(z_A, b_T)}, \quad e^{-g_B(z_B, b_T)}, \quad \text{and} \quad e^{-g_K(b_T) \ln \frac{Q^2}{Q_0^2}}, \quad (99)$$

where the nonperturbative transverse momentum dependence is encoded in the (coordinate dependence of) the lower-case g -functions in the exponents. (The g_A and g_B functions are placed inside exponents so that they retain the appearance of Sudakov form factor contributions.)

Then, in the usual presentation, the rest of the factors in the cross section automatically get expressed in terms of collinear functions by using the OPE to approximate the small b_T behavior. For a specific example of what we mean here, consider Eq.(13.81) of [3].

In this subsection, we will review the steps for transforming the low- q_T cross section (or rather $W(q_T, Q)$) in Eq. (20) into the form that involves Eq. (99) g -functions.

Setting up the usual presentation of the cross section begins with a partition of the coordinate space $\tilde{W}(b_T, Q)$ into regions considered large and small b_T . One does this by defining an arbitrary function of b_T , traditionally called $\mathbf{b}_*(b_T)$. The function should smoothly interpolate between \mathbf{b}_T at small values of b_T and a maximum transverse size \mathbf{b}_{max} as b_T grows to $b_T \gg \mathbf{b}_{\text{max}}$. It is otherwise arbitrary. In other words,

$$\mathbf{b}_*(b_T) = \begin{cases} \mathbf{b}_T & b_T \ll \mathbf{b}_{\text{max}} \\ \mathbf{b}_{\text{max}} & b_T \gg \mathbf{b}_{\text{max}} \end{cases}. \quad (100)$$

The value of \mathbf{b}_{max} is also arbitrary, but it is usually interpreted roughly as a value somewhere near the boundary between nonperturbatively large and perturbatively small regions of b_T . The purpose of the “ \mathbf{b}_* method” [99] is to sequester a purely perturbative calculation of transverse coordinate dependence away from a part that involves nonperturbative modeling or fitting. While any reasonably well-behaved, smooth function of b_T that obeys the right side of Eq. (100) is a valid $\mathbf{b}_*(b_T)$, the most often used choice is

$$\mathbf{b}_*(b_T) = \frac{\mathbf{b}_T}{\sqrt{1 + b_T^2/b_{\text{max}}^2}}. \quad (101)$$

Later on, we will also need to define another hard scale that approaches the RG improved value of $\mu = C_1/b_T$ appropriate to the $b_T \rightarrow 0$ limit but that levels off at a fixed scale at large b_T . The simplest (and standard) way to do this is to just use the inverse of \mathbf{b}_* and define

$$\mu_{b_*} \equiv C_1/\mathbf{b}_*. \quad (102)$$

The behavior of μ_{b_*} is similar to that of our $\overline{Q}_0(b_T)$, but $\overline{Q}_0(b_T)$ approaches Q_0 at large b_T while μ_{b_*} approaches $C_1/\mathbf{b}_{\text{max}}$. (Indeed, in our treatment below we could opt to use $\overline{Q}_0(b_T)$ instead of μ_{b_*} , but we will continue with μ_{b_*} to make the comparison with standard expressions clear.)

Next, one solves Eq. (18) to relate a TMD ff (for hadron A, for example) at an input scale Q_0 to the TMD ff at any other scale $\sqrt{\zeta}$ by

$$\begin{aligned} \tilde{D}_A(z, \mathbf{b}_T; \mu, \zeta) \\ = \tilde{D}_A(z, \mathbf{b}_T; \mu, Q_0^2) \exp \left\{ \tilde{K}(b_T; \mu) \ln \left(\frac{\sqrt{\zeta}}{Q_0} \right) \right\}. \end{aligned} \quad (103)$$

Exactly the same equation applies independently of the

transverse coordinate \mathbf{b}_T , so we also have

$$\begin{aligned} \tilde{D}_A(z, \mathbf{b}_*; \mu, \zeta) \\ = \tilde{D}_A(z, \mathbf{b}_*; \mu, Q_0^2) \exp \left\{ \tilde{K}(b_*; \mu) \ln \left(\frac{\sqrt{\zeta}}{Q_0} \right) \right\}. \end{aligned} \quad (104)$$

Then the ratio of Eq. (103) and Eq. (104) is

$$\begin{aligned} \frac{\tilde{D}_A(z, \mathbf{b}_T; \mu, \zeta)}{\tilde{D}_A(z, \mathbf{b}_*; \mu, \zeta)} &= \frac{\tilde{D}_A(z, \mathbf{b}_T; \mu, Q_0^2)}{\tilde{D}_A(z, \mathbf{b}_*; \mu, Q_0^2)} \times \\ &\times \exp \left\{ - \left[\tilde{K}(b_*, \mu) - \tilde{K}(b_T, \mu) \right] \ln \left(\frac{\sqrt{\zeta}}{Q_0} \right) \right\} \\ &= \frac{\tilde{D}_A(z, \mathbf{b}_T; \mu, Q_0^2)}{\tilde{D}_A(z, \mathbf{b}_*; \mu, Q_0^2)} \exp \left\{ -g_K(b_T) \ln \left(\frac{\sqrt{\zeta}}{Q_0} \right) \right\} \\ &= \frac{\tilde{D}_A(z, \mathbf{b}_T; \mu_{Q_0}, Q_0^2)}{\tilde{D}_A(z, \mathbf{b}_*; \mu_{Q_0}, Q_0^2)} \exp \left\{ -g_K(b_T) \ln \left(\frac{\sqrt{\zeta}}{Q_0} \right) \right\}, \end{aligned} \quad (105)$$

where on the second line we have *defined*

$$g_K(b_T) \equiv \tilde{K}(b_*, \mu) - \tilde{K}(b_T, \mu). \quad (106)$$

Since the μ -dependence of $\tilde{K}(b_T, \mu)$ is also b_T -independent, $g_K(b_T)$ is μ -independent. That is, μ -dependence cancels between the two terms, so $g_K(b_T)$ is μ -independent by definition. Also, on the last line of Eq. (105) we have used that the μ -dependence of $\tilde{D}_A(z, \mathbf{b}_T; \mu, Q_0^2)$ is a b_T -independent overall factor – recall the evolution equation in Eq. (19) – to specialize to the case of $\mu = \mu_{Q_0}$.

Next, one defines the logarithm of the ratio on the last line of Eq. (105) by the symbol $-g_A(z, \mathbf{b}_T)$:

$$-g_A(z, \mathbf{b}_T) \equiv \ln \left(\frac{\tilde{D}_A(z, \mathbf{b}_T; \mu_{Q_0}, Q_0^2)}{\tilde{D}_A(z, \mathbf{b}_*; \mu_{Q_0}, Q_0^2)} \right), \quad (107)$$

with the A subscript reminding of potential sensitivity to the identity of the final state hadron. Combining Eq. (105) and Eq. (107) gives

$$\begin{aligned} \tilde{D}_A(z, \mathbf{b}_T; \mu, \zeta) &= \tilde{D}_A(z, \mathbf{b}_*; \mu, \zeta) \times \\ &\times \exp \left\{ -g_A(z, b_T) - g_K(b_T) \ln \left(\frac{\sqrt{\zeta}}{Q_0} \right) \right\}. \end{aligned} \quad (108)$$

The $\tilde{D}_A(z, \mathbf{b}_*; \mu, \zeta)$ on the right-hand side is still the exact operator definition, but it is only ever evaluated at $b_T \leq b_{\max}$. The remaining exponential factor is sensitive to the large b_T region. As of yet, there are no approximations. In particular, any sensitivity to b_{\max} or the choice of the \mathbf{b}_* parametrization in Eq. (100) cancels exactly between the factors on the right-hand side of Eq. (108). We have simply taken the original definition of $\tilde{D}_A(z, \mathbf{b}_*; \mu, \zeta)$ and partitioned it into two factors.

The logarithm on the right side of the definition in Eq. (107) is cosmetic; expressing the nonperturbative ratio as the exponential of a function $-g_A(z, b_T)$ gives it the appearance of a type of contribution to a Sudakov exponent.

Despite the apparent arbitrariness of the above steps, one can anticipate the motivation for writing the TMD ff as in Eq. (108) by looking ahead. We obtain the full cross section by substituting Eq. (108) into the evolved $W(q_T, Q)$ in Eq. (20) with $\mu = \mu_{Q_0}$ and $\sqrt{\zeta} = Q_0$. In the resulting cross section expression, $\tilde{D}_A(z, \mathbf{b}_*; \mu_{Q_0}, Q_0^2)$ will be well-approximated by collinear factorization at $b_T \approx 1/Q_0$ so long as $b_{\max} \approx 1/Q_0$ and Q_0 is reasonably large compared to nonperturbative scales. This would be sufficient for calculations with $Q \approx Q_0$, where the $1/Q_0 \lesssim b_T < \infty$ region is the only relevant contribution. However, if we plan to evolve to very large Q , then we also need an accurate treatment of $\tilde{D}_A(z, \mathbf{b}_*; \mu_{Q_0}, Q_0^2)$ in the $b_T \ll 1/Q_0$ limit. But the fixed order calculations of $\tilde{D}_A(z, \mathbf{b}_*; \mu_{Q_0}, Q_0^2)$ in collinear factorization are poorly behaved as $b_T \mu_{Q_0} \rightarrow 0$, even though this is the limit where perturbative QCD should be most reliable.

As usual, therefore, we need to apply the evolution equations (Eq. (59)) once again in order to evolve $\tilde{D}_A(z, \mathbf{b}_*; \mu, \zeta)$ from μ, ζ to the RG-improved $\mu_{b_*}, \mu_{b_*}^2$. The evolution equations allow us to rewrite Eq. (108) as

$$\begin{aligned}
\tilde{D}_A(z, \mathbf{b}_T; \mu, \zeta) &= \tilde{D}_A(z, \mathbf{b}_*; \mu, \zeta) \exp \left\{ -g_A(z, b_T) - g_K(b_T) \ln \left(\frac{\sqrt{\zeta}}{Q_0} \right) \right\} \\
&= \tilde{D}_A(z, \mathbf{b}_*; \mu_{b_*}, \mu_{b_*}^2) \exp \left\{ \int_{\mu_{b_*}}^{\mu} \frac{d\mu'}{\mu'} \left[\gamma(\alpha_s(\mu'); 1) - \ln \frac{\sqrt{\zeta}}{\mu'} \gamma_K(\alpha_s(\mu')) \right] + \ln \frac{\sqrt{\zeta}}{\mu_{b_*}} \tilde{K}(b_*; \mu_{b_*}) \right\} \\
&\quad \times \exp \left\{ -g_A(z, b_T) - g_K(b_T) \ln \left(\frac{\sqrt{\zeta}}{Q_0} \right) \right\}.
\end{aligned} \tag{109}$$

Recall that μ_{b_*} is defined in Eq. (102). There is of course an exactly analogous equation for $\tilde{D}_B(z, \mathbf{b}_*; \mu_{b_*}, \mu_{b_*}^2)$. Substituting the evolved versions of $\tilde{D}_A(z, \mathbf{b}_*; \mu_{b_*}, \mu_{b_*}^2)$ and $\tilde{D}_B(z, \mathbf{b}_*; \mu_{b_*}, \mu_{b_*}^2)$ into the W -term factorization formula Eq. (15) and setting the final scales equal to $\mu = \mu_Q$ and $\zeta = Q^2$ in Eq. (15) gives

$$\begin{aligned}
W(q_T, Q) &= H(\mu_Q; C_2) \int \frac{d^2 \mathbf{b}_T}{(2\pi)^2} e^{-i \mathbf{q}_T \cdot \mathbf{b}_T} \tilde{D}_A(z_A, \mathbf{b}_*; \mu_{b_*}, \mu_{b_*}^2) \tilde{D}_B(z_B, \mathbf{b}_*; \mu_{b_*}, \mu_{b_*}^2) \\
&\quad \times \exp \left\{ 2 \int_{\mu_{b_*}}^{\mu_Q} \frac{d\mu'}{\mu'} \left[\gamma(\alpha_s(\mu'); 1) - \ln \frac{Q}{\mu'} \gamma_K(\alpha_s(\mu')) \right] + \ln \frac{Q^2}{\mu_{b_*}^2} \tilde{K}(b_*; \mu_{b_*}) \right\} \\
&\quad \times \exp \left\{ -g_A(z_A, b_T) - g_B(z_B, b_T) - g_K(b_T) \ln \left(\frac{Q^2}{Q_0^2} \right) \right\}.
\end{aligned} \tag{110}$$

Equation (110) is very close to the standard way of expressing the CSS-evolved W -term.³ As we have written it, there are still no approximations; the solutions to the evolution equations are exact and the steps above simply reorganize the original factorization formula in Eq. (15). However, by writing $W(q_T, Q)$ as in Eq. (110), we have isolated on the first two lines those factors that can be confidently approximated in perturbation theory using collinear factorization. The value of b_T never rises above b_{\max} and the scale μ_{b_*} never drops below C_1/b_{\max} . Therefore, one obtains well-behaved perturbative calculations by replacing $H(\mu_Q; C_2)$, $\gamma(\alpha_s(\mu'); 1)$, $\gamma_K(\alpha_s(\mu'))$ and $\tilde{K}(b_*; \mu_{b_*})$ by their n^{th} -order perturbative calculations.

For the TMD ffs themselves on the first line, the choice of $\mu = \sqrt{\zeta} = \mu_{b_*}$ implements RG improvement for the limit of small b_T . As long as b_{\max} is small enough, $\tilde{D}_{A,B}(z_{A,B}, \mathbf{b}_*; \mu_{b_*}, \mu_{b_*}^2)$ can be expanded in an OPE:

$$\begin{aligned}
&\tilde{D}^{(n, d_r)}(z, \mathbf{b}_*; \mu_{b_*}, \mu_{b_*}^2) \\
&= \int_z^1 \frac{d\hat{z}}{\hat{z}^{3-2\epsilon}} d_r(\hat{z}; \mu_{b_*}) \tilde{C}_D^{(n)}(z/\hat{z}, b_T; \mu_{b_*}^2, \mu_{b_*}, \alpha_s(\mu_{b_*})) \\
&+ O(mb_T),
\end{aligned} \tag{111}$$

which is a more explicit version of Eq. (25) but in b_T -space. (Here, as usual, m represents any of the

small intrinsic mass scales, including now $1/b_{\max}$.) Substituting Eq. (111) for both $\tilde{D}_A(z_A, \mathbf{b}_*; \mu_{b_*}, \mu_{b_*}^2)$ and $\tilde{D}_B(z_B, \mathbf{b}_*; \mu_{b_*}, \mu_{b_*}^2)$, along with the other perturbative approximations mentioned above, recovers the standard CSS expression – compare, for example, with the Drell-Yan version of TMD factorization in Eq. (22) of [66].

The b_* method, as it is explained here, has several desirable properties. There is the elegant feature that, in dealing with the nonperturbative region of large b_T , one never modifies or approximates the operator definitions of the TMD ffs themselves. Rather, on the first line of Eq. (110) we have simply changed their arguments from b_T to b_* . Along the same lines, the g -functions on the last line have explicit definitions in terms of the underlying QCD operators. The final result for the cross section, Eq. (110), is exactly independent of the choice of the $\mathbf{b}_*(b_T)$ function in Eq. (100) or of the value of parameters like b_{\max} . Since changing them simply amounts to reshuffling contributions between the perturbative and non-perturbative factors, the b_* -independence is a version of RG invariance that we can express as

$$\frac{d}{db_{\max}} W(q_T, Q) = 0. \tag{112}$$

Or, if we consider other more general $\mathbf{b}_*(b_T)$ functions determined by a collection of possibly many parameters {b-params}, we can express the same relation schematically as

$$\frac{d}{d\{\text{b-params}\}} W(q_T, Q) = 0. \tag{113}$$

These relations are exact for Eq. (110). Therefore, it is legitimate to say that perturbative calculations of the first

³ There are, however, a large number of minor but not always obvious variations in the form of the expression in the literature. There are also many different systems of notation. See [38] for some translation.

two lines in Eq. (110) is completely perturbative in that they have no dependence on nonperturbative parameters beyond whatever power suppressed errors are introduced when we substitute Eq. (111). Thus, the b_* -method is not itself a model when used as originally set up. It is only a method for reorganizing contributions between the various factors in Eq. (110).

For all of this to be preserved in practice when performing calculations and applying them to phenomenology, the Eq. (99) g -functions need to be parametrized nonperturbatively but in a way that preserves Eq. (113). If a change of b_* or b_{\max} induces a change in the perturbative parts, a compensating change is needed in the Eq. (99) functions. (For more on this, see for example the discussion in section 13.13.2 of [3].) When specific parametrizations and approximations are substituted for the symbols in Eq. (110), the statements above that are exact become approximate. Ideally, however, one hopes to do this in such a way that the errors are small and controlled.

But implementing this style of approach in practice is complicated by the fact that it leaves very little said about the details of the Eq. (99) g -functions other than that they must vanish like a power at small b_T . In particular, it leaves unaddressed the treatment of the transition between the purely perturbative and purely nonperturbative regions in the parametrizations, along with the role that integral relations like Eq. (96) play in that transition. For *very* large Q , where the g -functions are anyway expected to give only small corrections, these details might not have an important effect on calculations. But they become important once one enters regimes where one is sensitive to the details of hadron structure. In the earliest implementations, b_T^2 power-laws [100] and/or b_T power-laws [101] were proposed, and these work reasonably well for many applications. But if a g -function from Eq. (99) is modeled with a simple ansatz, relations like Eq. (113) tend to be violated in ways that can significantly affect results [65, 102]. In some applications, the b_* -method and the choice of functions like Eq. (100) get reinterpreted as being part of the nonperturbative model itself, due to the large b_* sensitivity that is introduced by most simple ansatzes as discussed above. But then the perturbative calculation of the small b_T behavior become intertwined with the nonperturbative modeling, which is a situation that the b_* method of organization in Eq. (110) is meant to avoid.

These and related complications are all very well

known, and efforts have been made to overcome them. One essentially needs to reverse engineer the ansatzes for the g -functions to recover some approximate consistency with relations like Eq. (113). For example, Refs. [65, 103] impose continuity for both the functions and their derivatives at a point b_{\max} in b_T -space that they designate as a boundary between perturbative and nonperturbative regions. Similarly, in treating $g_K(b_T)$ Ref. [66] proposed to expand the nonperturbative parametrization in a power series of b_{\max}^2 at small b_T and match to the corresponding powers in the perturbative part of $\bar{K}(b_*; \mu)$.

B. Bottom-up in the b_* method

Since the bottom-up procedure that we described in Secs. IV-VI explicitly interpolates between nonperturbative and perturbative transverse momentum dependence, there was no need for a b_* method. The $\bar{Q}_0(b_T)$ that we introduced in Eq. (42) plays a role that is in some sense analogous to the μ_{b_*} from Eq. (102) in that both impose an RG improved $\mu \sim 1/b_T$ scale in the small b_T limit. However, in the earlier sections of this paper we never attempted to completely sequester purely perturbative and purely nonperturbative parts.

Nevertheless, the steps for the b_* -method carry over directly to our final expressions from the bottom-up procedure and Eqs. (61)–(65), and the problems summarized at the end of the last subsection are automatically avoided. One simply arrives at expressions for Eq. (99) that are connected to specific nonperturbative TMD models or calculations, constrained from the outset to satisfy all important properties. In this subsection, we will show the details of how to rewrite the bottom-up expression in Eq. (65) using the b_* -method. Most steps are simply a repetition of the normal way of writing the CSS evolution in terms of b_* , μ_{b_*} , etc, that we reviewed in the last subsection but now using the underlined functions and their evolution equations.

By construction, all of the underlined objects satisfy the specific evolution equations in Eq. (48), Eq. (62), and Eq. (63) exactly. Therefore, steps identical to those leading from Eq. (103) to Eq. (110) apply also to Eq. (65) as long as we maintain all the appropriate underlines and “ (n) ” superscripts everywhere. They thus allow us to rewrite $W^{(n)}(q_T, Q)$ as

$$\begin{aligned}
W^{(n)}(q_T, Q) &= H^{(n)}(\mu_Q; C_2) \int \frac{d^2 \mathbf{b}_T}{(2\pi)^2} e^{-i \mathbf{q}_T \cdot \mathbf{b}_T} \tilde{\underline{D}}_A^{(n, d_{\overline{\text{MS}}})}(z_A, \mathbf{b}_*; \mu_{b_*}, \mu_{b_*}^2) \tilde{\underline{D}}_B^{(n, d_{\overline{\text{MS}}})}(z_B, \mathbf{b}_*; \mu_{b_*}, \mu_{b_*}^2) \\
&\times \exp \left\{ 2 \int_{\mu_{b_*}}^{\mu_Q} \frac{d\mu'}{\mu'} \left[\gamma^{(n)}(\alpha_s(\mu'); 1) - \ln \frac{Q}{\mu'} \gamma_K^{(n)}(\alpha_s(\mu')) \right] + \ln \frac{Q^2}{\mu_{b_*}^2} \tilde{\underline{K}}^{(n)}(b_*; \mu_{b_*}) \right\} \\
&\times \exp \left\{ -\underline{g}_A^{(n, d_{\overline{\text{MS}}})}(z_A, b_T) - \underline{g}_B^{(n, d_{\overline{\text{MS}}})}(z_B, b_T) - \underline{g}_K^{(n)}(b_T) \ln \left(\frac{Q^2}{Q_0^2} \right) \right\}, \quad (114)
\end{aligned}$$

but now with

$$\underline{g}_K^{(n)}(b_T) \equiv \tilde{\underline{K}}^{(n)}(b_*, \mu_{Q_0}) - \tilde{\underline{K}}^{(n)}(b_T, \mu_{Q_0}), \quad (115)$$

$$\begin{aligned}
&-\underline{g}^{(n, d_{\overline{\text{MS}}})}(z, \mathbf{b}_T) \\
&\equiv \ln \left(\frac{\tilde{\underline{D}}^{(n, d_{\overline{\text{MS}}})}(z, \mathbf{b}_T; \mu_{Q_0}, Q_0^2)}{\tilde{\underline{D}}^{(n, d_{\overline{\text{MS}}})}(z, \mathbf{b}_*; \mu_{Q_0}, Q_0^2)} \right). \quad (116)
\end{aligned}$$

The functions defined in Eq. (115) and Eq. (116) are now written in terms of whatever model or nonperturbative calculation is being used at $\mu = \mu_{Q_0}$, but just as with Eq. (106) and Eq. (107), they are μ -independent. The underlines and superscripts indicate that these g -functions are defined with specific model parametrization and perturbative calculations in mind, rather than the purely abstract g -functions of Eqs. (106)–(107).

It is instructive to substitute the example parametrizations, Eq. (78) and Eq. (92), that we constructed in Sec. VII into Eqs. (114)–(116) and confirm the b_{max} -independence and other expected properties. In Fig. 10, the solid black curves are the same $\tilde{\underline{K}}^{(1)}(b_T; \mu_{Q_0})$ as in Fig. 2 and Fig. 3, but for comparison we have also shown the separate $\tilde{\underline{K}}^{(1)}(b_*; \mu_{Q_0})$ and $-\underline{g}_K^{(1)}(b_T)$ curves. The two panels compare the graphs for different values of b_{max} : the top panel is for $b_{\text{max}} = 0.1 \text{ GeV}^{-1}$ while the bottom panel is for $b_{\text{max}} = 1.0 \text{ GeV}^{-1}$. In both cases, $-\underline{g}_K^{(1)}(b_T)$ approaches zero as $b_T m \rightarrow 0$, and $\tilde{\underline{K}}^{(1)}(b_*; \mu_{Q_0})$ approaches the unapproximated $\tilde{\underline{K}}^{(1)}(b_T; \mu_{Q_0})$ as $b_T m \rightarrow 0$. Ultimately, it is only

$$\tilde{\underline{K}}^{(1)}(b_T; \mu_{Q_0}) = \tilde{\underline{K}}^{(1)}(b_*; \mu_{Q_0}) - \underline{g}_K^{(1)}(b_T) \quad (117)$$

that appears in Eq. (65), and indeed the sum of the dashed and dot-dashed curves in Fig. 10 always reproduces exactly the solid black $\tilde{\underline{K}}^{(1)}(b_T; \mu_{Q_0})$ curve. The separate terms in Eq. (117) are different for different b_{max} but of course $\tilde{\underline{K}}^{(1)}(b_T; \mu_{Q_0})$ is not.

A similar comparison for $-\underline{g}_A^{(1, d_{\overline{\text{MS}}})}(z, \mathbf{b}_T)$ is shown in Fig. 11. Now from Eq. (116) the combination of terms that is independent of b_{max} is

$$\begin{aligned}
&\ln \left(\tilde{\underline{D}}^{(1, d_{\overline{\text{MS}}})}(z, \mathbf{b}_T; \mu_{Q_0}, Q_0^2) \right) \\
&= \ln \left(\tilde{\underline{D}}^{(1, d_{\overline{\text{MS}}})}(z, \mathbf{b}_*; \mu_{Q_0}, Q_0^2) \right) - \underline{g}^{(1, d_{\overline{\text{MS}}})}(z, \mathbf{b}_T). \quad (118)
\end{aligned}$$

The solid black curve in Fig. 11 is $\ln \left(\tilde{\underline{D}}^{(1, d_{\overline{\text{MS}}})}(z, \mathbf{b}_T; \mu_{Q_0}, Q_0^2) \right)$ and it is the same for the upper ($b_{\text{max}} = 0.1 \text{ GeV}^{-1}$) and lower ($b_{\text{max}} = 1.0 \text{ GeV}^{-1}$) panels. The dashed and dot-dashed curves are for $\ln \left(\tilde{\underline{D}}^{(1, d_{\overline{\text{MS}}})}(z, \mathbf{b}_*; \mu_{Q_0}, Q_0^2) \right)$ and $-\underline{g}^{(1, d_{\overline{\text{MS}}})}(z, \mathbf{b}_T)$ respectively. The sum of the latter two always reproduces $\ln \left(\tilde{\underline{D}}^{(1, d_{\overline{\text{MS}}})}(z, \mathbf{b}_T; \mu_{Q_0}, Q_0^2) \right)$ while $-\underline{g}^{(1, d_{\overline{\text{MS}}})}(z, \mathbf{b}_T)$ goes to zero like a power at small b_T .

Note carefully that there are no error terms in going from Eq. (65) to Eq. (114). So far, the expression is just another way to write Eq. (65). Plots of Eq. (114) that use our parametrization from Sec. VII produce figures identical to Fig. 7, Fig. 8, and Fig. 9.

There are actually two ways that we can recast the methods of Sec. IV–Sec. VI in the b_* -method. In the first, we can simply notice that Eq. (114) is already very close to the standard form. This version of the b_* -expression is literally identical to the bottom-up expression in Eq. (65). However, it requires that we use the exact $\tilde{\underline{K}}^{(1)}(b_T; \mu_{Q_0})$ and $\tilde{\underline{D}}_{A,B}^{(n, d_{\overline{\text{MS}}})}(z_A, \mathbf{b}_*; \mu_{b_*}, \mu_{b_*}^2)$. In our specific examples from earlier, this would be Eq. (78) and Eq. (92). Of course, this defeats the purpose of the b_* approach.

However, now we can also use that

$$\tilde{\underline{K}}^{(n)}(b_*; \mu_{b_*}) = \tilde{K}^{(n)}(b_*; \mu_{b_*}) + O(mb_{\text{max}}) \quad (119)$$

and

$$\begin{aligned}
&\tilde{\underline{D}}^{(n, d_{\overline{\text{MS}}})}(z, \mathbf{b}_*; \mu_{b_*}, \mu_{b_*}^2) \\
&= \tilde{D}_{\text{OPE}}^{(n, d_{\overline{\text{MS}}})}(z, \mathbf{b}_*; \mu_{b_*}, \mu_{b_*}^2) + O(mb_{\text{max}}), \quad (120)
\end{aligned}$$

where $\tilde{D}_{\text{OPE}}^{(n, d_{\overline{\text{MS}}})}(z, \mathbf{b}_*; \mu_{b_*}, \mu_{b_*}^2)$ is the first term on the right side of Eq. (111). In other words, we can use purely perturbative expressions for these functions since they are constrained to arguments $b_T < b_{\text{max}}$. Dropping the order mb_{max} terms and substituting Eqs. (119)–(120) gives us our last expression for $W^{(n)}(q_T, Q)$,

$$\begin{aligned}
W_{b_*}^{(n)}(q_T, Q) &= H^{(n)}(\mu_Q; C_2) \int \frac{d^2 \mathbf{b}_T}{(2\pi)^2} e^{-i \mathbf{q}_T \cdot \mathbf{b}_T} \tilde{D}_{A, \text{OPE}}^{(n, d_{\overline{\text{MS}}})}(z_A, \mathbf{b}_*; \mu_{b_*}, \mu_{b_*}^2) \tilde{D}_{B, \text{OPE}}^{(n, d_{\overline{\text{MS}}})}(z_B, \mathbf{b}_*; \mu_{b_*}, \mu_{b_*}^2) \\
&\times \exp \left\{ 2 \int_{\mu_{b_*}}^{\mu_Q} \frac{d\mu'}{\mu'} \left[\gamma^{(n)}(\alpha_s(\mu'); 1) - \ln \frac{Q}{\mu'} \gamma_K^{(n)}(\alpha_s(\mu')) \right] + \ln \frac{Q^2}{\mu_{b_*}^2} \tilde{K}^{(n)}(b_*; \mu_{b_*}) \right\} \\
&\times \exp \left\{ -\underline{g}_A^{(n, d_{\overline{\text{MS}}})}(z_A, b_T) - \underline{g}_B^{(n, d_{\overline{\text{MS}}})}(z_B, b_T) - \underline{g}_K^{(n)}(b_T) \ln \left(\frac{Q^2}{Q_0^2} \right) \right\}. \quad (121)
\end{aligned}$$

The b_* subscript on the left is to indicate that we have dropped the underlines on $\tilde{K}^{(n)}(b_*; \mu_{b_*})$ and $\tilde{D}^{(n, d_{\overline{\text{MS}}})}(z, \mathbf{b}_*; \mu_{b_*}, \mu_{b_*}^2)$ and we have neglected the $O(mb_{\text{max}})$ terms in Eqs. (119)–(120). These functions are just calculated in collinear perturbation theory now. Thus,

$$W^{(n)}(q_T, Q_0) - W_{b_*}^{(n)}(q_T, Q_0) = O(mb_{\text{max}}). \quad (122)$$

Equation (121) is the evolved $W(q_T, Q)$ as it is normally presented in the CSS formalism. (For comparison, consider Eq. (22) from Ref. [66].) However, now there is no ambiguity about what the functions $g_A^{(n, d_{\overline{\text{MS}}})}(z_A, b_T)$, $g_B^{(n, d_{\overline{\text{MS}}})}(z_B, b_T)$ and $g_K^{(n)}(b_T)$ are, assuming that one has already followed the steps in Sec. VI. Whatever model, parametrization, or calculational technique we have used to describe the nonperturbative small transverse momentum dependence near the input scale (steps A1, A2) simply gets substituted into the right side of Eqs. (115)–(116). The integrand in Eq. (121) equals that of Eq. (65) up to corrections that vanish like a power of $b_T \leq b_{\text{max}}$. As long as b_{max} is small relative to the intrinsic mass parameters in the model, Eq. (113) is satisfied automatically.

Now in the bottom-up approach here there are no drawbacks to choosing b_{max} small enough to make the right side of Eq. (122) as small as desired. It amounts simply to including more of the perturbative part of the calculation inside the g -functions.

Of course, the above applies to any other $\overline{\text{MS}}$ renormalization scheme, we have used $\overline{\text{MS}}$ because it is the most common.

One may check the above directly by using the explicit $n = 1$ example from Sec. VII. Equation (114) and Eq. (121) are both plotted in Fig. 12 for two values of Q and with a range of b_{max} . The solid black curves are the same $W^{(1)}(q_T, Q)$ from Sec. VII with the same sample parameters, while the other curves are generated by Eq. (121) for a sequence of decreasing b_{max} . As expected, Eq. (121) converges to Eq. (114)/Eq. (65), and b_{max} dependence vanishes, for small enough b_{max} . This happens more rapidly at the larger Q where there is less sensitivity to large b_T region. The size of the $O(mb_T)$ errors are of course dependent upon the size of the parameters M , m_K , m_D , and a in the parametrization of the g -functions.

In practice, we may of course simply choose b_{max} small enough that this error is negligible.

Compare what we have done above with the way that $g_A^{(n, d_{\overline{\text{MS}}})}(z_A, b_T)$ (and the analogous function for the B hadron) is often treated in top-down styles of approaches, where a g functions is usually modeled by an ansatz:

$$g_A^{(n, d_{\overline{\text{MS}}})}(z_A, b_T) \longrightarrow g_A^{(n, d_{\overline{\text{MS}}})}(z_A, b_T; \{c_1, c_2, \dots\}). \quad (123)$$

Here, the $\{c_1, c_2, \dots\}$ is a list of ansatz parameters. But notice that the integral

$$\int_0^{\mu_{Q_0}} dk_T k_T e^{-g_A^{(n, d_{\overline{\text{MS}}})}(z_A, b_T; \{c_1, c_2, \dots\})}$$

is constrained by Eqs. (56)–(57). Therefore, the initially postulated $\{c_1, c_2, \dots\}$ parameters are not independent if a separate set of collinear ffs is known and available. At least one of the parameters is fixed in terms of the other parameters and the collinear functions. In the example from Sec. VII, this corresponds to the step where we replaced the $C^{(d_c)}$ in Eq. (83) by the right side of Eq. (87).

Without that step, the parameters of $g_A^{(n, d_{\overline{\text{MS}}})}(z_A, b_T)$ are underconstrained, and the model of the nonperturbative transverse momentum will generally be inconsistent with the collinear correlation functions.⁴ To our knowledge, such a step is not explicitly performed in the top-down implementations of TMD factorization and evolution.

These constraints also mean that the nonperturbative g -functions are strongly correlated with the collinear functions, consistent with observed phenomenology [104].

Before closing this section, we emphasize once more that the steps above involving b_* are not strictly necessary if one has already adopted the bottom-up steps of Sec. VI and implemented Eq. (65), but they may be helpful in comparing with past results.

⁴ Alternatively, one could in principle leave the TMD ff model unconstrained by Eq. (56) and instead calculate all collinear ffs directly in terms of the parametrization for the TMD ff. This may be impractical, however, given the existing extensive phenomenology that constrains collinear functions as compared to the TMD ones.

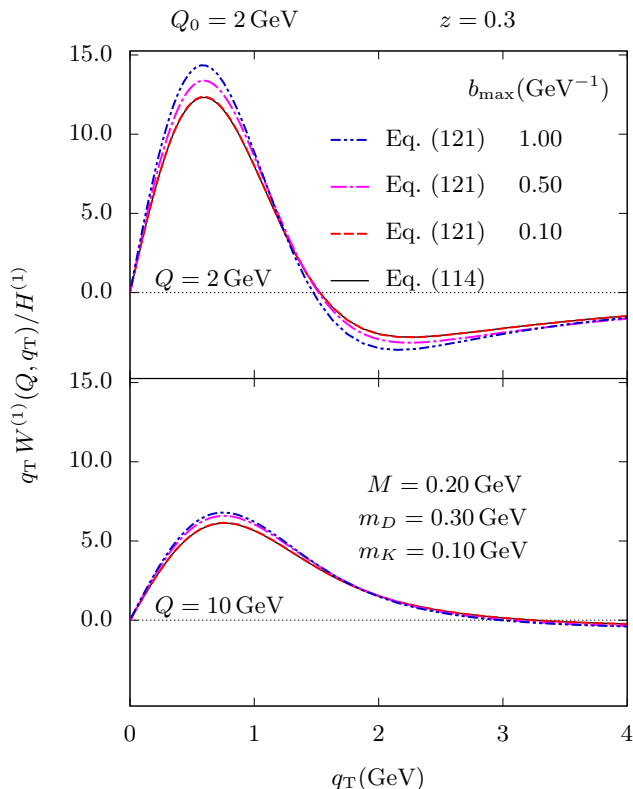


FIG. 12: A comparison of the cross section $W^{(1)}(q_T, Q)$ calculated using Eq. (114) and Eq. (121), with the example models from Sec. VII, at scales of $Q = 2$ GeV (top panel) and $Q = 10$ GeV (bottom panel), and with fixed values of intrinsic masses M , m_D and m_K as indicated in the labels. In each case, the solid lines implement the cross section in the usual notation of the CSS formalism, i.e. through the use of Eq. (114) and g functions defined in terms of our model examples, as in Eq. (115) and Eq. (116). The dashed lines are obtained by use of Eq. (121), with the same g as solid lines but with Eq. (121). Note that Eq. (114) is identical to Eq. (65) and is thus independent of b_{\max} by construction.

X. CONCLUSION

In this paper, we have explained the advantages of a bottom-up/forward-evolution style of treating TMD correlation functions modeled or calculated nonperturbatively at a moderate input scale. Before concluding, let us reemphasize that we have not made any fundamental modifications to standard TMD factorization and evolution – indeed, see Eq. (121). Rather, our purpose has been to make explicit the steps for combining any choice of nonperturbative model or parametrization of transverse momentum dependence with full TMD evolution in a reasonably automated way. This did lead to a significant amount of reorganization of previously known results, but we hope that the final prescription is fairly straightforward. Overall, our discussion in this paper

might be summarized as a prescription for constructing the “ g -functions” of typical CSS implementations in a way that conforms simultaneously with the TMD parton model viewpoint and TMD evolution.

The phenomenological strategy is to take TMDs generated from models, nonperturbative calculations, and/or fits near an input scale Q_0 , and use these to make predictions for higher Q measurements. Based on how successful those predictions are, models and/or fit parameters can be updated. The expected trend is that the amount of parameter adjustment diminishes as larger Q measurements are included.

Future steps involve constructing nonperturbative parametrizations analogous to our example functions in Sec. VII, but with more sophisticated input from nonperturbative QCD, including the models discussed in the introduction. It is likely (as was our intent) that many existing “Type I” phenomenological results can be combined with our approach with minimal modifications. Using the steps from Sec. VI to implement evolution with specific models like the spectator or bag models is a natural next task. Of course, all expressions need to be extended to all flavors and channels and to TMD pdfs. Other minor tasks still to be completed include extending to higher n (for \tilde{K} this is simple), including the singlet gluon channel, and extending it to a treatment of gluon TMDs [30].

Over the past several years, there has been significant progress also in lattice-based methods for calculating TMD functions [105–112]. The techniques discussed in this paper will also be important for connecting those developments to experimental data and phenomenological extractions.

We have focused on discussing unpolarized cross sections, but the same steps carry over in a straightforward way to polarized processes. A point of caution is that the integral relations analogous to Eq. (30) become more subtle in some spin dependent TMD functions, and the translation between correlation functions defined with cutoffs and in other schemes is not as straightforward [113, 114].

Nonperturbative g -functions exactly analogous to Eq. (99) appear in the TMD factorization formula for *double* scattering with double parton TMDs – see Eq.(6.31) of [115]. Therefore, techniques analogous to what we have described for single scattering should in principle apply there as well.

An application where our procedure also likely helps, but which we have not yet discussed in detail, is in the matching to large transverse momentum. The so-called “asymptotic” term discussed in, for example, [98] is the large k_T asymptote of Eq. (21), and it is an important ingredient for matching to the fixed order collinear calculation at large $q_T \approx Q$. In top-down/backward evolution approaches, errors that grow larger as Q decreases tend to spoil reasonable agreement between direct calculations of Eq. (21) and the asymptotic term [116]. By contrast, in the bottom-up approach we have laid out in this pa-

per, the matching to the asymptotic term at $Q \approx Q_0$ is automatic by construction. A separate but related issue is the difficulty observed in some processes, especially at moderate Q , of explaining $q_T \approx Q$ using standard fixed order collinear factorization and existing collinear pdfs and ffs [117–120].

In large Q measurements, there is reason to expect that nonperturbative transverse momentum eventually becomes phenomenologically irrelevant. It can remain important, however, when very high precision is a goal, such as measurements of vector boson masses [121–125].

We leave all of these considerations to future work.

Acknowledgments

Fatma Aslan and Abha Rajan were involved in early versions of this project and we thank her for useful discussions. We also thank Mariaelena Boglione for useful comments. T.R. was supported by the U.S. Department of Energy, Office of Science, Office of Nuclear Physics, under Award Number DE-SC0018106. This work was also supported by the DOE Contract No. DE-AC05-06OR23177, under which Jefferson Science Associates, LLC operates Jefferson Lab. The work of N.S. was supported by the DOE, Office of Science, Office of Nuclear Physics in the Early Career Program.

Appendix A: Notation Glossary

- $X^{(n)}$

An object X calculated *through* order α_s^n .

- $W(q_T, Q)$

The low- q_T contribution to the cross section TMD factorization, the “ W -term.” See Eq. (14).

- m

Any small mass scale of hadronic size or smaller, e.g., Λ_{QCD} , m_π , m_q etc.

- m_K, m_D, M

The nonperturbative mass scales in the parametrizations from Sec. VII. See Eq. (72) and Eq. (83).

- Renormalization group scales:

μ : A generic scale.

$\mu_Q = C_2 Q$,

$\mu_{Q_0} = C_2 Q_0$,

$\mu_{\overline{Q}_0} = C_2 \overline{Q}_0(b_T)$.

See below for $\overline{Q}_0(b_T)$, and see also Appendix C.

- Hard factors:

1. $H(\alpha_s(\mu_Q); C_2)$: The exact overall hard factor for the W -term in Eq. (20).
2. $H^{(n)}(\alpha_s(\mu_Q); C_2)$: The hard factor in perturbation theory truncated beyond order $\alpha_s(\mu_Q)^n$.
3. $\mathcal{C}_D^{(n)}(z k_T)$: The hard coefficient in the factorization formula relating the TMD ff to the collinear ff at $k_T \approx \mu_Q$, calculated in perturbation theory and truncated past order $\alpha_s(\mu_Q)^n$. See Eq. (25).
4. $\mathcal{C}_\Delta^{(n)}$: The hard coefficient in the correction term relating the cutoff integrated TMD ff to the collinear ff at $k_T \approx \mu_Q$, calculated in perturbation theory and truncated past order $\alpha_s(\mu_Q)^n$. See Eq. (28).

- $d_A(z_A; \mu)$

Definition: collinear fragmentation function for a quark with momentum fraction z_A fragmenting to hadron A .

- $d_{A,r}(z_A; \mu_Q)$

Definition: A more precise notation for $d_A(z_A; \mu_Q)$. Collinear fragmentation function with UV divergences handled in the r renormalization and/or regularization schemes. (e.g., $d_{\overline{\text{MS}}}$ is the standard collinear fragmentation function defined in the $\overline{\text{MS}}$ scheme.) The auxiliary scale μ is the renormalization scale and in the above we have already replaced it with $\mu = \mu_Q = C_2 Q$. Throughout this paper, we always assume $C_2 = 1$.

- $D_A(z_A, z_A \mathbf{k}_{AT}; \mu_Q, Q^2)$

Definition: The TMD quark ff for a quark with transverse momentum \mathbf{k}_{AT} fragmenting to hadron A . The auxiliary parameters associated with evolution are μ and ζ , and in the above they have already been replaced by $\mu = \mu_Q$ and $\zeta = \mu_Q^2 = Q^2$. We use different symbols for μ and ζ to keep derivatives clear.

- $D_A^{(n, d_r)}(z_A, z_A \mathbf{k}_{AT}; \mu_Q, Q^2)$

A *calculation* of a TMD quark ff in perturbative n^{th} -order collinear factorization optimized for $k_T \approx Q$ and using collinear ffs d_r defined in the r scheme.

- $d_{A,c}(z_A; \mu_Q)$

Definition: A special case of $d_{A,r}(z_A; \mu_Q)$ where the UV divergences are handled using the cutoff scheme. See Eq. (30).

- $\Delta^{(n,d_r)}(\alpha_s(\mu_Q))$

The correction term for relating $d_{A,c}(z_A; \mu_Q)$ to the collinear fragmentation function $d_{A,r}(z_A; \mu_Q)$ in another scheme r . See Eq. (27).

- $d_{A,c}^{(n,d_r)}(z_A; \mu_Q)$

The *approximate* expression for $d_{A,c}(z_A; \mu_Q)$ in terms of $d_{A,r}(z_A; \mu_Q)$, accurate up to order α_s^{n+1} and power suppressed errors. See Eqs. (31)–(32).

- $\underline{d}_{A,c}^{(n,d_r)}(z_A; \mu_Q)$

A parametrization of $d_{A,c}(z_A; \mu_Q)$ obtained from a the cutoff integral of the underlined TMD ff, $\underline{\tilde{D}}_A^{(n,d_r)}(z_A, \mathbf{b}_T; \mu_{Q_0}, Q_0^2)$. See Eqs. (56)–(57) and the definition of $\underline{\tilde{D}}_A^{(n,d_r)}(z_A, \mathbf{b}_T; \mu_{Q_0}, Q_0^2)$ below.

- $\tilde{K}(b_T; \mu)$

Definition: The coordinate space CS kernel. See Eqs. (17)–(18). Related to its momentum space version via

$$\tilde{K}(b_T; \mu) \equiv \int d^2 \mathbf{k}_T e^{i \mathbf{k}_T \mathbf{b}_T} K(k_T; \mu).$$

- $K^{(n)}(k_T; \mu)$

A fixed n^{th} -order, fixed scale perturbative calculation of $K(k_T; \mu)$. See Eqs. (36)–(37).

- $K_{\text{input}}^{(n)}(k_T; \mu_{Q_0})$

The *parametrization* of the momentum space CS kernel that interpolates between a nonperturbative parametrization of $K(k_T; \mu_{Q_0})$ at small k_T and $K^{(n)}(k_T; \mu_{Q_0})$ at large k_T . See Eq. (39). Optimized for applications in the $Q \approx Q_0$, $k_T \lesssim Q_0$ region of Eq. (20). The coordinate space version $\tilde{K}_{\text{input}}^{(n)}(b_T; \mu_{Q_0})$ is found from Eq. (40).

- $\overline{Q}_0(b_T)$

Transformation function for switching from $\mu = Q_0$ to $\mu = C_1/b_T$ RG scales. See Eq. (42). See also Appendix C.

- $\tilde{K}_{\text{input}}^{(n)}(b_T; \mu_{\overline{Q}_0})$

Same as $\tilde{K}_{\text{input}}^{(n)}(b_T; \mu_{Q_0})$ but with $\mu_{\overline{Q}_0} = C_2 \overline{Q}_0(b_T)$ as the scale.

- $\tilde{K}^{(n)}(b_T; \mu_{Q_0})$

Final parametrization of $\tilde{K}(b_T; \mu_{Q_0})$ optimized for all b_T , including the RG improved treatment of the $b_T \ll 1/Q_0$ region. See Eq. (46).

- $D_{\text{input}}^{(n,d_r)}(z, z \mathbf{k}_T; \mu_{Q_0}, Q_0^2)$

The input *parametrization* of the TMD ff with a nonperturbative parametrization for small k_T and interpolating to an n^{th} -order perturbative calculation at $k_T \sim Q_0$. Applicable to phenomenology at $Q \approx Q_0$ where $0 \leq k_T \lesssim Q_0$ is the relevant kinematical region. The perturbative part uses d_r collinear ffs in the r renormalization/regularization scheme. See Eq. (52).

- $\underline{\tilde{D}}_A^{(n,d_r)}(z_A, \mathbf{b}_T; \mu_{Q_0}, Q_0^2)$

The final *parametrization* of the coordinate space TMD ff at the input scale and optimized for all b_T , including the RG improved treatment of the $b_T \ll 1/Q_0$ region. The perturbative part uses d_r collinear ffs in the r renormalization/regularization scheme. See Eq. (61).

- $A^{(d_c)}(z; \mu), B^{(d_c)}(z; \mu), C^{(d_c)}$

Abbreviations for factors that involve collinear factorization. See Eq. (84), Eq. (85), and Eq. (87).

- $W^{(n)}(q_T, Q)$

A calculation of $W(q_T, Q)$ in Eq. (20) using $\underline{\tilde{D}}_{A,B}^{(n,d_r)}(z_{A,B}, \mathbf{b}_T; \mu_{Q_0}, Q_0^2)$, $H^{(n)}(\alpha_s(\mu_Q); C_2)$, $\tilde{K}^{(n)}(b_T; \mu_{Q_0})$, $\gamma_K^{(n)}(\alpha_s(\mu))$, and $\gamma^{(n)}(\alpha_s(\mu); 1)$.

Appendix B: Scale setting

The expansion in m/Q that gives the TMD factorization in Eq. (14) as its leading power must eventually break down as Q becomes small. In practice, this means one must choose a minimum Q_0 below which one stops trusting factorization in phenomenological applications, and this is what we have called the input scale Q_0 . Values of μ near Q_0 are understood to be close to the boundary where perturbative expansions in $\alpha_s(\mu)$ and power expansions in m/Q_0 cease to be valid even approximately. For the purposes of the present paper, Q_0 may be treated as a phenomenologically determined number. In practice it is usually taken to be somewhere in the range of 1–3 GeV.

The value of Q_0 fixes the overall RG (μ) and rapidity (ζ) scales in the input TMD ffs in Eq. (21). There is nothing incorrect in principle with working only with TMD factorization in the form that is written in Eq. (14) and Eq. (20). One may regard $\tilde{D}_A(z_A, \mathbf{b}_T; \mu_{Q_0}, Q_0^2)$, $\tilde{D}_B(z_B, \mathbf{b}_T; \mu_{Q_0}, Q_0^2)$, and $\tilde{K}(b_T; \mu_{Q_0})$ as entirely unknown functions to be determined phenomenologically or by other nonperturbative means. This is essentially the TMD parton model and is a standard approach to much phenomenology applied to nucleon structure studies near $Q \approx Q_0$. However, it leaves the TMD ffs very badly constrained at large k_T where perturbative calculations should be possible. When $k_{A,BT} \approx Q_0$ in Eq. (14), or equivalently when $b_T \approx 1/Q_0$ in Eq. (20), it is possible to expand the TMD functions perturbatively in collinear factorization and thereby increase predictive power. When $k_{A,BT}$ is much larger than Q_0 , one can further improve perturbative calculations by choosing $k_{A,BT}$ itself to set the hard scale in the individual TMD ffs rather than Q_0 . Of course, when $k_{A,BT}$ is small, it is not appropriate as a hard scale and one should instead continue to use Q_0 . Indeed, it is the nonperturbative k_T -dependence that is often of primary interest in TMD hadron structure studies.

In this appendix, we elaborate on the issue of the transition between the choices of Q_0 and k_T as scales for the TMD ffs, keeping in mind that the ultimate goal is to smoothly transition between traditional Type I and type II styles of approach. The discussion will be somewhat schematic and is meant to further motivate the main body of the text. Also, we will work in transverse momentum space where our main points will be somewhat more intuitive, but the discussion applies equally in transverse coordinate space, which is more common.

To see the issues clearly, recall that when k_T is large we may express the k_T -dependence in a single input TMD ff in the form

$$D(z, z\mathbf{k}_T; \mu_{Q_0}, Q_0^2) \stackrel{k_T \gg m}{\sim} \frac{1}{k_T^2} \left[\delta \left(\alpha_s(\mu_{Q_0}), \frac{k_T}{\mu_{Q_0}}, \frac{Q_0^2}{\mu_{Q_0}^2} \right) + O \left(\frac{m}{\mu_{Q_0}}, \frac{m}{k_T} \right) \right] \quad (\text{B1})$$

where δ is some function of the coupling and the ratios of the scales that generally appear in logarithms.

When $k_T \gg Q_0$, the k_T/μ_{Q_0} ratio on the right side of Eq. (B1) diverges so that perturbative calculations of δ with fixed μ_{Q_0} degrade in accuracy. Optimizing δ in perturbation theory requires another application of evolution from μ_{Q_0} to $\mu_{k_T} = C_k k_T$ and Q_0^2 to $\mu_{k_T}^2 = C_k^2 k_T^2$ where C_k is an order unity numerical constant analogous to C_1 and C_2 in the main body of the text. After evolution, the TMD ff that we work with instead has the general behavior

$$D(z, z\mathbf{k}_T; \mu_{k_T}, \mu_{k_T}^2) = \frac{1}{k_T^2} \left[\delta \left(\alpha_s(C_k k_T), O(1), O(1) \right) + O \left(\frac{m}{k_T} \right) \right] \quad (\text{B2})$$

Now as $k_T/Q_0 \rightarrow \infty$ the convergence properties of a perturbative expansion of δ only improves as the coupling and power suppressed terms vanish. Most of the standard Type II/top-down styles of TMD factorization implementations thus only use a scale choice analogous to Eq. (B2) (or rather its coordinate space analog) and rarely the fixed scale version in Eq. (B1).

However, small- α_s calculations of δ in Eq. (B2) come with numerically unstable truncation errors in the region around $k_T \approx Q_0$ simply because Q_0 is at the border between perturbative and nonperturbative scales. Small variations in, for example, the value of C_k can have a big effect on calculations. The problem is exacerbated by the fact that the transformation from μ_{Q_0}, Q_0^2 to $\mu_{k_T}, \mu_{k_T}^2$ effectively involves a resummation of many higher order logarithms in region of $k_{A,BT}$. That is, what appear in the factorization after the scale transformation is not Eq. (B2) alone but

$$\sim D(z, z\mathbf{k}_T; \mu_{k_T}, \mu_{k_T}^2) \times \left[1 + \sum_{\text{terms like}} \alpha_s(\mu_k)^m \ln^n \frac{\mu_{k_T}}{\mu_{Q_0}} \right] \quad (\text{B3})$$

However, when $k_T \approx \mu_{Q_0}$ the logarithms on the second line are anyway no larger than any other contributions that are higher order in $\alpha_s(k_T)$.⁵ The advantage of the scale transformation is lost here. More problematically, because of the rapidly rising coupling $\alpha_s(\mu_k)$ just below $k_T \approx Q_0$, the higher order logarithmic terms in Eq. (B3) are numerically unstable over the range of k_T extending from just below to just above Q_0 . Thus, calculations that use Eq. (B2) are rather poorly behaved in the $k_T \approx Q_0$ borderline region where we should expect a reasonably smooth transition to a nonperturbative region.

But calculations with a fixed scale can still be at least approximately valid around $k_T \approx Q_0$ where Eq. (B1) is

$$D(z, z\mathbf{k}_T; \mu_{Q_0}, Q_0^2) \stackrel{k_T \approx Q_0}{\sim} \frac{1}{k_T^2} \left[\delta \left(\alpha_s(\mu_{Q_0}), O(1), O(1) \right) + O \left(\frac{m}{Q_0} \right) \right] \quad (\text{B4})$$

As long as Q_0 is not very small, one can use low order perturbative calculations to approximate D . And there are no large logarithms in Eq. (B1) if $k_T \sim Q_0$, so the advantages of changing scales to Eq. (B2) are absent.

Therefore, our preferred choice of scale for the transition region around $k_T \approx Q_0$ is actually the fixed scale in Eq. (B1), not the $k_T \gg Q_0$ RG improved scale of Eq. (B2). Another advantage of using the fixed scale is that it automatically gives the fixed order asymptotic term in momentum space at $Q = Q_0$ and $q_T \approx Q_0$, which is also a fixed scale calculation in momentum space, when the TMD ff is substituted into Eq. (14).

⁵ It is also worth recalling here that QCD perturbation series are only asymptotic rather than convergent.

The above suggests that it is best to categorize the k_T -dependence not into just two regions of small k_T and large k_T , but into three regions: small k_T ($k_T \ll Q_0$), large k_T ($k_T \approx Q_0$), and very large k_T ($k_T \gg Q_0$). The large k_T region is where k_T is just barely large enough for small coupling descriptions of transverse momentum dependence to be reasonable.

In the discussion above we have worked in transverse momentum space because that better matches the intuition of models and phenomenology. However, the analogous observations apply straightforwardly to transverse coordinate space. In that case, there is a region of very large $b_T \gg 1/Q_0$ that is entirely nonperturbative, a region of very small $b_T \ll 1/Q_0$ that is purely perturbative as long as an RG improved $\mu \sim 1/b_T$ is used, and an intermediate region of $b_T \sim 1/Q_0$ where fixed order, fixed scale calculations are ideal.

One of our tasks in the main body of the paper is to interpolate between these three regions in our parameterizations. For the intermediate region of transverse momentum, transitioning between scales only introduces higher order errors.

Notice that our discussion of large logarithms above is a mirror image of how large logarithms are often introduced in explanations of top down approaches. There, one starts with Eq. (B1) but using μ_Q and Q^2 instead of the input μ_{Q_0} and Q_0^2 and assuming $Q \gg Q_0$:

$$D(z, z\mathbf{k}_T; \mu_Q, Q^2)^{k_T \gg m} = \frac{1}{k_T^2} \left[\delta \left(\alpha_s(\mu_Q), \frac{k_T}{\mu_Q}, \frac{Q^2}{\mu_Q^2} \right) + O \left(\frac{m}{\mu_Q}, \frac{m}{k_T} \right) \right] \quad (\text{B5})$$

Then the task is to determine how to resum large logarithms of $\ln(k_T/\mu_Q)$ as k_T gets *small* relative to Q , rather than as k_T gets large relative to Q_0 .

Appendix C: Scale transformation function

For the scale transition function in Eq. (42), we must arrange for the transition from $\sim 1/b_T$ to Q_0 to occur at b_T somewhat smaller than $1/Q_0$ to avoid modifying the treatment of Eq. (20) in the $Q \approx Q_0$ region. One choice that satisfies this for a $Q_0 = 2$ GeV is

$$\begin{aligned} \bar{Q}_0(b_T) &= 2.0 \text{ GeV} \left[1 - \left(1 - \frac{C_1}{(2.0 \text{ GeV})b_T} \right) e^{-(4 \text{ GeV}^2)b_T^2} \right]. \end{aligned} \quad (\text{C1})$$

If we wish to adjust the exact shape in the $\approx 1/Q_0$ transition region by adding a parameter as in Eq. (49), we may modify Eq. (C1) by introducing a parameter a ,

$$\begin{aligned} \bar{Q}_0(b_T, a) &= 2.0 \text{ GeV} \left[1 - \left(1 - \frac{C_1}{(2.0 \text{ GeV})b_T} \right) e^{-b_T^2 a^2} \right]. \end{aligned} \quad (\text{C2})$$

Here the transition between the two RG scales takes place around $b_T \sim 1/a$. We can use the Eq. (C2) form to check approximate scale independence in the transition region by varying a slightly. C_1 is the usual numerical constant, $C_1 = 2e^{-\gamma_E} \approx 1.123$.

-
- [1] J. C. Collins and D. E. Soper, Nucl. Phys. **B193**, 381 (1981), erratum: **B213**, 545 (1983).
 - [2] J. C. Collins, D. E. Soper, and G. Sterman, Nucl. Phys. **B250**, 199 (1985).
 - [3] J. C. Collins, *Foundations of Perturbative QCD* (Cambridge University Press, Cambridge, 2011).
 - [4] T. Becher, M. Neubert, and B. D. Pecjak, JHEP **01**, 076 (2007), hep-ph/0607228.
 - [5] T. Becher and M. Neubert, Eur. Phys. J. **C71**, 1665 (2011), 1007.4005.
 - [6] M. G. Echevarría, A. Idilbi, and I. Scimemi, JHEP **1207**, 002 (2012), 1111.4996.
 - [7] R. K. Ellis, D. A. Ross, and S. Veseli, Nucl. Phys. B **503**, 309 (1997), hep-ph/9704239.
 - [8] D. de Florian and M. Grazzini, Phys. Rev. Lett. **85**, 4678 (2000), hep-ph/0008152.
 - [9] G. Bozzi, S. Catani, D. de Florian, and M. Grazzini, Nucl. Phys. **B737**, 73 (2006), hep-ph/0508068.
 - [10] S. Catani, L. Cieri, D. de Florian, G. Ferrera, and M. Grazzini, Eur. Phys. J. **C72**, 2195 (2012), 1209.0158.
 - [11] S. Catani, L. Cieri, D. de Florian, G. Ferrera, and M. Grazzini, Nucl. Phys. **B881**, 414 (2014), 1311.1654.
 - [12] C. W. Gardiner and D. P. Majumdar, Phys. Rev. D **2**, 2040 (1970).
 - [13] R. Tangerman and P. Mulders, Phys. Rev. **D51**, 3357 (1995), hep-ph/9403227.
 - [14] P. J. Mulders and R. D. Tangerman, Nucl. Phys. **B461**, 197 (1996), hep-ph/9510301.
 - [15] M. Anselmino, M. Boglione, and F. Murgia, Phys. Lett. B **362**, 164 (1995), hep-ph/9503290.
 - [16] A. Bacchetta et al., JHEP **02**, 093 (2007), hep-ph/0611265.
 - [17] M. Anselmino, M. Boglione, U. D'Alesio, A. Kotzinian, F. Murgia, A. Prokudin, and C. Turk, Phys. Rev. D **75**, 054032 (2007), hep-ph/0701006.
 - [18] P. Schweitzer, T. Teckentrup, and A. Metz, Phys. Rev. **D81**, 094019 (2010), 1003.2190.
 - [19] M. Anselmino, M. Boglione, and F. Murgia, Phys. Rev. D **60**, 054027 (1999), hep-ph/9901442.
 - [20] R. P. Feynman, R. D. Field, and G. C. Fox, Phys. Rev. **D18**, 3320 (1978).
 - [21] X. Ji, J.-P. Ma, and F. Yuan, Phys. Rev. **D71**, 034005 (2005), hep-ph/0404183.
 - [22] X. Ji, J.-P. Ma, and F. Yuan, Phys. Lett. **B597**, 299 (2004), hep-ph/0405085.
 - [23] S. M. Aybat and T. C. Rogers, Phys. Rev. **D83**, 114042 (2011), 1101.5057.
 - [24] M. Anselmino, M. Boglione, and S. Melis, Phys. Rev.

- D86**, 014028 (2012), 1204.1239.
- [25] S. M. Aybat, J. C. Collins, J. Qiu, and T. C. Rogers, *Phys. Rev. D* **85**, 034043 (2012), 1110.6428.
 - [26] R. M. Godbole, A. Misra, A. Mukherjee, and V. S. R. Rao, *Phys. Rev. D* **88**, 014029 (2013), 1304.2584.
 - [27] M. G. Echevarria, A. Idilbi, Z.-B. Kang, and I. Vitev, *Phys. Rev. D* **89**, 074013 (2014), 1401.5078.
 - [28] F. Hautmann, H. Jung, M. Krämer, P. J. Mulders, E. R. Nocera, T. C. Rogers, and A. Signori, *Eur. Phys. J. C* **74**, 3220 (2014), 1408.3015.
 - [29] A. Bacchetta, M. G. Echevarria, P. J. G. Mulders, M. Radici, and A. Signori, *JHEP* **11**, 076 (2015), 1508.00402.
 - [30] F. Scarpa, D. Boer, M. G. Echevarria, J.-P. Lansberg, C. Pisano, and M. Schlegel, *Eur. Phys. J. C* **80**, 87 (2020), 1909.05769.
 - [31] M. Boglione, J. O. Gonzalez-Hernandez, and R. Taghavi, *Phys. Lett. B* **772**, 78 (2017), 1704.08882.
 - [32] A. Bacchetta, F. Delcarro, C. Pisano, M. Radici, and A. Signori, *JHEP* **06**, 081 (2017), [Erratum: *JHEP* **06**, 051 (2019)], 1703.10157.
 - [33] M. Anselmino, M. Boglione, U. D'Alesio, F. Murgia, and A. Prokudin, *Phys. Rev. D* **98**, 094023 (2018), 1809.09500.
 - [34] A. Bacchetta, V. Bertone, C. Bissolotti, G. Bozzi, F. Delcarro, F. Piacenza, and M. Radici, *JHEP* **07**, 117 (2020), 1912.07550.
 - [35] I. Scimemi and A. Vladimirov, *JHEP* **06**, 137 (2020), 1912.06532.
 - [36] S. Bastami, L. Gamberg, B. Parsamyan, B. Pasquini, A. Prokudin, and P. Schweitzer, *JHEP* **02**, 166 (2021), 2005.14322.
 - [37] M. Boglione and A. Simonelli, *JHEP* **02**, 076 (2021), 2011.07366.
 - [38] J. Collins and T. C. Rogers, *Phys. Rev. D* **96**, 054011 (2017), 1705.07167.
 - [39] M. Aghasyan et al. (COMPASS), *Phys. Rev. D* **97**, 032006 (2018), 1709.07374.
 - [40] L. P. Gamberg, G. R. Goldstein, and K. A. Oganessyan, *Phys. Rev. D* **67**, 071504 (2003), hep-ph/0301018.
 - [41] A. Bacchetta, F. Conti, and M. Radici, *Phys. Rev. D* **78**, 074010 (2008), 0807.0323.
 - [42] Z.-B. Kang, J.-W. Qiu, and H. Zhang, *Phys. Rev. D* **81**, 114030 (2010), 1004.4183.
 - [43] J. V. Guerrero and A. Accardi (2020), 2010.07339.
 - [44] B. Pasquini, S. Cazzaniga, and S. Boffi, *Phys. Rev. D* **78**, 034025 (2008), 0806.2298.
 - [45] B. Pasquini and P. Schweitzer, *Phys. Rev. D* **83**, 114044 (2011), 1103.5977.
 - [46] A. Bacchetta, S. Cotogno, and B. Pasquini, *Phys. Lett. B* **771**, 546 (2017), 1703.07669.
 - [47] B. Pasquini and P. Schweitzer, *Phys. Rev. D* **90**, 014050 (2014), 1406.2056.
 - [48] Z. Hu, S. Xu, C. Mondal, X. Zhao, and J. P. Vary (2022), 2205.04714.
 - [49] S. Sakai, *Prog. Theor. Phys.* **63**, 1815 (1980).
 - [50] S. Sakai, *Prog. Theor. Phys.* **63**, 1311 (1980).
 - [51] F. Yuan, *Phys. Lett. B* **575**, 45 (2003), hep-ph/0308157.
 - [52] H. Avakian, A. V. Efremov, P. Schweitzer, and F. Yuan, *Phys. Rev. D* **81**, 074035 (2010), 1001.5467.
 - [53] A. I. Signal and F. G. Cao, *Phys. Lett. B* **826**, 136898 (2022), 2108.12116.
 - [54] H. H. Matevosyan, W. Bentz, I. C. Cloet, and A. W. Thomas, *Phys. Rev. D* **85**, 014021 (2012), 1111.1740.
 - [55] H. H. Matevosyan, A. W. Thomas, and W. Bentz, *Phys. Rev. D* **86**, 034025 (2012), 1205.5813.
 - [56] S. Noguera and S. Scopetta, *JHEP* **11**, 102 (2015), 1508.01061.
 - [57] C. Shi and I. C. Cloët, *Phys. Rev. Lett.* **122**, 082301 (2019), 1806.04799.
 - [58] W. Broniowski and E. Ruiz Arriola, *Phys. Lett. B* **773**, 385 (2017), 1707.09588.
 - [59] S. Bastami, A. V. Efremov, P. Schweitzer, O. V. Teryaev, and P. Zavada, *Phys. Rev. D* **103**, 014024 (2021), 2011.06203.
 - [60] R. K. Ellis and S. Veseli, *Nucl. Phys. B* **511**, 649 (1998), hep-ph/9706526.
 - [61] A. Kulesza and W. J. Stirling, *Nucl. Phys. B* **555**, 279 (1999), hep-ph/9902234.
 - [62] Y. L. Dokshitzer, D. Diakonov, and S. I. Troian, *Phys. Rept.* **58**, 269 (1980).
 - [63] J. C. Collins and D. E. Soper, *Nucl. Phys. B* **194**, 445 (1982).
 - [64] J. C. Collins, D. E. Soper, and G. Sterman, *Phys. Lett. B* **109**, 388 (1982).
 - [65] J. Qiu and X.-F. Zhang, *Phys. Rev. D* **63**, 114011 (2001), hep-ph/0012348.
 - [66] J. Collins and T. Rogers, *Phys. Rev. D* **91**, 074020 (2015), 1412.3820.
 - [67] M. A. Kimber, A. D. Martin, and M. G. Ryskin, *Phys. Rev. D* **63**, 114027 (2001), hep-ph/0101348.
 - [68] G. Watt, A. D. Martin, and M. G. Ryskin, *Eur. Phys. J. C* **31**, 73 (2003), hep-ph/0306169.
 - [69] B. Guiot (2022), 2205.02873.
 - [70] K. Golec-Biernat and A. M. Stasto, *Phys. Lett. B* **781**, 633 (2018), 1803.06246.
 - [71] B. Guiot, *Phys. Rev. D* **101**, 054006 (2020), 1910.09656.
 - [72] M. A. Ebert, J. K. L. Michel, I. W. Stewart, and Z. Sun (2022), 2201.07237.
 - [73] P. Sun and F. Yuan, *Phys. Rev. D* **88**, 034016 (2013), 1304.5037.
 - [74] P. Sun and F. Yuan, *Phys. Rev. D* **88**, 114012 (2013), 1308.5003.
 - [75] D. Boer, *Nucl. Phys. B* **806**, 23 (2009), 0804.2408.
 - [76] D. Boer, R. Jakob, and P. J. Mulders, *Nucl. Phys. B* **504**, 345 (1997), hep-ph/9702281.
 - [77] E. Moffat, T. C. Rogers, N. Sato, and A. Signori, *Phys. Rev. D* **100**, 094014 (2019), 1909.02951.
 - [78] E. Moffat, W. Melnitchouk, T. C. Rogers, and N. Sato (Jefferson Lab Angular Momentum (JAM)), *Phys. Rev. D* **104**, 016015 (2021), 2101.04664.
 - [79] A. Buckley, J. Ferrando, S. Lloyd, K. Nordström, B. Page, M. Rüfenacht, M. Schönherr, and G. Watt, *Eur. Phys. J. C* **75**, 132 (2015), 1412.7420.
 - [80] T. C. Rogers, *Eur. Phys. J. A* **52**, 153 (2016), 1509.04766.
 - [81] M. Diehl, *Eur. Phys. J. A* **52**, 149 (2016), 1512.01328.
 - [82] M. Anselmino, U. D'Alesio, and F. Murgia, *Phys. Rev. D* **67**, 074010 (2003), hep-ph/0210371.
 - [83] J. Collins, A. Efremov, K. Goeke, S. Menzel, A. Metz, et al., *Phys. Rev. D* **73**, 014021 (2006), hep-ph/0509076.
 - [84] A. Signori, A. Bacchetta, M. Radici, and G. Schnell, *JHEP* **1311**, 194 (2013), arXiv:1309.3507.
 - [85] S. J. Brodsky, D.-S. Hwang, B.-Q. Ma, and I. Schmidt, *Nucl. Phys. B* **593**, 311 (2001), hep-th/0003082.
 - [86] J. C. Collins, *Acta Phys. Polon. B* **34**, 3103 (2003), hep-ph/0304122.
 - [87] C. Davies and W. J. Stirling, *Nucl. Phys. B* **244**, 337

- (1984).
- [88] Y. Li and H. X. Zhu, Phys. Rev. Lett. **118**, 022004 (2017), 1604.01404.
 - [89] Y. Li, D. Neill, and H. X. Zhu, Nucl. Phys. B **960**, 115193 (2020), 1604.00392.
 - [90] M. G. Echevarria, I. Scimemi, and A. Vladimirov, JHEP **09**, 004 (2016), 1604.07869.
 - [91] T. L  bber, J. Oredsson, and M. Stahlhofen, JHEP **03**, 168 (2016), 1602.01829.
 - [92] A. A. Vladimirov, Phys. Rev. Lett. **125**, 192002 (2020), 2003.02288.
 - [93] C. Aidala, B. Field, L. Gamberg, and T. Rogers, Phys. Rev. D **89**, 094002 (2014), 1401.2654.
 - [94] P. Shanahan, M. Wagman, and Y. Zhao, Phys. Rev. D **102**, 014511 (2020), 2003.06063.
 - [95] M. Anselmino, M. Boglione, A. Prokudin, and C. Turk, Eur. Phys. J. A **31**, 373 (2007), hep-ph/0606286.
 - [96] M.-X. Luo, X. Wang, X. Xu, L. L. Yang, T.-Z. Yang, and H. X. Zhu, JHEP **10**, 083 (2019), 1908.03831.
 - [97] M.-x. Luo, T.-Z. Yang, H. X. Zhu, and Y. J. Zhu, JHEP **06**, 115 (2021), 2012.03256.
 - [98] J. Collins, L. Gamberg, A. Prokudin, T. C. Rogers, N. Sato, and B. Wang, Phys. Rev. D **94**, 034014 (2016), 1605.00671.
 - [99] J. C. Collins and D. E. Soper, Nucl. Phys. B **197**, 446 (1982).
 - [100] C. T. H. Davies, B. R. Webber, and W. J. Stirling, **1**, 1.95 (1984).
 - [101] G. Ladinsky and C. Yuan, Phys. Rev. D **50**, R4239 (1994), hep-ph/9311341.
 - [102] J. Qiu and X.-F. Zhang, Phys. Rev. Lett. **86**, 2724 (2001), hep-ph/0012058.
 - [103] M. Grewal, Z.-B. Kang, J.-W. Qiu, and A. Signori, Phys. Rev. D **101**, 114023 (2020), 2003.07453.
 - [104] M. Bury, F. Hautmann, S. Leal-Gomez, I. Scimemi, A. Vladimirov, and P. Zurita (2022), 2201.07114.
 - [105] M.-H. Chu et al. (2022), 2204.00200.
 - [106] X. Ji, Y.-S. Liu, Y. Liu, J.-H. Zhang, and Y. Zhao, Rev. Mod. Phys. **93**, 035005 (2021), 2004.03543.
 - [107] M. Constantinou et al., Prog. Part. Nucl. Phys. **121**, 103908 (2021), 2006.08636.
 - [108] K. Cichy and M. Constantinou, Adv. High Energy Phys. **2019**, 3036904 (2019), 1811.07248.
 - [109] M. A. Ebert, S. T. Schindler, I. W. Stewart, and Y. Zhao (2022), 2201.08401.
 - [110] M. A. Ebert, I. W. Stewart, and Y. Zhao, JHEP **03**, 099 (2020), 1910.08569.
 - [111] M. A. Ebert, I. W. Stewart, and Y. Zhao, JHEP **09**, 037 (2019), 1901.03685.
 - [112] M. A. Ebert, I. W. Stewart, and Y. Zhao, Phys. Rev. D **99**, 034505 (2019), 1811.00026.
 - [113] J.-W. Qiu, T. C. Rogers, and B. Wang, Phys. Rev. D **101**, 116017 (2020), 2004.13193.
 - [114] T. Rogers, Mod. Phys. Lett. A **35**, 2030021 (2020), 2008.05351.
 - [115] M. G. A. Buffing, M. Diehl, and T. Kasemets, JHEP **01**, 044 (2018), 1708.03528.
 - [116] M. Boglione, J. O. G. Hernandez, S. Melis, and A. Prokudin, JHEP **02**, 095 (2015), 1412.1383.
 - [117] A. Daleo, D. de Florian, and R. Sassot, Phys. Rev. D **71**, 034013 (2005), hep-ph/0411212.
 - [118] J. O. Gonzalez-Hernandez, T. C. Rogers, N. Sato, and B. Wang, Phys. Rev. D **98**, 114005 (2018), 1808.04396.
 - [119] A. Bacchetta, G. Bozzi, M. Lambertsen, F. Piacenza, J. Steiglechner, and W. Vogelsang, Phys. Rev. D **100**, 014018 (2019), 1901.06916.
 - [120] B. Wang, J. O. Gonzalez-Hernandez, T. C. Rogers, and N. Sato, Phys. Rev. D **99**, 094029 (2019), 1903.01529.
 - [121] A. Banfi, M. Dasgupta, and S. Marzani, Phys. Lett. B **701**, 75 (2011), 1102.3594.
 - [122] A. Bacchetta, G. Bozzi, M. Radici, M. Ritzmann, and A. Signori, Phys. Lett. B **788**, 542 (2019), 1807.02101.
 - [123] M. Guzzi, P. M. Nadolsky, and B. Wang, Phys. Rev. D **90**, 014030 (2014), 1309.1393.
 - [124] P. M. Nadolsky, AIP Conf. Proc. **753**, 158 (2005), hep-ph/0412146.
 - [125] T. Aaltonen et al. (CDF), Science **376**, 170 (2022).